NASA TN D-908

TECHNICAL NOTE

D-908

THE DEVELOPMENT OF AN 8-INCH BY 8-INCH SLOTTED TUNNEL FOR MACH NUMBERS UP TO 1.28

By B. H. Little, Jr., and James M. Cubbage, Jr.

Langley Research Center
Langley Air Force Base, Va.

NATIONAL AERONAUTICS AND SPACE ADMINISTRATION
WASHINGTON
August 1961

NATIONAL AERONAUTICS AND SPACE ADMINISTRATION

TECHNICAL NOTE D-908

THE DEVELOPMENT OF AN 8-INCH BY 8-INCH SLOTTED TUNNEL FOR MACH NUMBERS UP TO 1.28[1]

By B. H. Little, Jr., and James M. Cubbage, Jr.

SUMMARY

An 8-inch by 8-inch transonic tunnel model with test section slotted on two opposite walls was constructed in which particular emphasis was given to the development of slot geometry, slot-flow re-entry section, and short-diffuser configurations for good test-region flow and minimum total-pressure losses. Center-line static pressures through the test section, wall static pressures through the other parts of the tunnel, and total-pressure distributions at the inlet and exit stations of the diffuser were measured.

With a slot length equal to two tunnel heights and 1/14 open-area-ratio slotted walls, a test region one tunnel height in length was obtained in which the deviation from the mean Mach number was less than ±0.01 up to Mach number 1.15. With 1/7 open-area-ratio slotted walls, a test region 0.84 tunnel heights in length with deviation less than ±0.01 was obtained up to Mach number 1.26.

Increasing the tunnel diffuser angle from 6.4° to 10° increased pressure loss through the tunnel at Mach number 1.20 from 15 percent to 20 percent of the total pressure. The use of other diffusers with equivalent angles of 10° but contoured so that the initial diffusion angle was less than 10° and the final angle was 20° reduced the losses to as low as 16 percent.

A method for changing the test-section Mach number rapidly by controlling the flow through a bypass line from the tunnel settling chamber to the slot-flow plenum chamber of the test section was very effective. The test-section Mach number was reduced approximately 5 percent in 1/8 second by bleeding into the test section a flow of air equal to 2 percent of the mainstream flow and 30 percent in 1/4 second with bleed flow equal to 10 percent of the mainstream flow. The rate of reduction was largely determined by the opening rate of the bleed-flow-control valve.

---

[1]Supersedes declassified NACA Research Memorandum L55B08 by B. H. Little, Jr., and James M. Cubbage, Jr., 1955.

INTRODUCTION

The urgent need for aerodynamic data in the transonic range has resulted in a rapid development of the slotted tunnel. The pattern of development consists, to a large degree, of the efforts to convert available subsonic wind tunnels to transonic operation. It is not surprising, therefore, to find data in the literature (refs. 1 to 4) from a number of slotted tunnels whose geometries differ over a wide range but few data from systematic investigations of the basic variables. Most of that in the latter category is concerned with flow generation. (For example, see refs. 5 and 6.) The available data do provide a valuable guide in designing subsequent tunnels, but each new design remains, to some extent, a new development problem.

The present paper deals with the development program for converting the Langley 19-foot pressure tunnel for transonic operation. This development was done in a 1/24-scale model of that tunnel. Originally, it was thought that the tunnel conversion must be made without altering the overall dimensions of the tunnel circuit. This condition meant that the lengthening of the test section that was necessary for satisfactory flow generation could only be accomplished by shortening the diffuser. The slotted tunnel, with its mass of low-energy slot-flow air which is introduced into the diffuser, presents a difficult pressure-recovery problem even with a long, low-angle diffuser. With a shorter diffuser, a small percentagewise increase in pressure losses can easily result in significant increases in tunnel power requirements or decreases in maximum Mach number attainable. During the course of this development, the possibility arose of lengthening the tunnel circuit to permit use of a 6.4° included-angle conical diffuser. This configuration was included in the test program and affords a good standard geometry with which the short-diffuser configurations may be compared.

Since some research was planned in which this tunnel would be used to study flutter characteristics of various models and model components, it was desired that a method be devised to change the test-section Mach number almost instantaneously when the models were in danger of destruction. It was suggested that this be done by establishing a bypass line through which flow could be bled directly from the tunnel settling chamber into the test-section plenum chamber. Tunnel deceleration would be accomplished by increasing the bypass flow and acceleration by decreasing the bypass flow. The investigation of this method is reported herein.

The Reynolds numbers obtained in the development of this tunnel range up to about 5.5×10^6 per foot and the test-section Mach numbers range from 0.7 to 1.28. The data presented include center-line static-pressure distributions, static-pressure-recovery coefficients at the

diffuser exit, total-pressure losses at the diffuser inlet and exit stations, and time histories of the tests for rapid change of test-section Mach number.

SYMBOLS

A	cross-sectional area
A_o	total bypass, or bleed, line orifice area
A^*	cross-sectional area at tunnel throat (61.2 sq in.)
a	speed of sound
atm	atmospheric pressure
C	total periphery of test section
d_s	depth of untapered portion of slot
h	height of test section at minimum section
H	total pressure
ΔH	difference in total pressure from diffuser inlet to exit
ΔH_T	difference in total pressure from tunnel entrance cone to diffuser exit
L	length of slot-opening taper
m	mass flow
m'	bleed mass flow
Δm	measured mass flow minus true mass flow
M	Mach number
M_c	Mach number computed by using p_c and H_o
$\bar{M}_i$	mean inlet Mach number
ΔM	change in Mach number
n	number of slots per wall
p	static pressure
p_c	static pressure in test-section plenum chamber
Δp	difference in static pressure from diffuser inlet to exit
q	dynamic pressure

t	time from energization of solenoid, sec
u	velocity at point in boundary layer
U	free-stream velocity
w_s	width of untapered portion of slot
x	longitudinal distance
δ_F	flap-position angle
δ_T	flap-tab angle
ρ	free-stream density

Subscripts:

o	stagnation or reference conditions
L	local condition (at a measuring point)
i	diffuser inlet
e	diffuser exit

APPARATUS AND METHODS

High-pressure air was supplied by multistage centrifugal compressors capable of handling a maximum of 60 pounds per second at pressures up to 50 lb/sq in. absolute. The stagnation temperature was variable but was generally set at about 150° F or at whatever higher value was necessary to avoid visible condensation in the test section.

MODEL TUNNEL

A drawing of the model tunnel is shown in figure 1, and a line diagram of the tunnel and auxiliary ducting is shown in figure 2. The tunnel system was of the nonreturn type exhausting to the atmosphere, but the pressure level was controlled by the butterfly valve in the exhaust ducting (fig. 2). The supply line from the compressors was expanded to form a settling chamber upstream of the inlet bell and screens were located, as shown in figure 2, to damp out large-scale turbulence. Duplication of the Langley 19-foot pressure tunnel began at the entrance bell which had a contraction ratio of about 10:1 and was contoured to form a transition from the circular plenum chamber to the filleted square shape of the test section.

Test Section

The test section is shown in detail in figures 1 to 3. This square cross section with two slotted and two solid walls was chosen for the structural simplicity of a two-dimensional shape and the ease with which slotted-wall changes could be made. In order to obtain the maximum tunnel span for the model throat area of 61.2 square inches, which was fixed by the full-scale-tunnel power considerations, corner fillets were installed. These fillets increased test-section height and breadth to 8 inches. Both solid and slotted walls diverged in the direction of the flow about 0° 8' with respect to the center line. The solid walls extended outboard of the slotted walls to form, with the side and end plates, pressure-tight plenum chambers which were interconnected.

For the tests of rapid Mach number change by test-section bleed, the test-section plenum manifolds were connected to the tunnel settling chamber as shown in figure 2. The connecting ducts contained rapid-opening butterfly valves which were operated by a solenoid-controlled air cylinder. Flow-measuring and metering orifices were placed in the ducts between the butterfly valves and the test section.

Details of the slotted-wall construction are also shown in figures 1 to 3. The slotted-wall plates were attached to longitudinal wall beams which were held in place by the nozzle block upstream and a simple bracket downstream. The slot shape is readily changed by changing wall plates. All screw heads were filled after each change to keep the test-section interior aerodynamically smooth. Development of the test section was planned to indicate the general configuration rather than to carry out a program of detailed modifications which it would probably be necessary to repeat in the full-size tunnel. The slotted-wall plates were constructed to form walls having open-area-to-total-area ratios $\left(\frac{nw_s}{C/4}\right)$ of 1/14 and 1/7. A tapered slot opening of length equal to one tunnel height was chosen as that which would provide a probable minimum slot opening rate. Greater opening rates were obtained by machining the wall plates.

Slot-Flow Re-entry Section

A large portion of the tunnel losses was shown in reference 3 to occur in the slot-flow re-entry section at the downstream end of the test section. In this region, the slots must be terminated and the slot flow guided into the diffuser. Several configurations were designed to accomplish these results. The basic boattail configuration is shown in

figures 1 and 3 and in greater detail in figure 4(a). In this configuration, the slotted-wall plates and beams taper for $8\frac{3}{4}$ inches to a point at the diffuser entrance and straight flaps move between the wall beams, as shown in figure 5(a), to control the slot flow. The flaps are hinged just ahead of the diffuser entrance and the leading edges extend forward to the point where the taper starts.

In the shroud configuration (shown in fig. 4(b)) the slots, instead of widening in the slot-flow re-entry section, were extended at a constant width so that the overall slot length was increased by $4\frac{1}{4}$ inches. The shroud itself was a 0.050-inch-thick plate which spanned the slotted wall through the last $4\frac{1}{2}$ inches of the slot-flow re-entry section. The leading edge of the shroud faired into the slotted-wall surface, but provisions were made for moving the shroud trailing edge outboard to incline the shroud relative to the tunnel center line as is shown in figure 5(a). This inclination was made possible by constructing the floor beams with two removable wedges. When the wedges were in place, the shroud was parallel to the tunnel center line; when one wedge was removed, the shroud trailing edge was moved outboard or closer to the wall so that the gap between the shroud and flap upper surface was decreased to three-fourths its original size; and when the second wedge was removed, the shroud was placed so that this gap was decreased to one-half its original size. This last position is the one shown in figure 5(a).

The no-boattail configuration, as shown in figure 4(c), differed from the basic boattail configuration in that the tapered or boattail wall plates were removed and the flaps were shortened 3/4 inch. (See fig. 5(a).)

The short-flap configuration, figure 4(d), was formed by shortening the flaps and boattails $5\frac{1}{4}$ inches; the slots were thereby lengthened by the same amount.

The flap hinge lines were located 0.60 inch outboard of the wall surface so that the top surface of the flap faired into the transition-section surface. Flap position δ_F was designated by the angle the main body of the flap made with the most closed flap position. This most closed flap position was determined by the position at which the flap nose touched the wall plates or the corner inserts, whichever occurred first, and was called $\delta_F = 0^\circ$. Positive values of δ_F are for greater flap openings. The long flaps are approximately parallel to the tunnel center line at $\delta_F = 3^\circ$ and the short flaps, at $\delta_F = 6^\circ$.

In the no-boattail configuration, several flap shapes were tested. These shape variations were produced by deflecting the forward portion or nose tab of the flap up or down. The tab-deflection angles δ_T and flap positions tested are shown in figure 5(b). For these flaps, δ_F defines the position of the main body of the flap and was determined from the straight-flap positions (fig. 5(a)).

Transition Section

Between the test section and diffuser is the transition section which is so called because its primary purpose was to afford a geometric transition from the square test section to the circular diffuser. The transition section was also designed to act as a mixing tube in which the slot-flow air might be re-energized as much as possible before entering the diffuser. The first transition section was designed to maintain a constant area throughout its length. This involved the use of elements of compound curvature and was a relatively complex job. In some preliminary tests, static-pressure distributions indicated an area reduction in the last few inches of this transition section. In order to eliminate this condition, the downstream end was bored out slightly (the area was increased about 2.5 percent). The 4°, 20° diffuser, which had been constructed to match the transition-section exit, was then similarly altered to fit the new transition-section exit diameter. This transition section was used with all the short diffusers. A second transition section with an equivalent conical angle of approximately 1.4° or an area increase of 5.6 percent was used with the 6.4° diffuser. This transition section was designed with straight-line elements so that the area variation was not a linear function of distance from the inlet.

Diffusers

With reasonably good boundary layers at subsonic velocities, the optimum diffuser angle is considered to be about 6°; at angles greater than 12° separated flow can be expected. But for the thick, low-momentum, boundary-layer flow at near-sonic mean velocities that exists at the diffuser entrance of a slotted tunnel, separation can be expected at much lower diffuser angles. Therefore, the necessity of using a diffuser with an equivalent conical angle of about 10°, as dictated by the available length and existing geometry of this tunnel, suggested that separation would be the critical factor in the diffuser performance and that the geometry should be chosen to delay separation as long as possible. In order to test this line of reasoning, three equal-length diffusers were designed (shown in fig. 6) each with equivalent angles of 10° but having initial expansion angles of 4°, 6°, and 8°. In each diffuser, the initial conical section joined a 20° conical section to reach the exit

area. A straight 10° diffuser was also designed and, later, a straight 6.4° diffuser as shown. The area ratio of all the diffusers was 2.4.

INSTRUMENTATION

Static-Pressure Measurements

Static-pressure orifices were installed in a line extending through the entrance cone, test section (except where prevented by the windows), transition section, and diffuser. These orifices were connected to multitube manometer boards, and pressures were recorded photographically. The reference total pressure was measured in the settling chamber upstream of the entrance cone and reference total temperature was measured in the supply ducting upstream of the settling chamber.

Static-pressure distributions along the center line of the test section were measured with the survey tube shown in figure 1. This tube was driven fore and aft by a friction drive system mounted outside the elbow downstream of the diffuser and its position was transmitted by a synchro generator wheel driven directly by the tube. The first distributions were obtained from U-tube manometer readings at each survey tube position. Later, this laborious process was greatly improved by using a pressure cell on the survey tube which, with the position synchro, fed into a two-variable recorder. Thus it became possible to obtain a continuous plot of pressure against distance as the tube traversed the tunnel. The estimated accuracy of the static-pressure measurements with the U-tube manometer is about ±0.01 lb/sq in. and with the pressure cells about ±0.03 lb/sq in. In the range of total pressures used in these tests, these figures result in estimates for Mach number accuracy of ±0.001 for the U-tube measurements and ±0.003 for the pressure-cell measurements. Two total-pressure rakes were used - one for the diffuser exit station and one for the diffuser inlet station. The exit rake is shown installed in figure 1. These rakes spanned the tunnel and could be rotated to provide complete coverage of the cross section; data were taken along eight equally spaced diameters. All rake pressures were photographically recorded from multitube manometers. The forward support strut which was used to steady the survey tube and inlet rake was removable and all rake surveys were made with the tunnel clear upstream of the rake.

Total-Pressure Measurements

The mean value of total pressure at each rake position was determined by a numerical integration performed on International Business Machines. Each tube was given a weighting factor (A_L/A_{total}) in

proportion to the area it represented. Then the mass-weighted value was obtained from the following equation:

$$\frac{\Delta H}{H_o} = \frac{\sum \left(1 - \frac{H_L}{H_o}\right)\left(\frac{\rho U}{\rho_o a_o}\right)_L \frac{H_L}{H_o} \frac{A_L}{A_{total}}}{\sum \left(\frac{\rho U}{\rho_o a_o}\right)_L \frac{H_L}{H_o} \frac{A_L}{A_{total}}}$$

where the subscript L denotes values measured locally, that is, at each tube, and the subscript o denotes the reference condition for which pressure and temperature are known. The mean value of $\frac{\Delta H}{H_o}$ for any Mach number was then obtained by averaging the values from the eight rake positions.

Measurements of Rapid Flow Changes With Bleed

In order to determine the rate of change of the test-section Mach number with test-section bleed, the survey tube was replaced by a similar tube which simultaneously measured total pressure, static pressure, and differential pressures for pitch and yaw. This tube, shown in figure 7, occupied the position that a model would ordinarily have in the test section. The tube was constructed with pressure cells inside the tube as close as possible to the measuring orifices in order to minimize the time lag in the readings. These pressure cells were connected to a recording magnetic oscillograph which plotted the pressures against time. Pressures across the orifice plates in the bleed lines were recorded on the same plot. The electrical impulse which initiated the bleed-valve opening also produced a signal on the oscillograph record.

RESULTS AND DISCUSSION

SLOTTED-TEST-SECTION INVESTIGATION

Mach number distributions along the center line of the test section are presented in figures 8 to 12. A plan view of the corresponding slot configuration and boattail shape is shown on each of the figures to facilitate orientation of the distribution with respect to the slots.

Effect of Flap Setting

The effect of flap setting δ_F on the Mach number distributions can be seen in figures 8(a) to 8(c) where distributions at $\delta_F = 0^\circ$, 5°, and 10° are plotted for the 1/14-open L/h = 1.0 walls and in figures 10(a) to 10(c) where distributions at $\delta_F = 0^\circ$, 5°, and 10° are plotted for the 1/7-open L/h = 0.5 walls. There is little or no effect of δ_F on the initial rate of expansion in either case. Flap setting, however, did affect the test-section flow in the region of the flaps. At $\delta_F = 0^\circ$ (closed position), the flaps were at a diverging angle with respect to the flow, and at Mach numbers greater than 1.0 this condition produced an acceleration of the test-section flow over the flaps (figs. 8(a) and 10(a)). The magnitude of this acceleration decreased as δ_F increased and at $\delta_F = 10^\circ$ the flow decelerated over the flaps. Subsonically, at $\delta_F = 0^\circ$, the flow accelerated in the region at the nose of the flaps and then decelerated slowly over the length of the flaps (figs. 8(a) and 10(a)). This acceleration of the flow at subsonic speeds was eliminated entirely at $\delta_F = 10^\circ$ (fig. 8(c)) and reduced to a small amount at $\delta_F = 5^\circ$ (fig. 8(b)). At sonic speeds and above, flap setting had a small effect on the flow through the test region, better distributions being obtained at $\delta_F = 10^\circ$ than at $\delta_F = 0^\circ$.

Effect of Open-to-Closed-Area Ratio

The effect of open-to-closed-area ratio can be seen by comparing the 1/14-open L/h = 1.0 walls of figure 8 with the 1/7-open L/h = 1.0 walls of figure 9. At subsonic speeds the open-to-closed-area ratio had no noticeable effect on the Mach number distributions. At supersonic speeds, increasing the open-to-closed-area ratio increased the rate of initial expansion. This effect is most clearly seen by comparing the high Mach number curves of figures 8 and 9. For pressures indicating $M_c = 1.32$, a slot length of $9\frac{1}{2}$ inches is required to generate a Mach number of 1.2 for the 1/14-open walls (fig. 8(b)) whereas a length of only $7\frac{1}{2}$ inches is required for the 1/7-open walls (fig. 9) for pressures indicating $M_c = 1.24$. The velocity gradient over the entire length of the 1/14-open slots at $M_c = 1.32$ plus the fact that the local Mach number never reached 1.32 indicate that these slots were choked.

Both the 1/7- and 1/14-open walls generated satisfactory distributions for Mach numbers up to approximately 1.15, the 1/14-open walls producing a better distribution at $M_c = 1.15$ than the 1/7-open walls.

Effect of Slot Taper Length

Mach number distributions for the 1/7-open walls with a nondimensional slot taper length $L/h = 1/2$ are shown in figure 10. Comparison with the distributions for $L/h = 1.0$ (fig. 9) shows that the reduction in slot taper length (or increase in rate of slot opening) increased the rate of initial expansion of the flow by about one-third. This is in general agreement with the findings of reference 5 that pressure distributions can be obtained to first-order approximation by the longitudinal distribution of slot area.

This increased rate of initial expansion, however, caused a small amount of overexpansion of the flow to local Mach numbers greater than those indicated by the chamber static pressure. This overexpansion in turn produced flow disturbances downstream in the test region; thereby, poorer Mach number distributions than those obtained with the longer slot taper resulted.

Effect of Variable Slot Depth Along the Slot Taper

It was shown in references 5 and 6 that a linear decrease in slot depth along the tapered portion of a 1/8-open slot configuration ($w_s = 0.141$ inch, $d_s = 0.063$ inch) from 1/2 inch at the slot origin to 1/16 inch at the end of the slot taper produced good distributions for a Mach number range up to 1.4. The addition of this variable depth along the slot taper in references 5 and 6 decreased the amount of overexpansion of the flow during its initial expansion without affecting the rate of initial expansion materially. For this investigation, depth varying linearly from 1.5 inches at the slot origin to 0.050 inch at the end of the taper was added to the slot configuration of figure 10 (1/7 open, $L/h = 0.5$, $w_s = 0.341$ inch, $d_s = 0.050$ inch) in an attempt to reduce the initial overexpansion of the flow and still retain approximately the same rate of expansion. The Mach number distributions resulting from this modification are shown in figure 11 for $\delta_F = 10^\circ$. Comparison of figures 10(c) and 11 shows that the addition of variable depth along the slot taper increased the rate of initial expansion somewhat but did not reduce or eliminate the initial overexpansion of the flow. No significant changes in the distributions occurred for this investigation as occurred for those of references 5 and 6. The distribution for $M_c = 1.06$ in figure 11 is somewhat better than that for $M_c = 1.07$ in figure 10(c) but the distribution for $M_c = 1.28$ in figure 11 is not so uniform as that for $M_c = 1.26$ in figure 10(c). A strict comparison between the configuration for this investigation and the configurations of references 5 and 6 cannot be made since the rate at which the slot depth along the slot taper decreased for the former

was approximately 2.6 times greater than that for the latter. Furthermore, the original slot configuration of references 5 and 6 had a slot-depth-to-slot-width ratio 24.2 times greater than the original configuration of this investigation.

Effect of Slot and Flap Length

Lengthening the slots and shortening the flaps $5\frac{1}{4}$ inches as shown in figure 4(d) was intended to provide more test-section length for damping of disturbances originating in the flow generation. Mach number distributions for this configuration at $\delta_F = 10^\circ$ are shown in figure 12. These particular distributions were obtained by using the two-variable, continuous-recording potentiometer, one variable being the local static pressure as measured by the probe and the other being the axial position of the probe.

L 1 0 0 5

Figure 12 shows that the effective length of the slot was only increased about 2 inches at the higher Mach numbers with no noticeable improvement of the flow through the test region when compared with the shorter slots of figure 10. The shorter flaps appear to have had an adverse effect at subsonic speeds since the distribution for $M_c = 0.92$ in figure 12 is not so good as that obtained previously with other slot configurations.

Summary of Slotted-Test-Section Findings

The data indicate that a test region one tunnel height in length in which the local Mach number variation from the mean is less than ± 0.01 can be obtained for values of M_c up to 1.15 by using 1/14-open walls with taper length $L/h = 1.0$. Acceptable flow can be obtained up to $M_c = 1.26$ over a region about 0.84h in length by increasing the open area to 1/7 or slightly less and shortening the slot taper to about $L/h = 1/2$ to obtain the necessary expansion rate.

TOTAL-PRESSURE LOSSES AND STATIC-PRESSURE RECOVERY

A comparison between the 1/7-open and 1/14-open wall configurations on the basis of total pressure required for tunnel operation is shown in figure 13 where $\frac{H_o - atm}{H_o}$ is plotted against M_c. The atmospheric-pressure reference is justified because the butterfly valve in the exhaust line was open for both configurations. In both configurations,

the choice of flap position δ_F makes little difference at $M_c = 0.7$, but, as M_c increases, increasingly more total pressure is required for $\delta_F = 0^\circ$ than for $\delta_F = 5^\circ$ or 10°. At $\delta_F = 0^\circ$, less pressure is required for the 1/14-open walls than for the 1/7-open walls at M_c values greater than 1.0, but for $\delta_F = 5^\circ$ and 10° there is no significant difference between the 1/14-open and 1/7-open walls at M_c values less than 1.20. The data for the 1/14-open walls at higher values of M_c cannot be used because the slots choked and the higher Mach numbers were not obtained except in small regions near the end of the slots (fig. 8(b)). This is shown in figure 14 where the Mach number at $x = 13.5$ inches (a point about in the center of the test region) is plotted against M_c. For the 1/7-open walls, M_c is a good indication of the test-section Mach number at values up to 1.28, but, for the 1/14-open walls, M_c indicates the test-section Mach number only up to about $M_c = 1.20$. Therefore, in investigating the pressure losses through the tunnel system, the 1/7-open wall configuration was used because the range of Mach number in which the data are significant can be extended to about $M_c = 1.30$ and, for the case of minimum-power operation ($\delta_F = 5^\circ$ or 10°), there is little or no difference between the 1/14- and 1/7-open walls.

Total-Pressure Measurements

In order to check the accuracy of the method of measuring and reducing the total-pressure-loss data, mass-flow values computed from the rake total-pressure measurements were compared with values computed from a wall static pressure in the tunnel throat (upstream of the slots) and the reference stagnation pressure by assuming zero boundary-layer thickness. Since this throat station is at the end of a continuously contracting channel, it is believed that the values of mass flow obtained are accurate to ±1 percent. When the throat mass-flow values were compared with rake values measured at the diffuser inlet, the discrepancies were negligible. A similar comparison with the rake values measured at the diffuser exit, however, revealed that the rake values were higher than the true values. This is shown in figure 15 where the ratio of the difference between measured and true mass flow Δm to the true mass flow m is plotted against M_c for each diffuser configuration at $\delta_F = 5^\circ$. For the 6.4° diffuser, values of $\frac{\Delta m}{m}$ vary from about 0.10 to 0.15 as M_c increases. Values for the short diffusers range from about 0.15 to 0.35. In the short diffusers, at low values of M_c, $\frac{\Delta m}{m}$ decreases slightly with increasing initial diffuser angle;

at $M_c = 1.0$, values of $\frac{\Delta m}{m}$ are about the same for all initial diffuser angles; and at $M_c > 1.0$, the trend has reversed and $\frac{\Delta m}{m}$ increases sharply with increasing initial diffuser angle. Similar discrepancies are pointed out in references 7 and 8 and are attributed to the presence of turbulent-flow fluctuations. A theoretical discussion of the way in which turbulence can cause such errors in pitot-static-tube readings is given in reference 9.

Inasmuch as the exit mass-flow values are in error, the mean total-pressure values must also be in error and the only index to the degree of error is the mass-flow discrepancy $\frac{\Delta m}{m}$. By assuming a one-dimensional incompressible flow and also that the static-pressure error is negligible, an expression can be derived which relates the total-pressure error to the mass-flow discrepancy. This expression is

$$\left(\frac{\Delta H}{H_i - p_i}\right)_{True} = \left(\frac{\Delta H}{H_i - p_i}\right)_{Measured} + \left(\frac{H_e - p_e}{H_i - p_i}\right)_{Measured}\left[1 - \left(\frac{1}{1 + \frac{\Delta m}{m}}\right)^2\right]$$

or

$$\left(\frac{\Delta H}{H_o}\right)_{True} = \left(\frac{\Delta H}{H_o}\right)_{Measured} + \frac{\left(H_e - p_e\right)_{Measured}}{H_o}\left[1 - \left(\frac{1}{1 + \frac{\Delta m}{m}}\right)^2\right]$$

Although this correction is not exact, it has proven useful in obtaining correlations of diffuser data that otherwise appeared to have no correlation. In this report, it was used wherever comparisons between different diffuser configurations were desired, but in every case the uncorrected data are also presented.

Overall Tunnel Performance

In order to evaluate the different configurations from the standpoint of overall tunnel performance, total-pressure loss and static-pressure recovery between the entrance bell and the end of the diffuser are presented as a function of the test-section Mach number M_c. The total-pressure loss is plotted as the ratio $\frac{\Delta H_T}{H_o}$ against M_c in figures 16(a) to 16(e) for the five diffusers used. In each figure, different curves are presented for each of the diffuser flap positions tested. The general effects of δ_F and M_c on $\frac{\Delta H_T}{H_o}$ are the same for all the

diffuser configurations. Increasing M_c always increases $\frac{\Delta H_T}{H_o}$. At Mach numbers up to about 1.0 the effect is gradual but, as M_c approaches the value at which the minimum downstream area is such that the combined slot and mainstream flow cannot pass without choking, the rate of increase of $\frac{\Delta H_T}{H_o}$ increases. When choking does occur, further increases in tunnel power merely increase $\frac{\Delta H_T}{H_o}$ without increasing M_c. The effects of varying δ_F at low Mach numbers are small, but, at Mach numbers greater than 1.0, the position of the flap becomes one of the factors which determine the choking Mach number. As can be seen in figure 5, the flaps are almost parallel to the tunnel center line at $\delta_F = 5^\circ$. At values of δ_F from 0° up to about 5°, the leading edge of the flaps determines the area through which mainstream and slot flow must pass by producing a throat which chokes the tunnel at low supersonic values of M_c. When the flaps are opened further, this flow constriction is relieved until M_c is increased (and therefore the slot flow is increased) sufficiently to form another throat at a higher value of M_c. When δ_F is large enough so that choking does not occur on the flaps, the limiting Mach number for the tunnel is fixed by the area of the transition section and the quantity of slot-flow air induced into that section. But if δ_F is too large, the limiting value of M_c is again reduced. An example of this effect can be seen in figure 16(a) where opening the flaps beyond 5° progressively lowers the limiting Mach number. This phenomenom was also observed in reference 10, and it is believed that it occurs when the leading edge of the flap is far enough into the slot-flow plenum chambers to intercept some of the secondary circulating flow, which, in burbling over the leading edge of the flap, effectively thickens it and produces another throat smaller than that produced by the transition section. The maximum M_c obtained in this tunnel was about 1.28. Higher values could be obtained by moving the flap hinges outboard and increasing the transition-section inlet area correspondingly.

Envelope curves of $\frac{\Delta H_T}{H_o}$ against M_c were obtained from figure 16 for each of the various diffuser configurations and are plotted in figure 17. In addition, envelope curves for the pressure-loss ratio measured at the diffuser inlet are also shown. It can be seen that the diffuser losses are a substantial part of the overall tunnel loss but only at the higher values of M_c do they equal or exceed the losses through the rest of the tunnel. The values as measured, without the $\frac{\Delta m}{m}$

correction previously discussed, show the 6.4° diffuser to be no better than the short diffusers; in fact, it appears to be inferior to the 6°,20° diffuser at all Mach numbers and also to the 4°,20° diffuser at high Mach numbers. This conclusion is inconsistent with other available experimental results. The corrected values of $\frac{\Delta H_T}{H_o}$, however, indicate that the long 6.4° diffuser is superior to the short diffusers at all Mach numbers. Therefore, it is felt that the corrected curves give a more accurate picture of the results. At low Mach numbers, there is little to choose from among the short diffusers, but, at higher Mach numbers, the short diffuser curves, with the exception of the 4°,20° diffuser, fan out to show a consistent increase in $\frac{\Delta H_T}{H_o}$ with increasing initial diffuser angle. Values for the 4°,20° diffuser are slightly higher than those for the 6°,20° diffuser at all except the highest Mach numbers where the 4°,20° diffuser values are a little lower than the 6°,20° diffuser values. These curves show that, at $M_c = 1.15$, the use of a 6°,20° diffuser permits operation with a total-pressure loss equal to 84 percent of that for a 10° diffuser, and, at $M_c = 1.25$, operation with a total-pressure loss equal to 72 percent of the 10° diffuser value. These curves also show that use of the 4°,20° or 6°,20° diffuser permits operation at $M_c = 1.21$ for the same value of $\frac{\Delta H_T}{H_o}$ obtained with the 10° diffuser at $M_c = 1.15$.

Wall Static-Pressure Distributions

Wall static-pressure distributions through the tunnel are presented for the 4°,20°, 6°,20°, 8°,20°, 10°, and 6.4° diffusers in figures 18 to 22, respectively. Area distributions are also plotted through the transition section and diffuser in each figure. Data are presented for $\delta_F = 5°$ only, because in nearly every case this value gave lowest values of $\frac{\Delta H_T}{H_o}$ and thus appears to be the optimum operating condition. Since there were no wall static-pressure orifices in the test section, the curves are connected by dotted lines through this region and do not represent true pressure distributions.

In the short-diffuser transition section (figs. 18 to 21), the pressure is rising at $x = 48$, the beginning of the transition section, and continues to rise for several inches even though the flow is passing through a constant-area channel. This effect undoubtedly results from the diffusive mixing of the mainstream and slot flow in this region.

The fact that the pressure levels off at about $x = 56.0$ probably indicates that the optimum mixing tube length has been reached. The constant-area portion of the $4^\circ,20^\circ$ diffuser configuration extends down to about $x = 61.0$ because the inlet of this diffuser was rebored as described in the section entitled "APPARATUS AND METHODS." In the other short diffuser configurations, the diffuser starts at $x = 58.8$.

In the $4^\circ,20^\circ$ diffuser (fig. 18), the static pressure rises steadily through the 4° part and at about $x = 79$ begins a more rapid rise as the flow enters the 20° part of the diffuser. At about $x = 82$, however, the pressure starts to level off; this leveling off of the curve indicates that the flow has separated and is no longer expanding with the diffuser geometry. In the $6^\circ,20^\circ$ diffuser (fig. 19) at $M_c \leq 1.05$, the pressure rises steadily through the 6° part but gives no indication of ever starting the 20° expansion. Separation probably occurs at or just upstream of the $6^\circ,20^\circ$ juncture. At $M_c = 1.24$, the abrupt changes in slope of the curves at $x = 70$ indicate that separation probably occurs near that point. In the $8^\circ,20^\circ$ and 10° diffusers (figs. 20 and 21), it is more difficult to determine exactly the position where separation begins to break down the pressure rise but the curves indicate it to be at about $x = 65$ in both.

The static-pressure distribution in the 6.4° diffuser transition section, which has an equivalent conical angle of about 1.4° (fig. 22), is considerably different from that in the short-diffuser transition sections. The mixture of slot and mainstream flow issuing from the test section appears to be very sensitive to changes in area as evidenced by the rapid rise in static pressure at the transition-section inlet and the leveling off in pressure which follows as the rate of area change decreases. Comparison with the distributions of figures 18 to 21 shows that a slight gain in pressure rise results from use of this transition section. These results emphasize the need for more knowledge of ejectors and mixing tubes. The pressure distributions in the diffuser show no indication of severe separation except that at $M_c = 1.27$ the possibility of separation is suggested by the abrupt change in slope of the curve downstream of $x = 75$.

In figure 23, the ratio p_e/H_o is plotted against M_c to show the relative value of the various diffuser configurations in converting the dynamic pressure of the stream back to static pressure. Also shown is the ideal curve of p_e/H_o - that value that would be obtained if there were no boundary layer and the flow were isentropic. None of the short-diffuser configurations can match the pressure recovery of the long 6.4° diffuser configuration. The $6^\circ,20^\circ$ diffuser configuration has the highest pressure recovery of the short diffusers except at $M_c = 0.7$ where the larger angle diffusers are as good or slightly better. These results for the short diffusers follow the performance

trends indicated by the total-pressure-loss parameters in that the larger initial angle diffusers perform best at low Mach numbers and the smaller initial angle diffusers perform best at high Mach numbers.

Effect of Some Tunnel Modifications

Shroud configuration.- Although three shroud positions (parallel to the center line, trailing edge moved one-fourth the distance to the wall, and the trailing edge moved one-half the distance to the wall (fig. 5(a))) were designed, total-pressure-loss data were taken only for the last position. This position was chosen as the most significant in the following way. Velocity profiles were measured behind the slotted and solid walls at the transition-section exit for all three shroud positions and for the unshrouded or boattail configuration. Little change in profile shape from that with the boattails was observed with the undeflected shroud. A slight improvement in shape, indicative of better mixing action, was observed for the first deflection and still more improvement for the larger deflection. It was assumed that the greatest shroud effect would be felt for this last case; therefore, total-pressure-loss data were taken for that case only and are shown in figure 24 where $\frac{\Delta H_T}{H_o}$ is plotted against M_c. Also shown is the envelope curve from the $4^\circ,20^\circ$ diffuser configuration with boattails. Only at low Mach numbers is the shroud configuration as good as the boattail configuration. At Mach numbers near 1.0, the pressure losses produced by the shroud exceed any possible gains from diffuser performance, and, at supersonic Mach numbers, it is obvious that the shroud choked the tunnel at all flap angles. It seems likely that, with the leading edge of the shroud downstream of the flap leading edge, the slot-flow air spilled over to the top side of the shroud to choke the tunnel under all conditions. For $\delta_F = 5^\circ$, at $M_c = 1.14$, the shroud configuration, despite the poor performance at lower Mach numbers, performs almost as well as the boattail configuration. Perhaps if the choke condition were relieved by moving the shroud inboard and/or upstream, some advantage in performance might be gained.

Performance with lengthened slots and shortened flap section.- It has already been shown that the effective test section is lengthened about 2 inches by lengthening the wall plates and shortening the flap section (figs. 4(d) and 5(a)), but, in order to evaluate this modification fully, the effects on the total-pressure-loss parameter must be considered. These effects are shown in figure 25 where $\frac{\Delta H_T}{H_o}$ is plotted against M_c for the short-flap configuration and compared with the

envelope curve of $\frac{\Delta H_T}{H_o}$ for the long-flap configuration. (These data were taken in the long 6.4° diffuser.) For the short flaps, the curves of $\frac{\Delta H_T}{H_o}$ against M_c behaved in about the same manner as those for the long flaps as δ_F varied, except that the choking Mach number increases continuously as the flaps open and gives no indication of a reversal of this trend - probably because these flaps are too short to reach into the secondary flow. Values of $\frac{\Delta H_T}{H_o}$ were about 10 percent higher for the short flaps than for the long flaps at all Mach numbers.

Flap section with boattailed wall plates removed.- The no-boattail data were taken with the 1/14-open-area walls and flaps 3/4 inch shorter than the original long flaps (figs. 4(c) and 5(a)). Values of $\frac{\Delta H_T}{H_o}$ for this configuration are plotted against M_c in figure 26. These curves behave with varying M_c and δ_F in the same manner as did those for the standard flap configuration.

It was shown in figure 13 that, for $\delta_F = 5°$ and $10°$, the total pressure required for tunnel operation was the same for both 1/14-open and 1/7-open slotted walls. If the effect of the slight shortening of the flaps is considered negligible, the results of figure 26 can then be compared with those of figure 16. This comparison is made in figure 27 for $\delta_F = 10°$. Although the difference in these curves is not great, it can be seen that some improvement in performance was obtained at the lower values of M_c by removing the boattails.

Effects of flap shape with no-boattail configurations.- The bent-flap (fig. 5(b)) tests were made in the 6.4° diffuser configuration with 1/14-open walls and the boattails removed (fig. 4(c)). The results are presented in figure 28 where envelope curves of $\frac{\Delta H_T}{H_o}$ against M_c (from curves of different δ_F values shown in fig. 5(b)) are plotted for tab angles δ_T of -15°, -10°, 5°, and 10°. Also shown is the curve for $\delta_T = 0°$ or the straight flap. (This is the envelope curve from fig. 26.) The only effect of bending the flaps was a variation of the maximum Mach number which was produced by choking on the tab leading edge at positive tab angles and choking from secondary-flow effects at negative tab angles. The straight flaps had the highest choking Mach number.

Summary of flap-section results.- The general results of the various modifications to the flap section can be briefly summarized as follows. The best configuration tested from the standpoint of total-pressure losses was the no-boattail configuration with straight flaps which was as good as the boattail configuration at all values of M_c and slightly better at the lower values. Deflecting the nose tab of the flaps only reduced the maximum Mach number. Lengthening the slots by shortening the boattails and flaps increased the pressure loss. Closing over the slot-flow re-entry section with the shroud increased the pressure losses and considerably reduced the maximum Mach number.

Diffuser Performance

The nature of the diffuser problem can best be understood through an examination of the flow entering the diffuser. Under ordinary conditions with reasonably good entering flows, good performance characteristics could be expected of a 10° diffuser. Reference 11 has pointed out, however, that for 12° and 23° diffusers, inlet boundary-layer thickness and shape factor affect the total-pressure losses and static-pressure recovery considerably.

In figure 29, inlet velocity contours, or lines of constant velocity at the inlet cross section, are plotted for the 6.4° diffuser with $\delta_F = 5°$. The parameter u/U is the ratio of local velocity to center-line velocity; thus, the edge of the boundary layer lies at $u/U = 1.0$. Since the fully developed turbulent pipe flow has often been used as an inlet condition in diffuser investigations, contour lines representing such a flow are also shown on these figures by the broken lines. It can be seen that the boundary layer downstream of the slotted wall is about twice as thick as that downstream of the solid wall. Also downstream of the slotted wall, velocities near the wall are not as great as they would be for a pipe flow even though the pipe-flow boundary layer is much thicker. This type of flow in which the momentum near the wall is disproportionately low separates from the wall very easily under the influence of an adverse pressure gradient. Therefore, it must be expected that separation will be a real source of trouble even for small-angle diffusers that would ordinarily be expected to have good performance characteristics.

Loss coefficients $\frac{\Delta H}{H_i - p_i}$ for the various diffusers are plotted in figure 30 against mean inlet Mach number. The corrected values will be used for analysis since it is believed that those curves more nearly represent the true picture than do the uncorrected curves. For the short diffusers on the tunnel, the diffuser contour has little effect on $\frac{\Delta H}{H_i - p_i}$ at $M_i = 0.5$. This result is in agreement with reference 12

which indicates that the area ratio and equivalent conical angle are the governing variables for incompressible flow. The effects at higher Mach numbers, however, show very clearly the large increases in $\frac{\Delta H}{H_i - p_i}$ that result when the flow separates first in the 10° diffuser, at a slightly higher Mach number in the 8°,20° diffuser, and near the top Mach number in the 6°,20° diffuser. The 4°,20° diffuser losses increase gradually with increasing Mach number in a manner similar to those in the long 6.4° diffuser and at the highest Mach number are only about 10 percent greater than the 6.4° diffuser losses as contrasted with the 10° diffuser which has losses about 100 percent greater than the 6.4° diffuser. Also shown in figure 30 are corrected values of $\frac{\Delta H}{H_i - p_i}$ for the 6.4° and 10° diffusers alone. In order to obtain these data, the diffusers were removed from the tunnel and flow was induced through an inlet bell directly to the diffusers. These curves give an indication of the losses that might be expected with a good inlet boundary-layer flow. Total-pressure losses through the diffusers under these conditions are approximately half as large as the losses when the diffusers are used behind the slotted test section.

In figure 31, static-pressure-rise coefficients $\frac{\Delta p}{H_i - p_i}$ are plotted against mean inlet Mach number for the five diffusers on the tunnel and for the 6.4° and 10° diffusers with inlet bells only. It can be seen that the pressure recovery of the 6.4° and 10° diffusers on the tunnel was from 15 to 30 percent lower than for the diffusers with inlet bells. Also, the pressure recovery for the short diffusers varied from 10 percent to 20 percent lower than that for the 6.4° diffuser. The curves for the short diffusers form an interesting envelope in which the 10° diffuser has the highest static-pressure recovery at $M_i = 0.5$ followed by the 8°,20°, 6°,20°, and 4°,20° diffusers, each of which momentarily has the highest value of $\frac{\Delta p}{H_i - p_i}$ at a successively higher Mach number.

Reference back to the static-pressure distributions of figure 22 and the results of figures 30 and 31 yields some general conclusions about the diffusers. No separated flow was observed in the long 6.4° diffuser but, since separation was very extensive in the 8°,20° diffuser at $M_i > 0.7$, it is unlikely that diffuser angles greater than about 6° can be satisfactorily used when the inlet-flow conditions are similar to those for this configuration. The performance results indicate that, when length restrictions preclude the use of a diffusion

angle of 6°, it is better to keep a small initial angle in a trumpet-shaped diffuser and thereby delay separation as long as possible. The optimum initial angle decreases with increasing Mach number. The big differences in diffuser-performance characteristics with good and bad inlet boundary layers emphasize the need for more research along this line.

THE EFFECTS OF BLEEDING AIR INTO THE TEST SECTION TO OBTAIN RAPID MACH NUMBER CHANGES

A sample of the results obtained when air was bled from the settling chamber to the test-section plenum chamber can be seen in the pressure-time records of figure 32. In these tests, a certain initial value of M_c was set by varying the tunnel total pressure with the bleed-line butterfly valve closed. The butterfly valve was then opened and the flow permitted to reach equilibrium. A solenoid which controlled pressure to the air cylinder which actuated the butterfly valve also produced a signal on the pressure records. Another signal was produced when the solenoid was de-energized and the butterfly valve closed. The flow then returned to its initial equilibrium condition. Data were taken at several initial Mach numbers with four sets of orifices in the bleed line to simulate four different bleed-line sizes. The ratios of total orifice area A_o to tunnel throat area were 0.014, 0.026, 0.103, and 0.231.

The records of figure 32 are for $A_o/A^* = 0.103$. Since H_o did not vary during the tests (fig. 32), the curves of p_c give a good indication of the Mach number variation. The values of Δp across the orifices permit determination of the bleed mass flow. The yaw and pitch curves show no significant variations. The p_c variation when the valve closes is almost exactly opposite the variation when the valve opens; this condition was also the case for the other orifice area ratios.

For application to the investigation of flutter, the lower Mach number limit could be approached by raising tunnel pressure with the bleed valve closed. When the model began to flutter, opening the valve would reduce the Mach number very rapidly. The upper Mach number limit could be approached from above by opening the bleed valve while holding the tunnel pressure constant. When flutter started, closing the valve would increase the Mach number rapidly.

The amount of reduction of Mach number that was obtained with a particular amount of bleed is shown in figure 33. There appears to be no consistent effect of Mach number. The points fall into four groups at different values of m'/m depending upon the bleed-orifice-area ratio.

The rate at which the Mach number changed is shown in figure 34. The points shown are transient points picked from the pressure records for all Mach numbers and bleed orifices. Most of the points shown are for $A_o/A^* = 0.103$ and 0.231 since the changes in Mach number at the lower area ratios were too small to obtain many points with any degree of accuracy. The grouping of these points about a single line indicates that the time required for a change in Mach number was independent of orifice area. This result suggests that the rate of opening of the butterfly valve might have been the controlling factor. The butterfly-valve action was recorded by a high-speed motion-picture camera and from that record the projected open area at any time was obtained. The ratio of that open area to the tunnel throat area is also plotted against time in figure 34. The bleed-orifice-area ratios are also indicated in that figure. It can be seen that, for $A_o/A^* = 0.103$, the projected open area of the butterfly valve was less than the orifice area until $t = 0.23$ second. By referring back to figure 32, it can be seen that, for all three initial Mach numbers, practically all the change in Mach number had occurred by the time $t = 0.23$ second. The same situation was found to apply for the other bleed-orifice records - the time required for most of the Mach number change to occur was the same as the time required for the butterfly valve to open an amount equal to the bleed-orifice area.

If the butterfly valve did form the controlling area, it should be possible to obtain additional points of $\frac{\Delta M}{M_c}$ and m'/m for the curve of figure 33. This has been done by using the faired curve of figure 34 to obtain a value of t for a certain $\frac{\Delta M}{M_c}$. That value of t was used to get the butterfly-valve restricting-area value from figure 34 also. Then, by assuming the Mach number at the restricting area to be the same as that at the tunnel throat,

$$\frac{m'}{m} = \frac{\text{Butterfly-valve projected open area}}{\text{Tunnel-throat area}}$$

The curve of m'/m against $\frac{\Delta M}{M_c}$ obtained in this manner is plotted in figure 35 and the faired curve of figure 33 is also presented for comparison. The excellent agreement of the two curves offers strong

evidence that the time required for a change in Mach number was fixed by the opening rate of the butterfly valve. Inasmuch as the rates of change measured were well within the limits desired, however, no further effort was made to determine the effects of orifice size on rate of change of Mach number. From figures 33 and 34, it can be seen that, with bleed flow only 2 percent of the mainstream flow, the Mach number was reduced 5 percent in less than 0.12 second and, with bleed flow equal to 11 percent of the mainstream flow, the Mach number was reduced 30 percent in about 0.24 second.

CONCLUSIONS

From the results observed in the development of an 8-inch by 8-inch slotted tunnel for Mach numbers up to 1.28 and Reynolds numbers to 5.5×10^6 per foot, the following conclusions are drawn:

1. With a slot length equal to two tunnel heights, a test region with length equal to one tunnel height was obtained with Mach number deviation from the mean of less than ± 0.01 up to a Mach number of 1.15 by using 1/14-open-area slotted walls. By reducing the test-region length to 0.84 tunnel heights and using 1/7-open-area walls, good distributions were obtained up to Mach number 1.26.

2. The effective-test-region length was increased by increasing the slot length and shortening the slot-flow re-entry section, but tunnel-pressure losses were also increased.

3. Tunnel-total-pressure losses were lowest for the slot-flow re-entry section in which the slotted wall plates were ended abruptly at the leading edge of the flaps. Losses increased slightly when the wall plates were tapered down in this region. Covering over the slots in this region with a shroud increased the losses further and considerably reduced the maximum Mach number.

4. The optimum flap position for the test-section Mach number distribution and the tunnel-pressure loss was that in which the flaps were approximately parallel to the tunnel center line.

5. Tunnel-total-pressure losses were considerably higher with a 10° conical diffuser than with a 6.4° conical diffuser of the same area ratio. In the 10° diffuser shell, the use of other diffuser contours consisting of a small-angle truncated cone from the diffuser inlet and a 20° truncated cone from the diffuser exit resulted in a decrease in total-pressure loss and an increase in static-pressure recovery. Initial-cone-angle configurations of 4°, 6°, and 8° were all better than the 10° diffuser. Optimum initial angle decreased with increasing tunnel Mach number.

6. Rapid changes in test-section Mach number were obtained by using a bleed or bypass flow from the tunnel settling chamber to the test section plenum chamber. By bleeding air into the test section, the Mach number was reduced about 5 percent in 1/8 second with bleed mass flow equal to 2 percent of the stream mass flow and about 30 percent in 1/4 second with 10-percent bleed flow. Similar increases in Mach number were obtained by diminishing the bleed flow. The rate of Mach number change was primarily dependent on the rate of opening or closing of the valve which controlled the flow.

Langley Aeronautical Laboratory,
National Advisory Committee for Aeronautics,
Langley Field, Va., January 28, 1955.

REFERENCES

1. Wright, Ray H., and Ward, Vernon G.: NACA Transonic Wind-Tunnel Test Sections. NACA Rep. 1231, 1955. (Supersedes NACA RM L8J06.)

2. Osborne, James I., and Zeck, Howard: Progress Report on Development of a Transonic Test Section for the Boeing Wind Tunnel (BWT 188). Vol. I - December 1950 to June 1951. Doc. No. D-11955, Boeing Airplane Co., Sept. 1951.

3. Whitcomb, Richard T., Carmel, Melvin M., and Morgan, Francis G., Jr.: An Investigation of the Stream-Tube Power Losses and an Improvement of the Diffuser-Entrance Nose in the Langley 8-Foot Transonic Tunnel. NACA RM L52E20, 1952.

4. Osborne, James I.: Distribution of Losses in Model Transonic Wind Tunnel at a Mach No. of 1.25. Doc. No. D-11934, Boeing Airplane Co., June 19, 1951.

5. Nelson, William J., and Cubbage, James M., Jr.: Effects of Slot Size and Geometry on the Flow in Rectangular Tunnels at Mach Numbers up to 1.4. NACA RM L53B16, 1953.

6. Nelson, William J., and Cubbage, James M., Jr.: Effects of Slot Location and Geometry on the Flow in a Square Tunnel at Transonic Mach Numbers. NACA RM L53J09, 1953.

7. Persh, Jerome, and Bailey, Bruce M.: Effect of Various Arrangements of Triangular Ledges on the Performance of a 23° Conical Diffuser at Subsonic Mach Numbers. NACA TN 3123, 1954.

8. Wood, Charles C., and Higginbotham, James D.: Effects of Diffuser and Center-Body Length on Performance of Annular Diffusers With Constant-Diameter Outer Walls and With Vortex-Generator Flow Controls. NACA RM L54G21, 1954.

9. Fluid Motion Panel of the Aeronautical Research Committee and Others: Modern Developments in Fluid Dynamics. Vols. I and II, S. Goldstein, ed., The Clarendon Press (Oxford), 1938.

10. Dennard, John S., and Little, Barney H., Jr.: Effects of Auxiliary and Ejector Pumping on the Mach Number Attainable in a $4\frac{1}{2}$- by $4\frac{1}{2}$-Inch Slotted Tunnel at Low Pressure Ratios. NACA RM L53K19, 1954.

11. Little, B. H., Jr., and Wilbur, Stafford W.: Performance and Boundary-Layer Data From 12° and 23° Conical Diffusers of Area Ratio 2.0 at Mach Numbers up to Choking and Reynolds Numbers up to 7.5×10^6. NACA Rep. 1201, 1954. (Supersedes NACA RM L9H10 by Copp and Klevatt, RM L9K10 by Persh, and RM L50C02a by Little and Wilbur.)

12. Henry, John R.: Design of Power-Plant Installations. Pressure-Loss Characteristics of Duct Components. NACA WRL-208, 1944. (Formerly NACA ARR L4F26.)

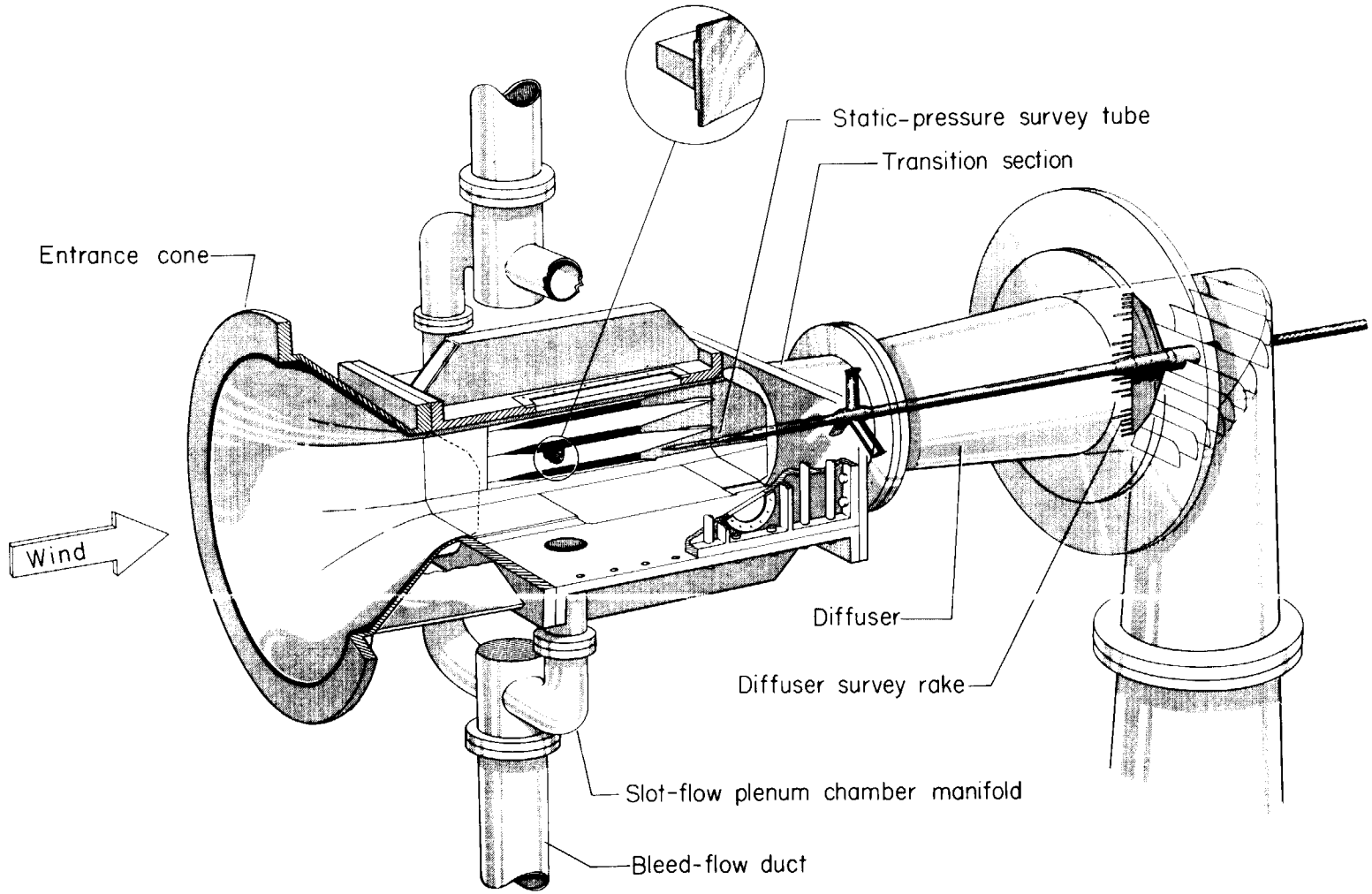

L-87573.1

Figure 1.- 8- by 8-inch slotted-tunnel configuration.

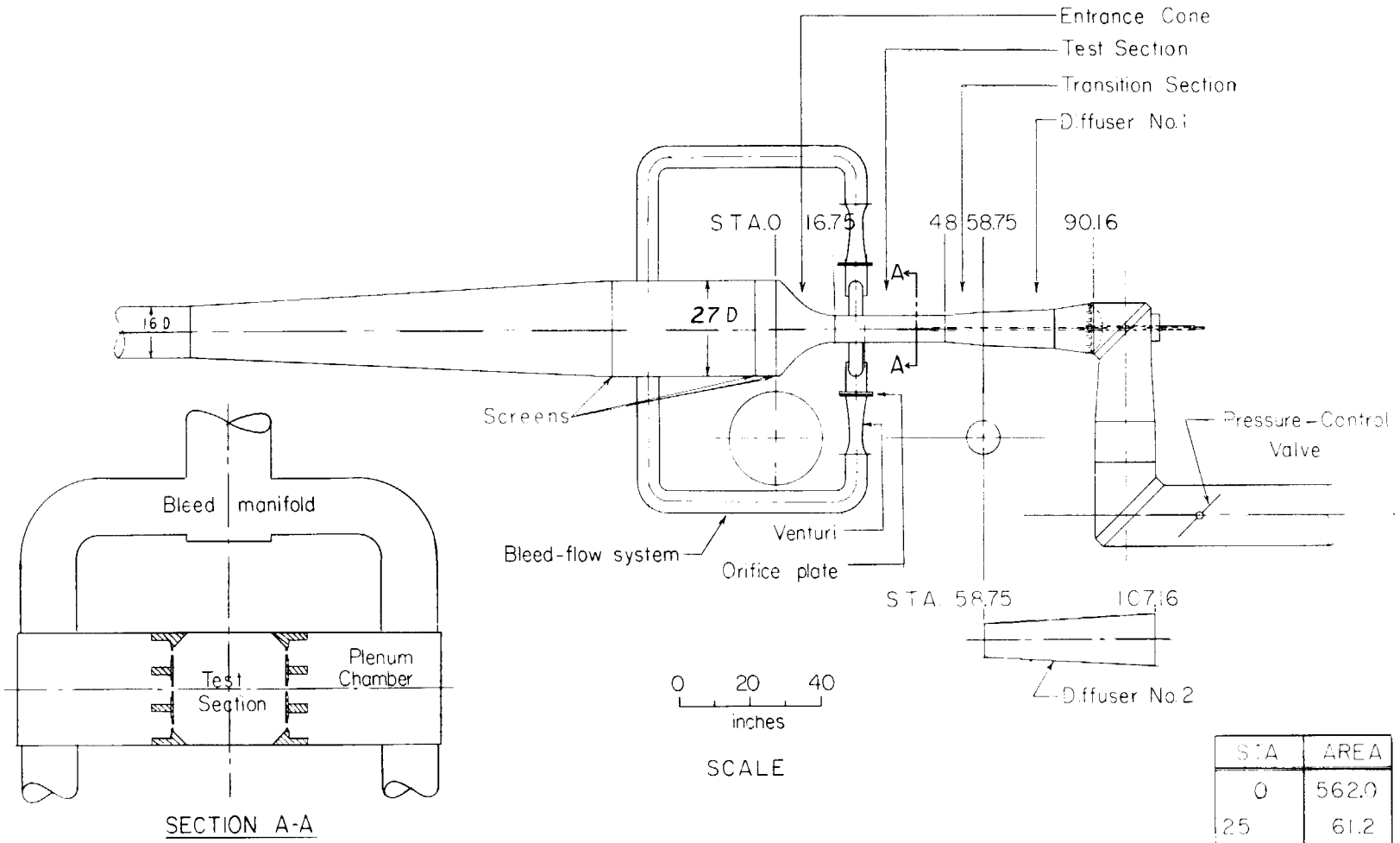

STA	AREA
0	562.0
25	61.2
58.75	73.0
90.16	173.7

Figure 2.- Line drawing of apparatus.

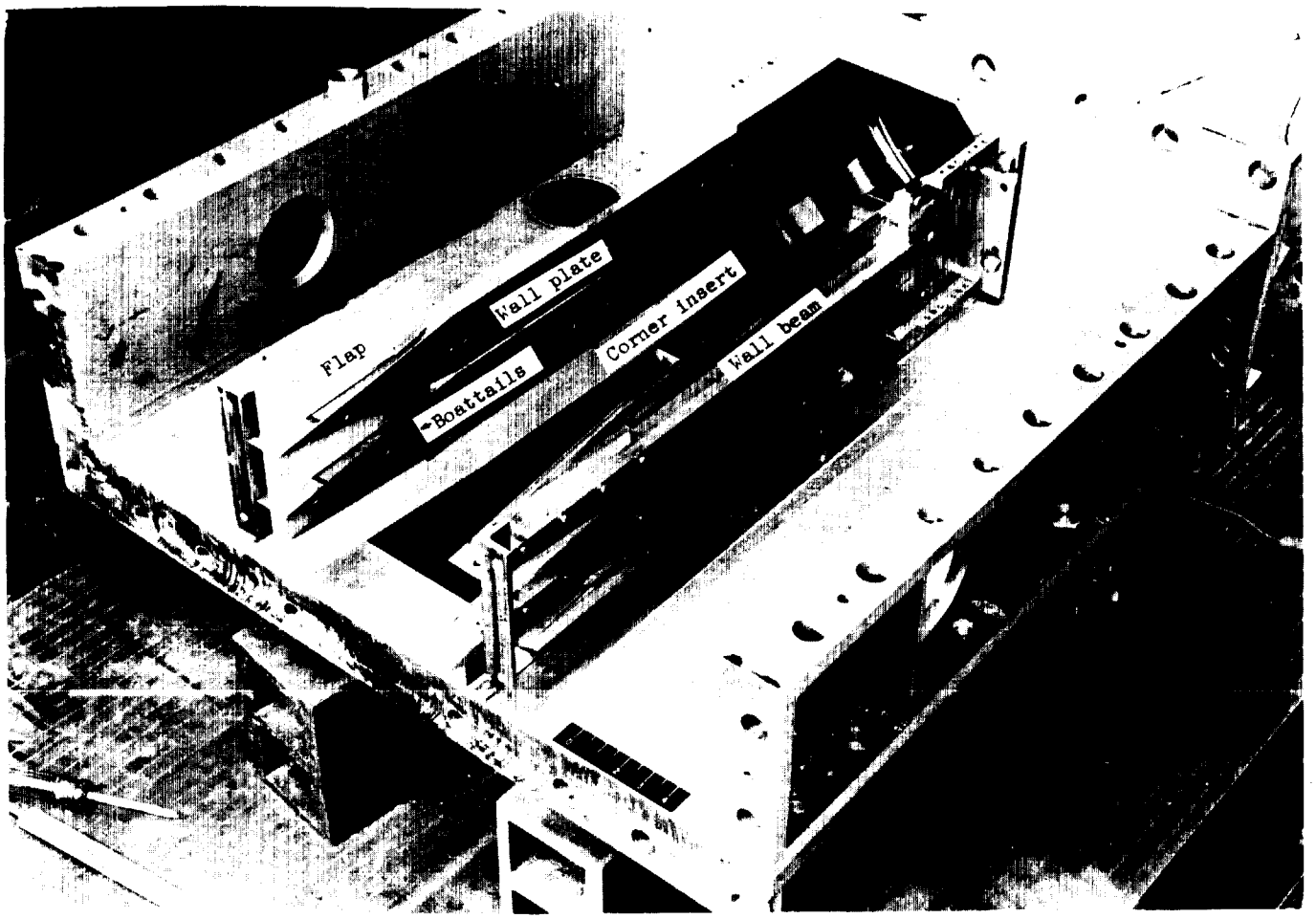

(a) View upstream. L-78334.1

Figure 3.- Photographs of partially assembled test section.

L-78337.1

(b) View downstream.

Figure 3.- Concluded.

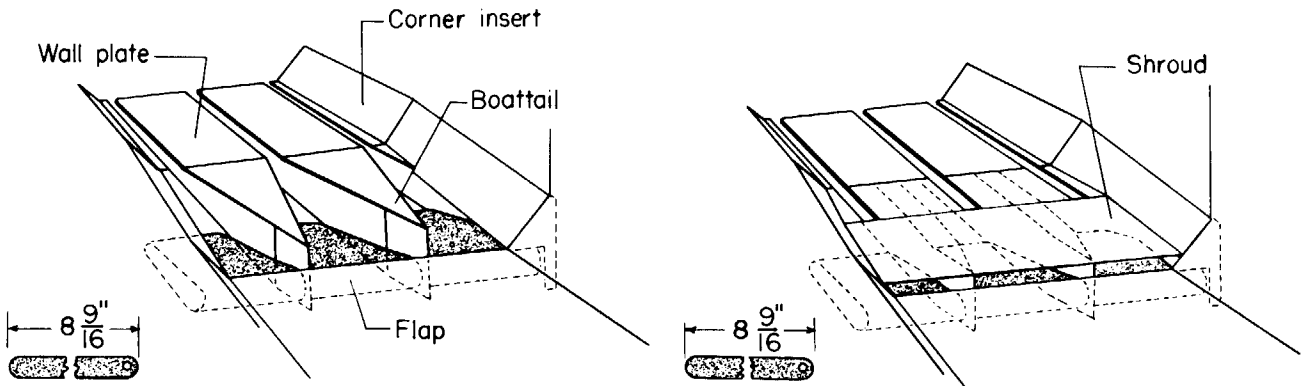

(a) Basic boattail configuration. (b) Shroud configuration.

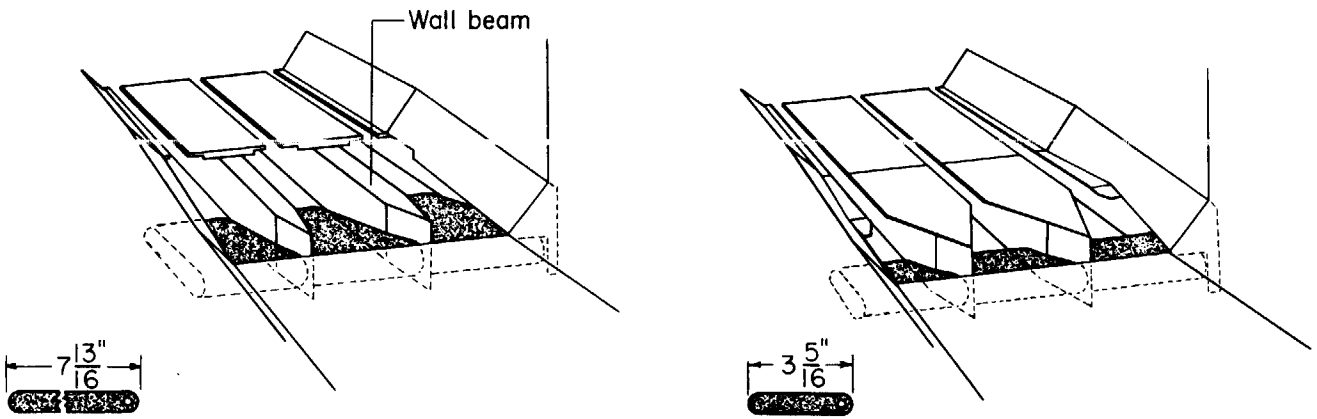

(c) No-boattail configuration. (d) Short-flap configuration.

Figure 4.- Slot-flow re-entry sections.

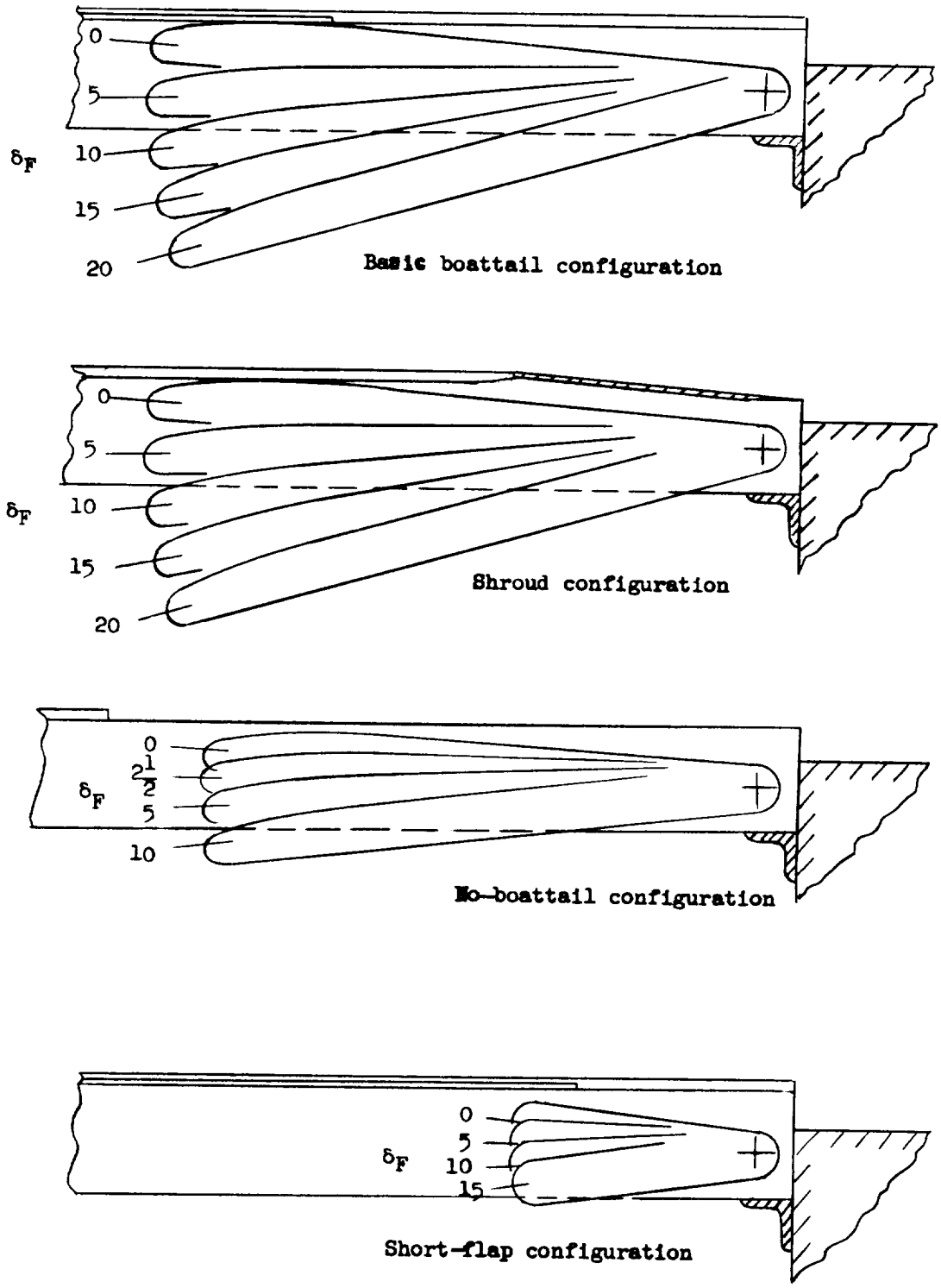

(a) Straight flaps.

Figure 5.- Flap positions.

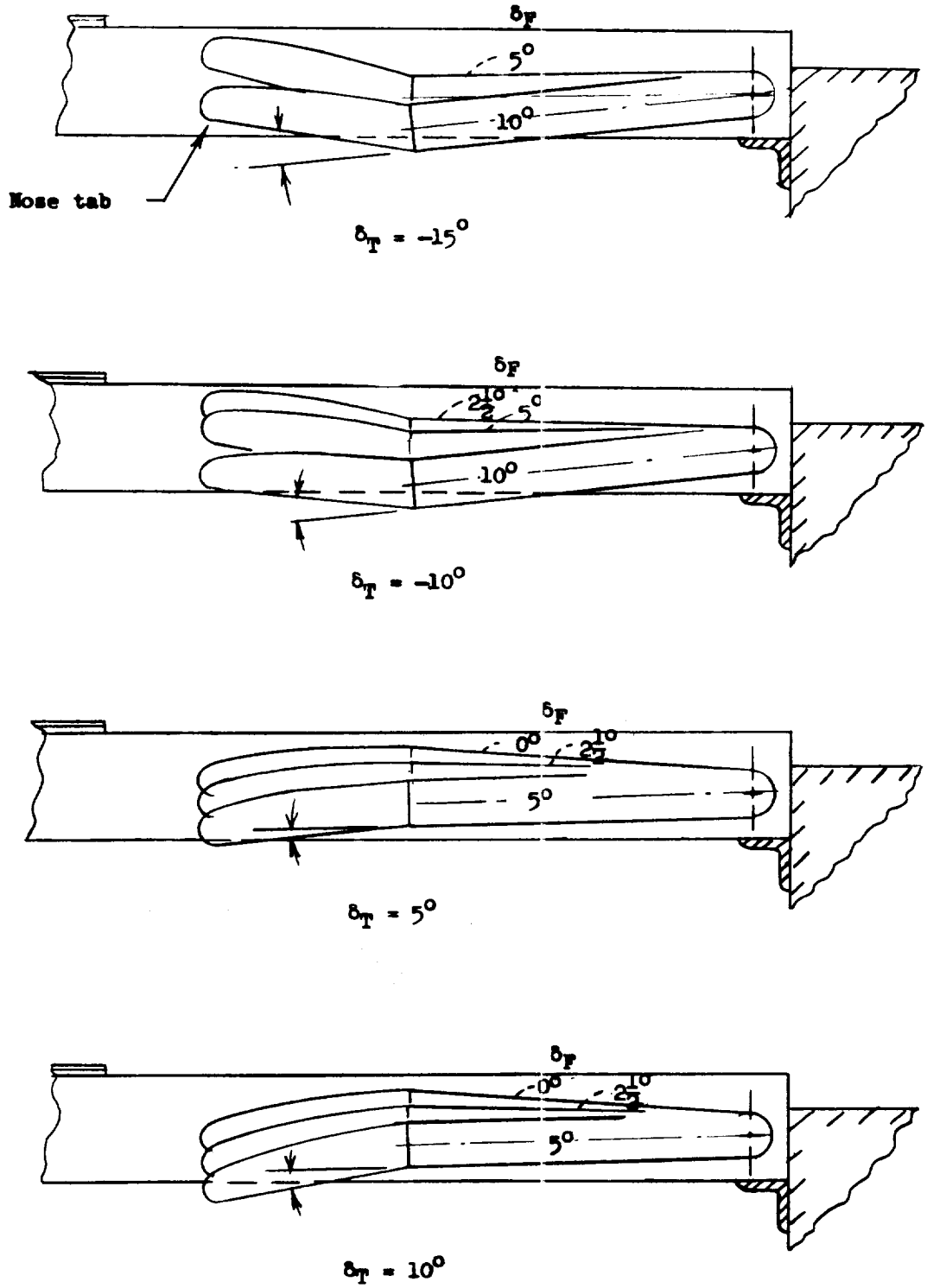

(b) Bent flaps.

Figure 5.- Concluded.

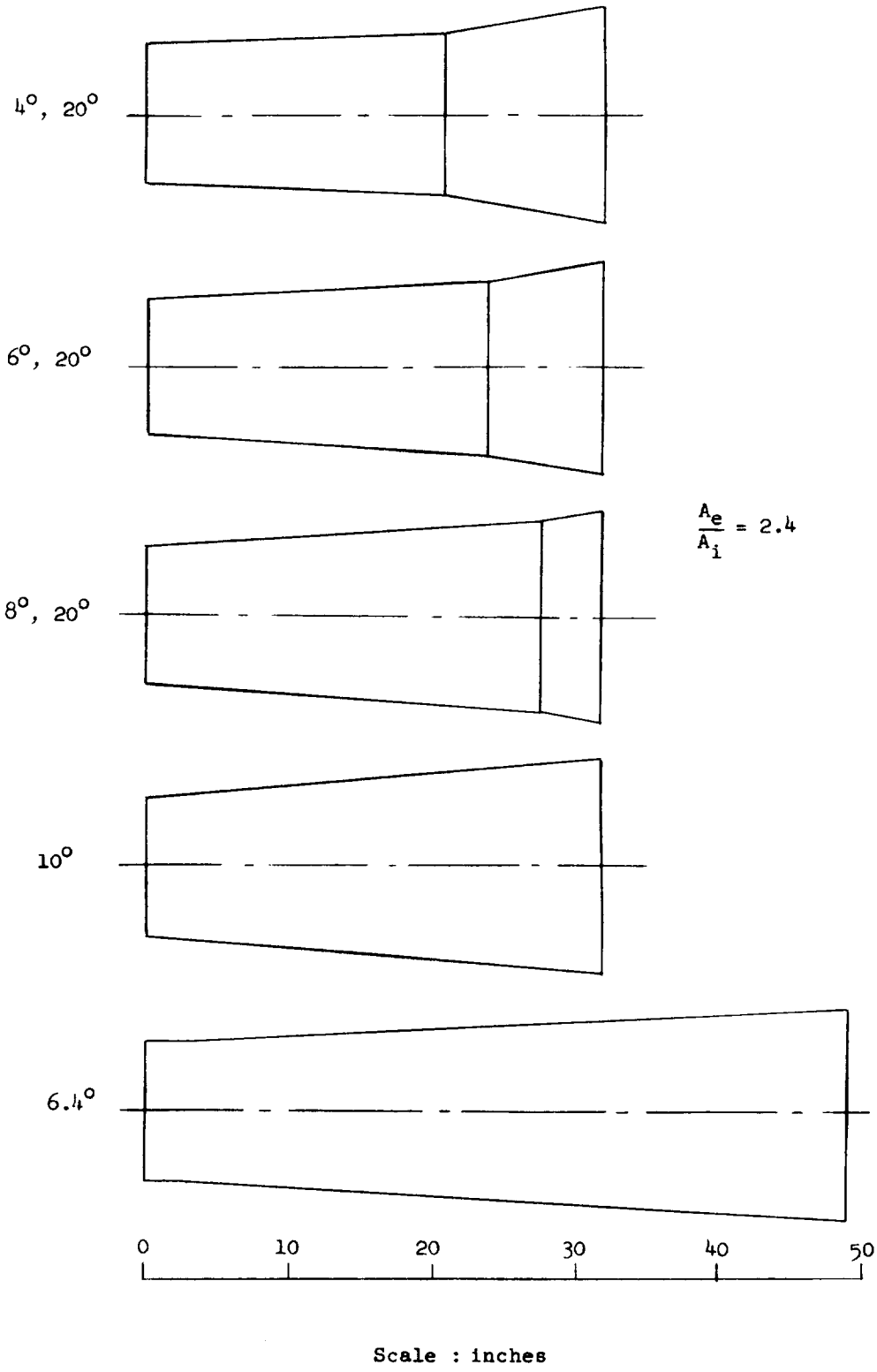

Figure 6.- Comparison of diffuser geometries.

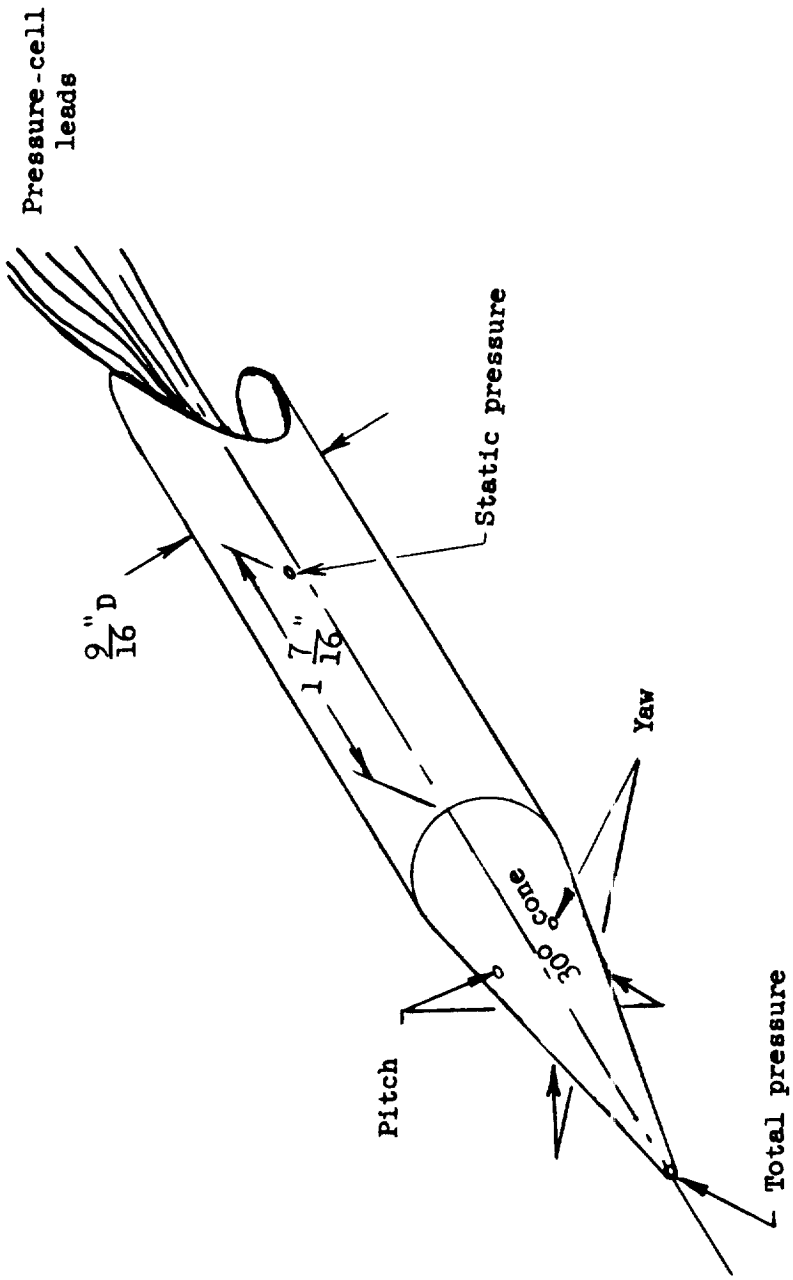

Figure 7.- Schematic view of pressure tube for rapid deceleration tests.

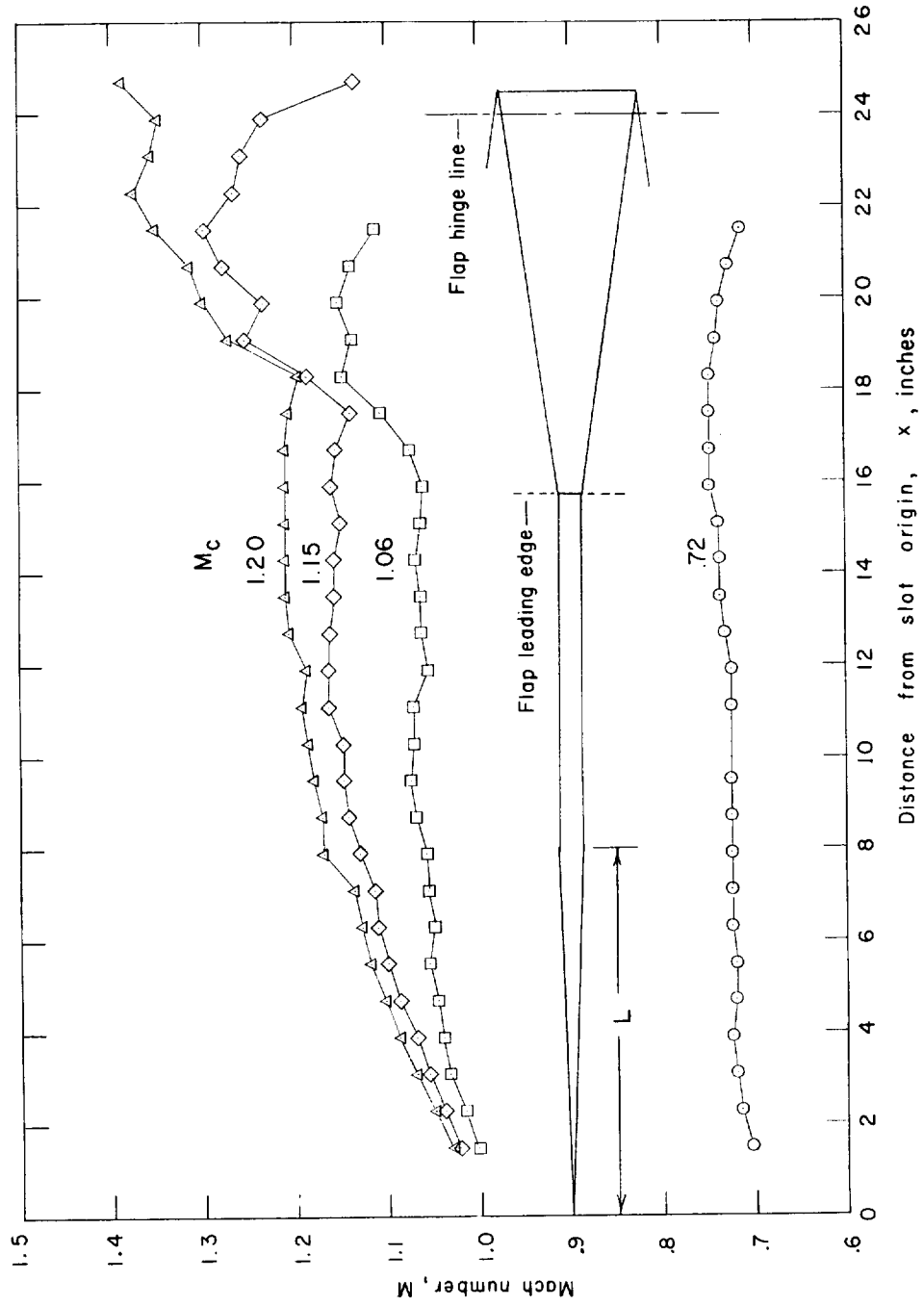

(a) $\delta_F = 0^\circ$.

Figure 8.- Center-line Mach number distributions. $\frac{nw_s}{C/4} = \frac{1}{14}$; $\frac{L}{h} = 1.0$.

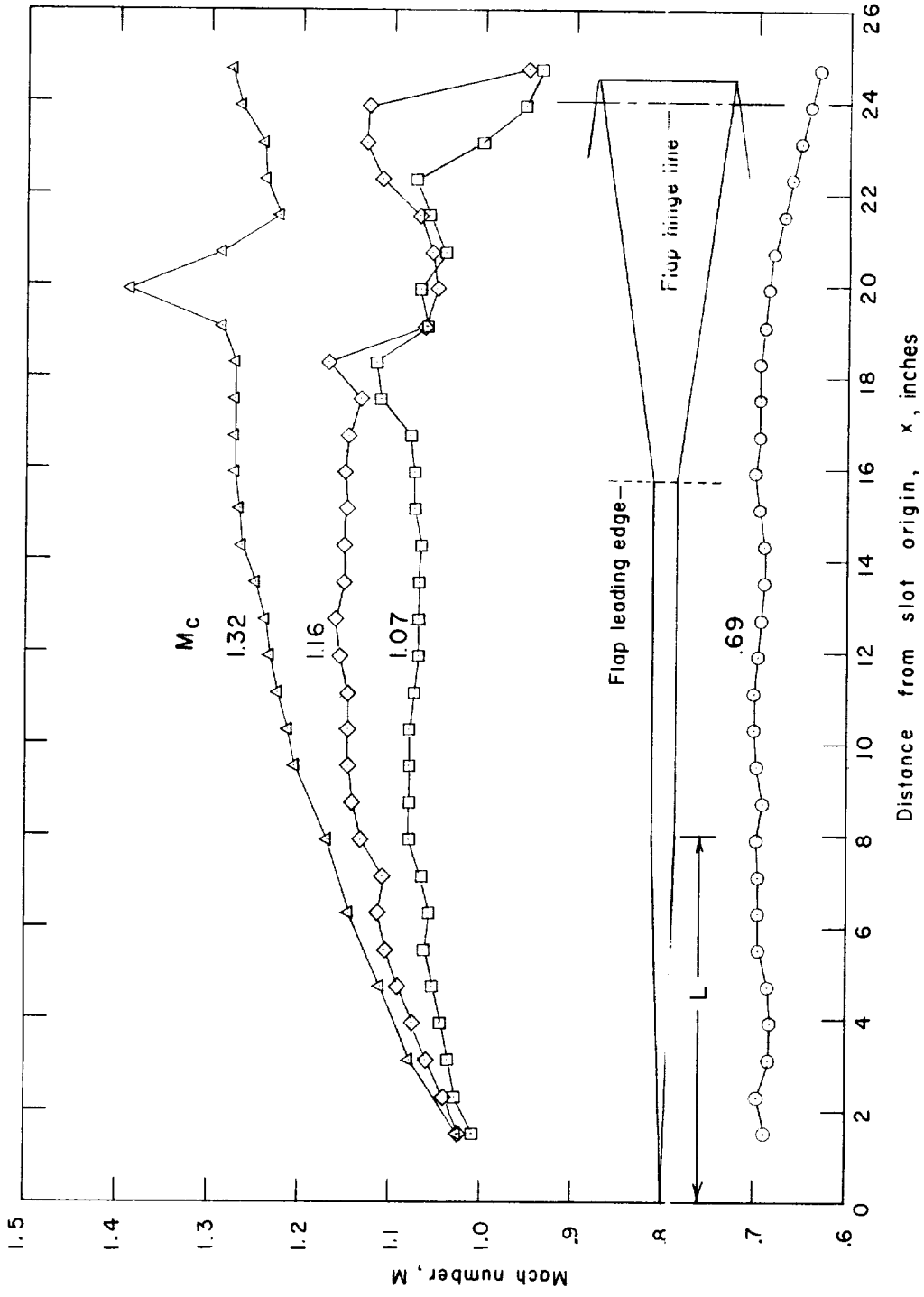

(b) $\delta_F = 5°$.

Figure 8.- Continued.

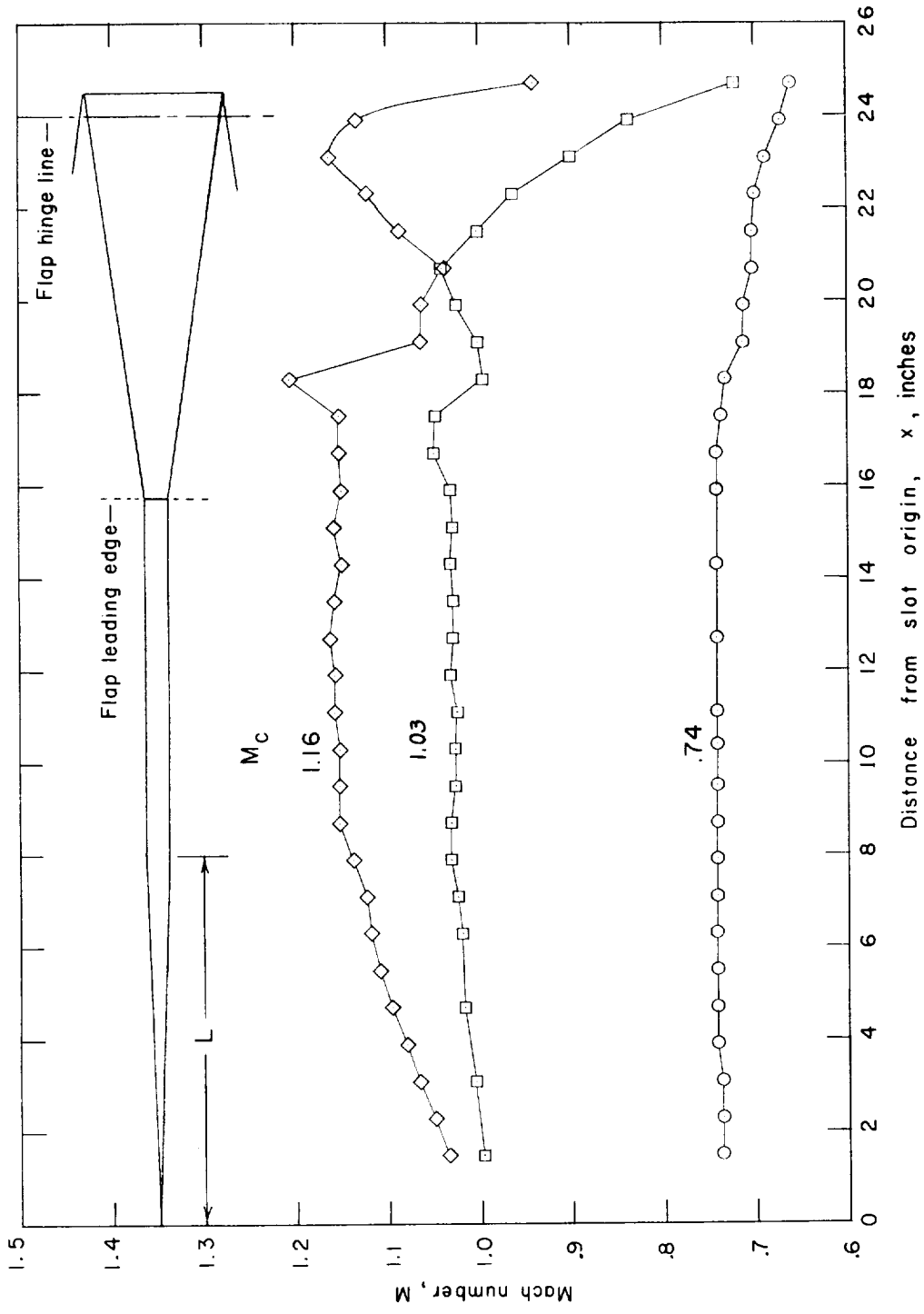

(c) $\delta_F = 10^o$.

Figure 8.- Concluded.

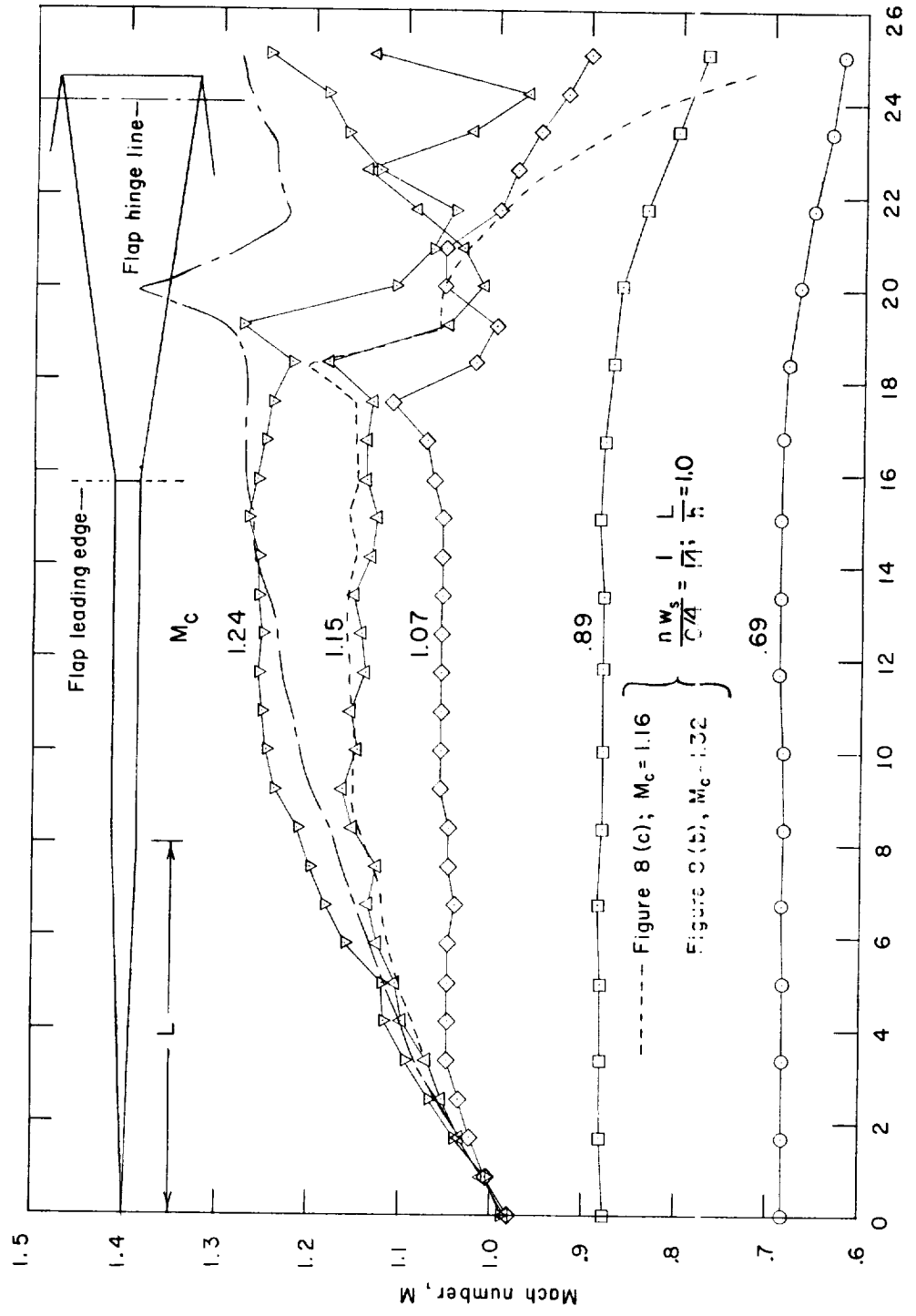

Figure 9.- Center-line Mach number distributions. $\frac{nw_s}{C/4} = \frac{1}{7}$; $\frac{L}{h} = 1.0$;

$\delta_F = 10^o$.

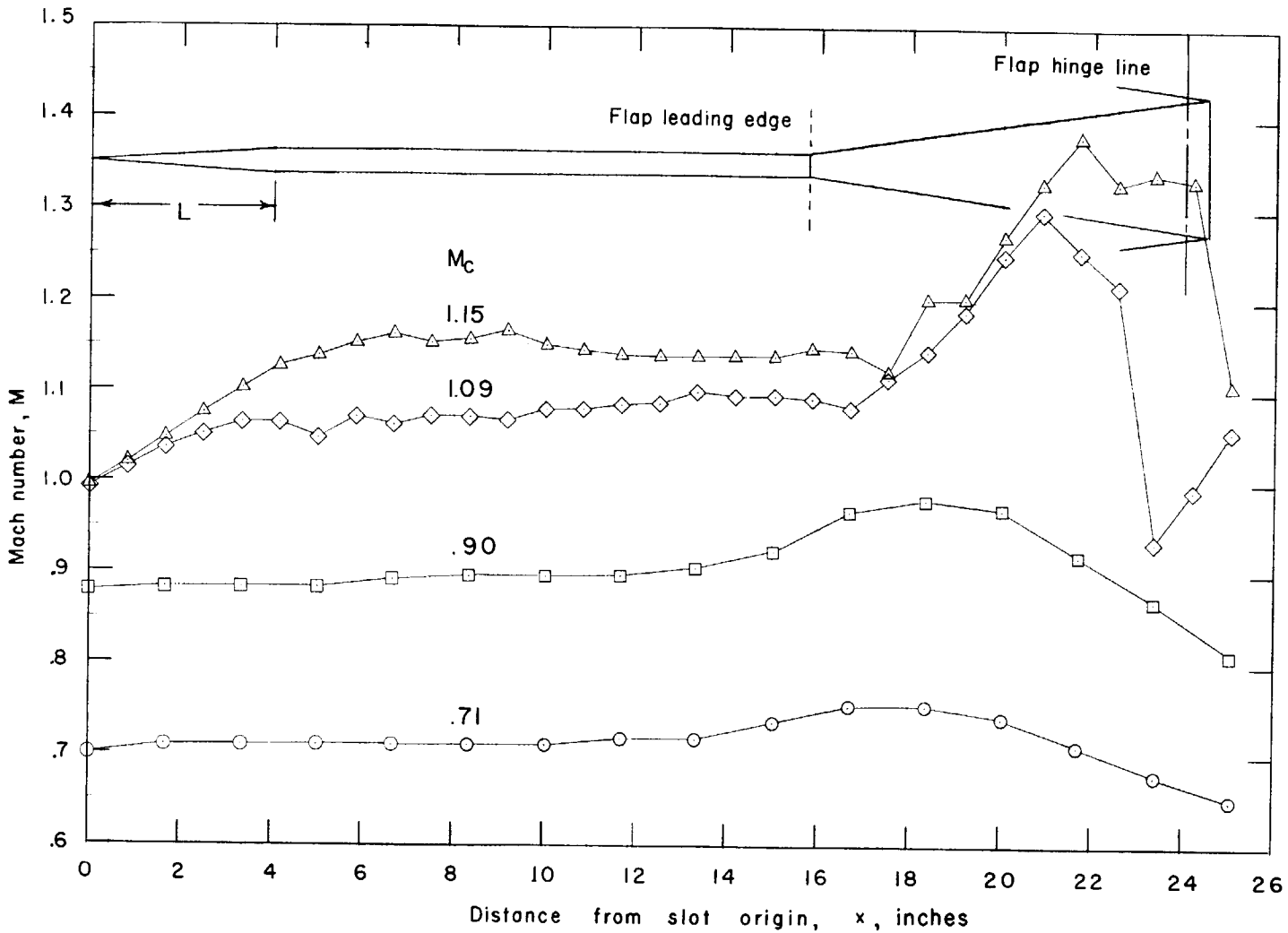

(a) $\delta_F = 0^\circ$.

Figure 10.- Center-line Mach number distributions. $\frac{nw_s}{C/4} = \frac{1}{7}$; $\frac{L}{h} = 1/2$.

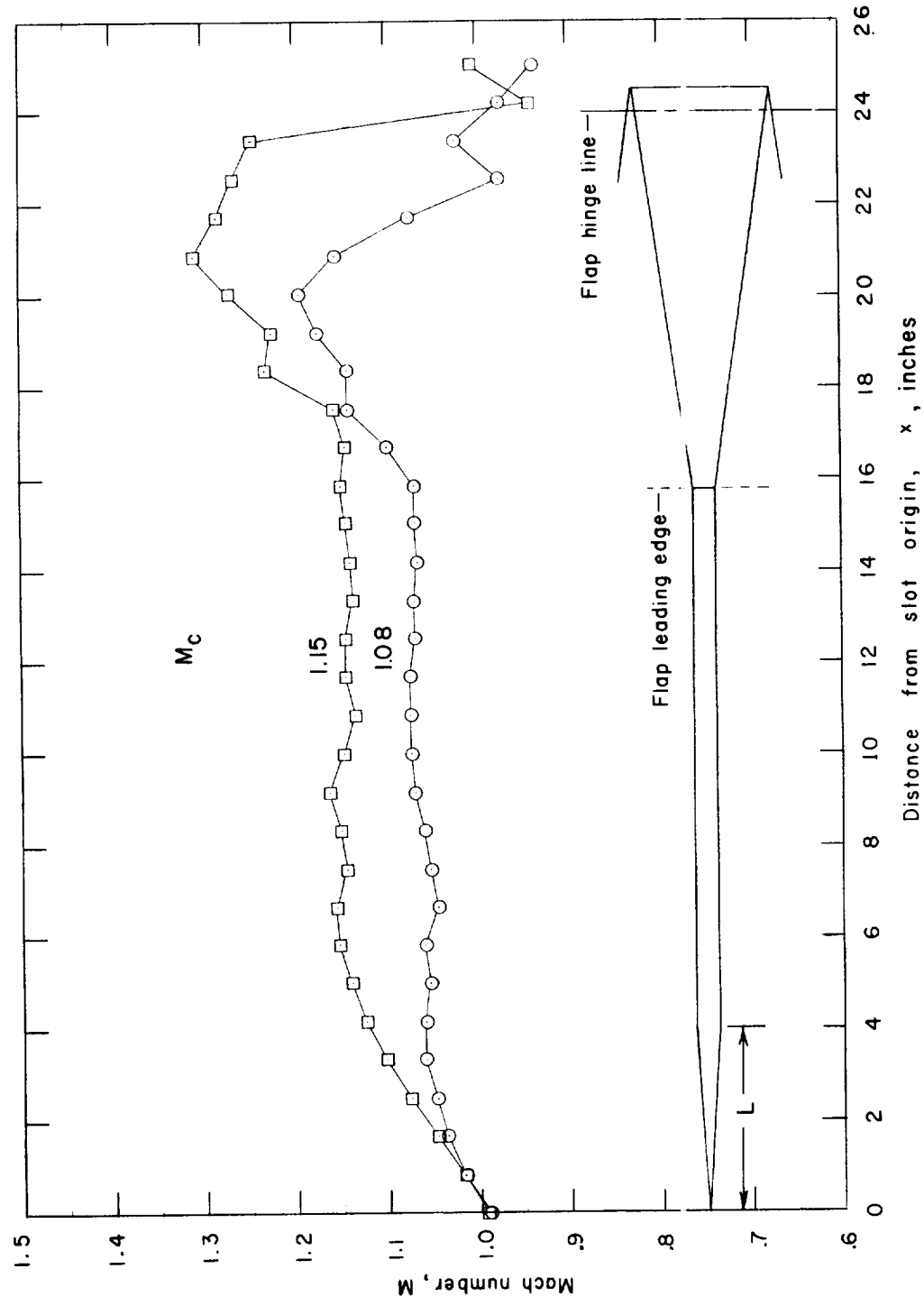

(b) $\delta_F = 5°$.

Figure 10.- Continued.

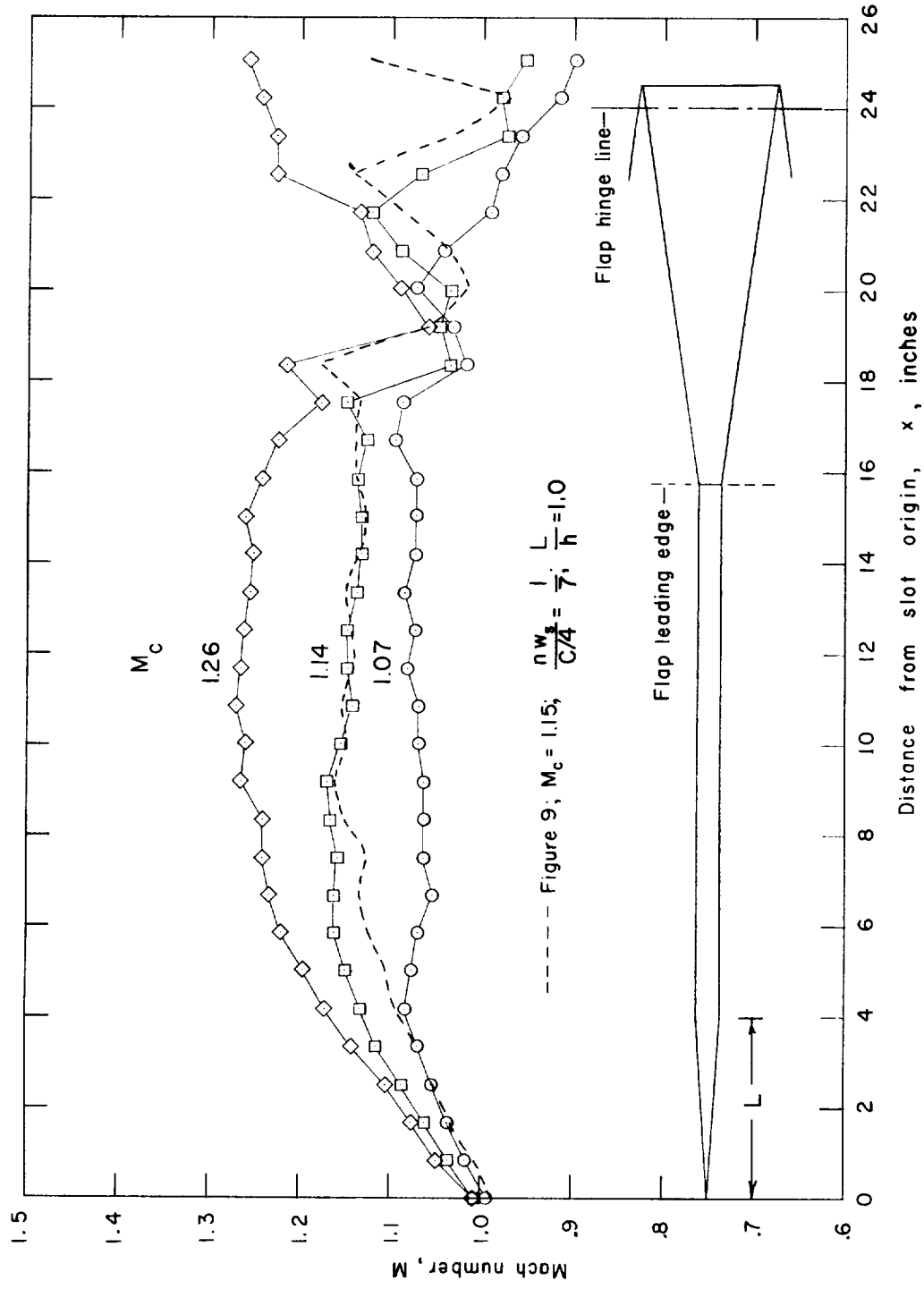

(c) $\delta_F = 10^\circ$.

Figure 10.- Concluded.

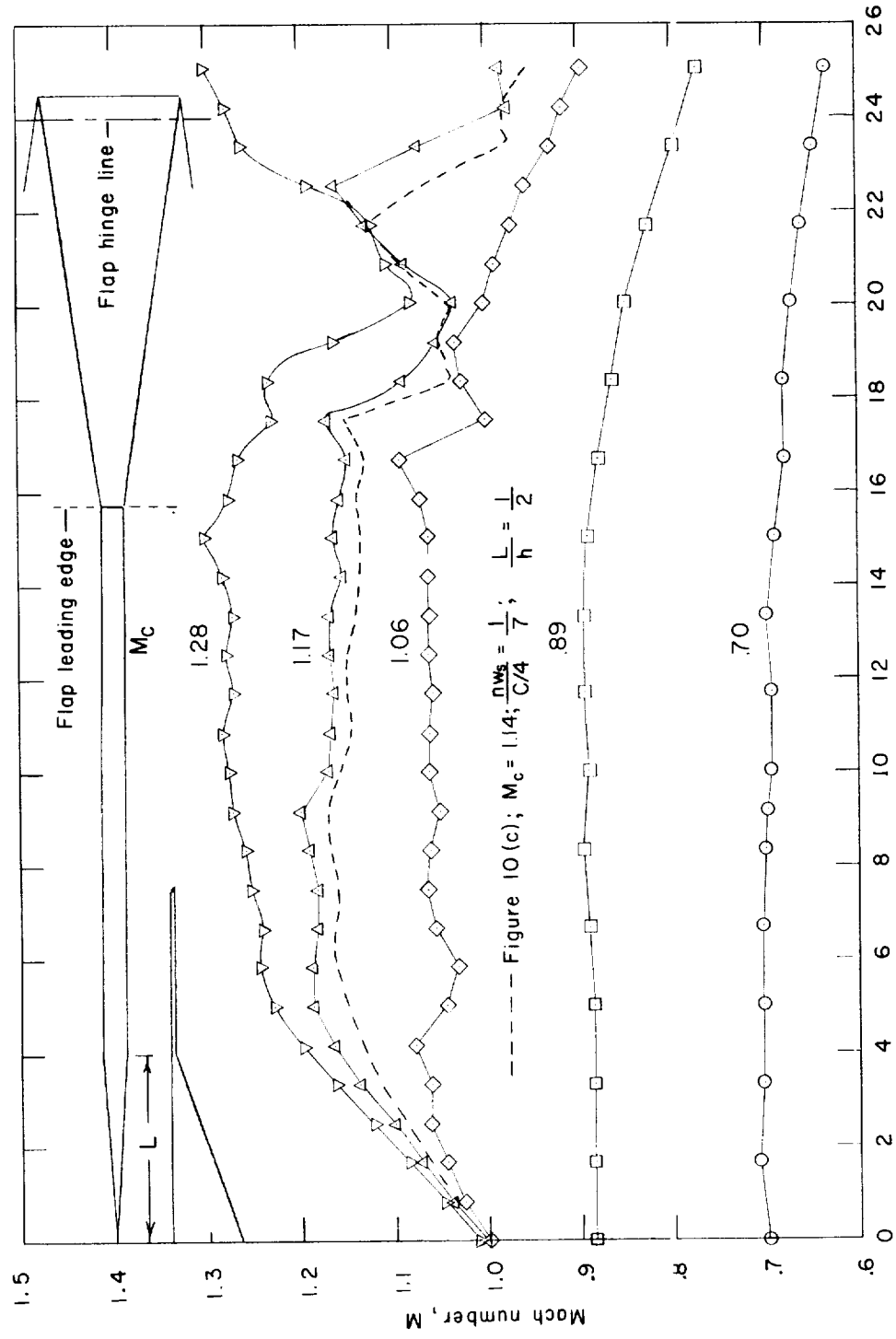

Figure 11.-Center-line Mach number distributions. $\frac{nw_s}{C/4} = \frac{1}{7}$; $\frac{L}{h} = \frac{1}{2}$; $\delta_F = 10^\circ$; variable depth taper.

L-1005

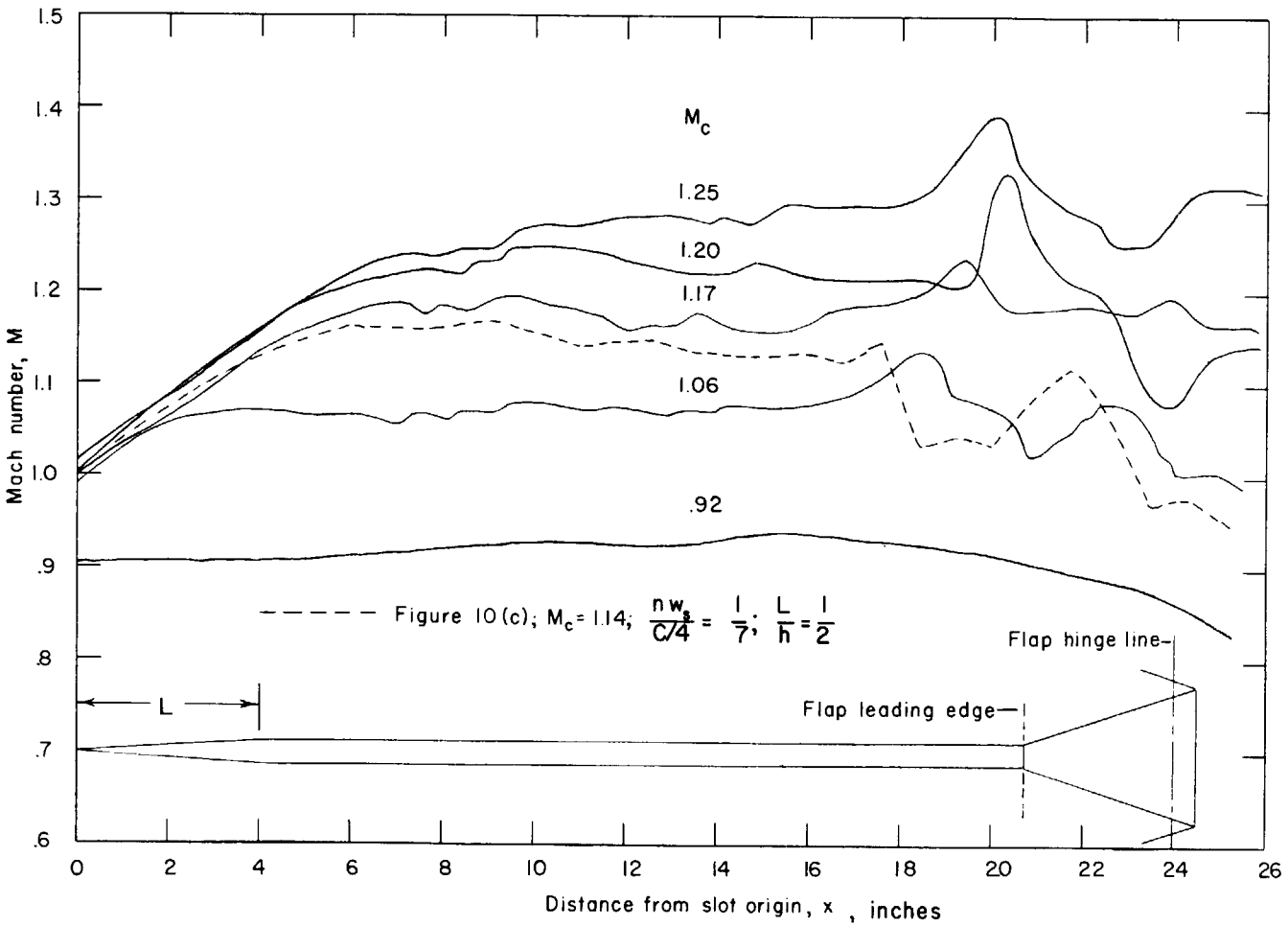

Figure 12.- Center-line Mach number distributions for shortened flaps and lengthened slots. $\frac{nw_s}{C/4} = \frac{1}{7}$; $\frac{L}{h} = \frac{1}{2}$; $\delta_F = 10^\circ$.

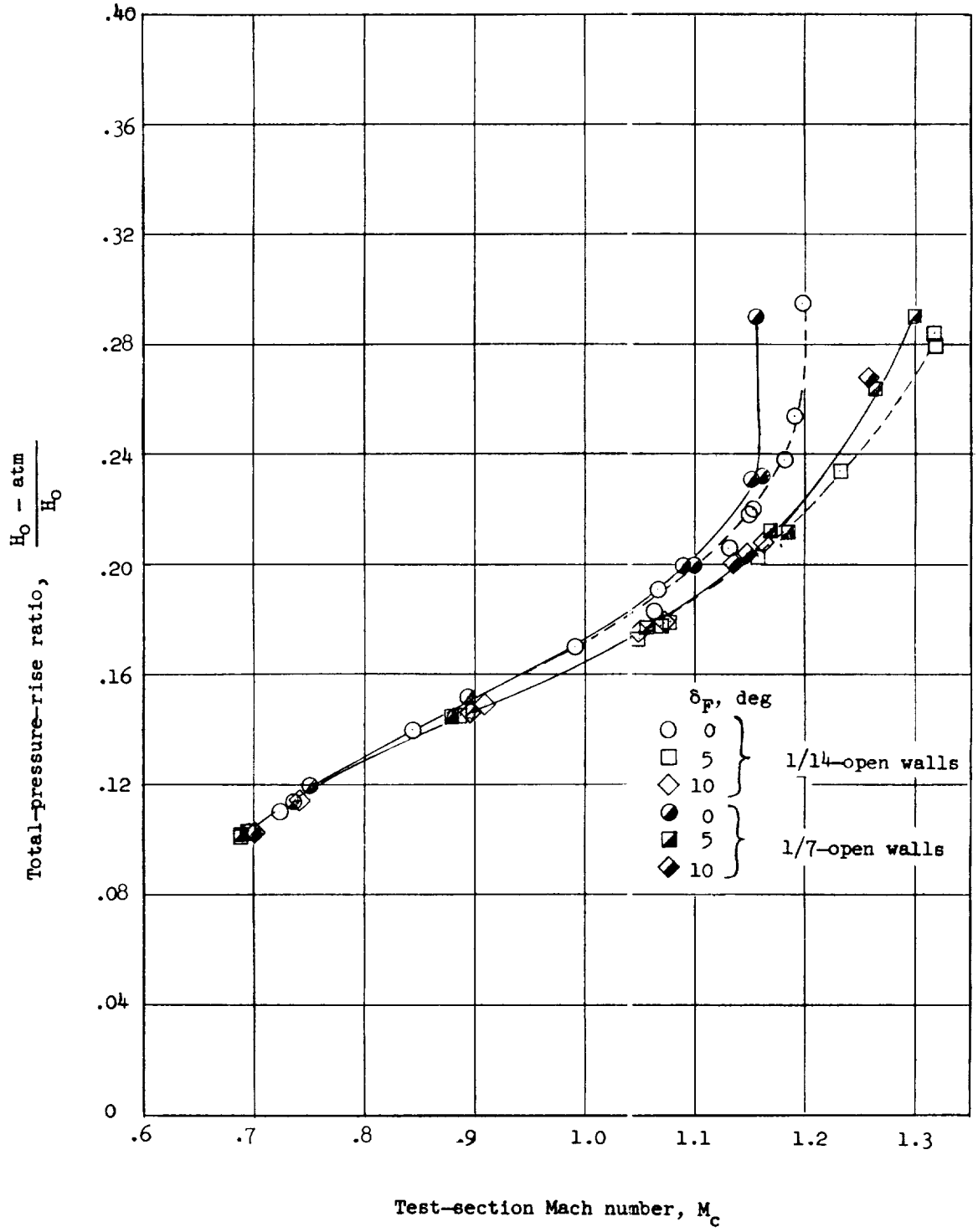

Figure 13.- Total-pressure rise required for tunnel operation with 1/14-open and 1/7-open slotted walls.

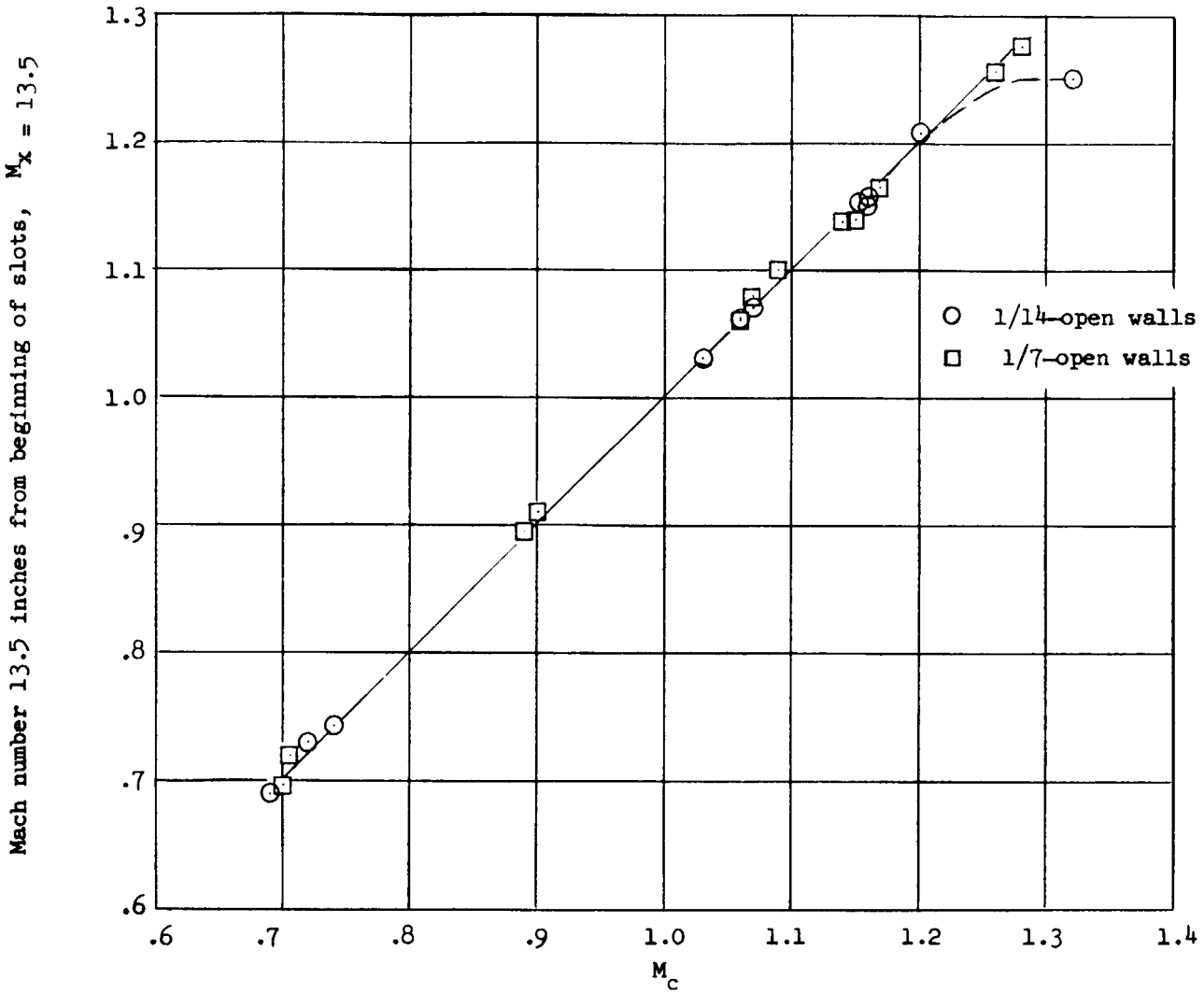

Figure 14.- Relationship between M_c and Mach number near midpoint of test region.

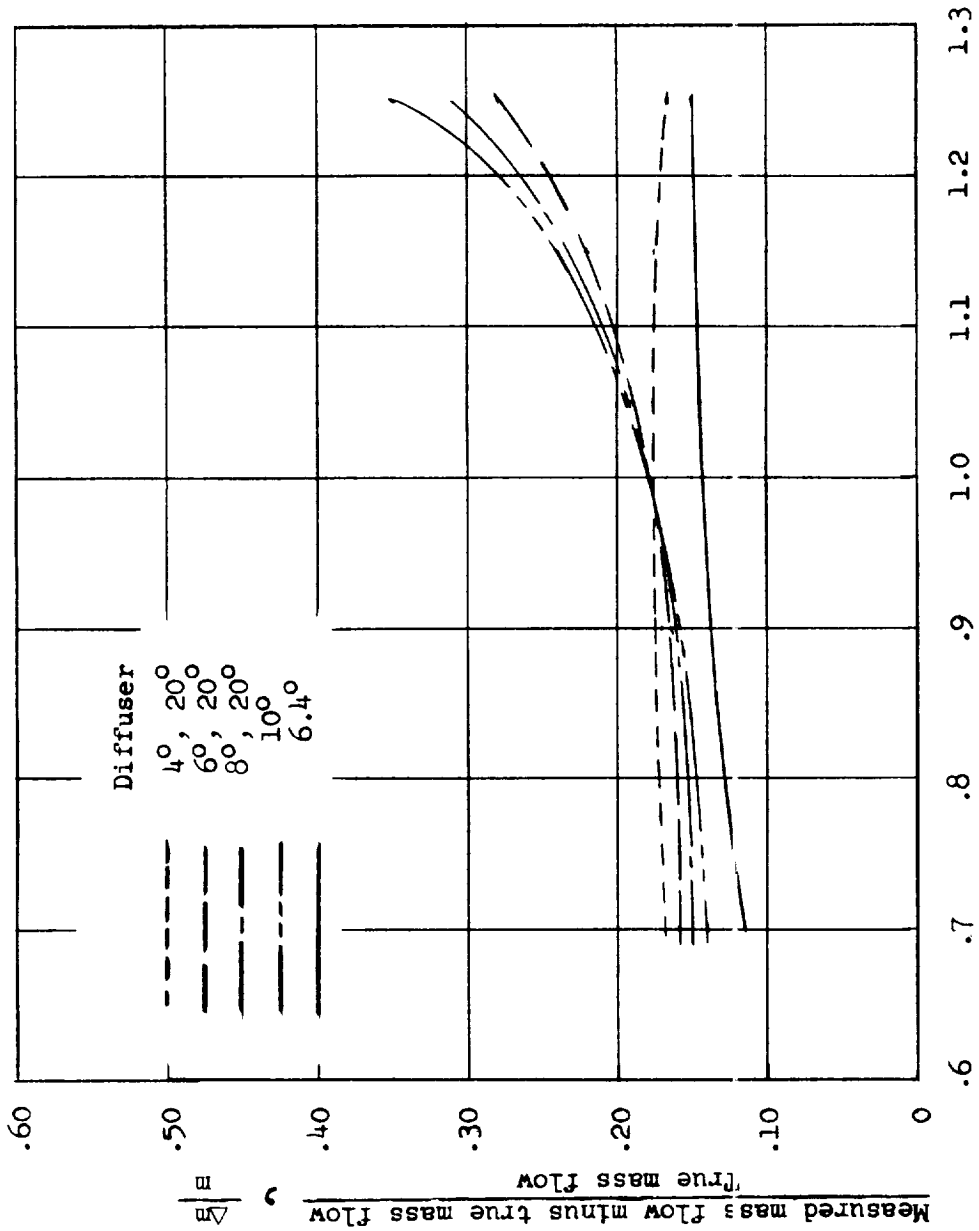

Figure 15.- Discrepancies in measured mass flow for the various diffusers. Envelope curves.

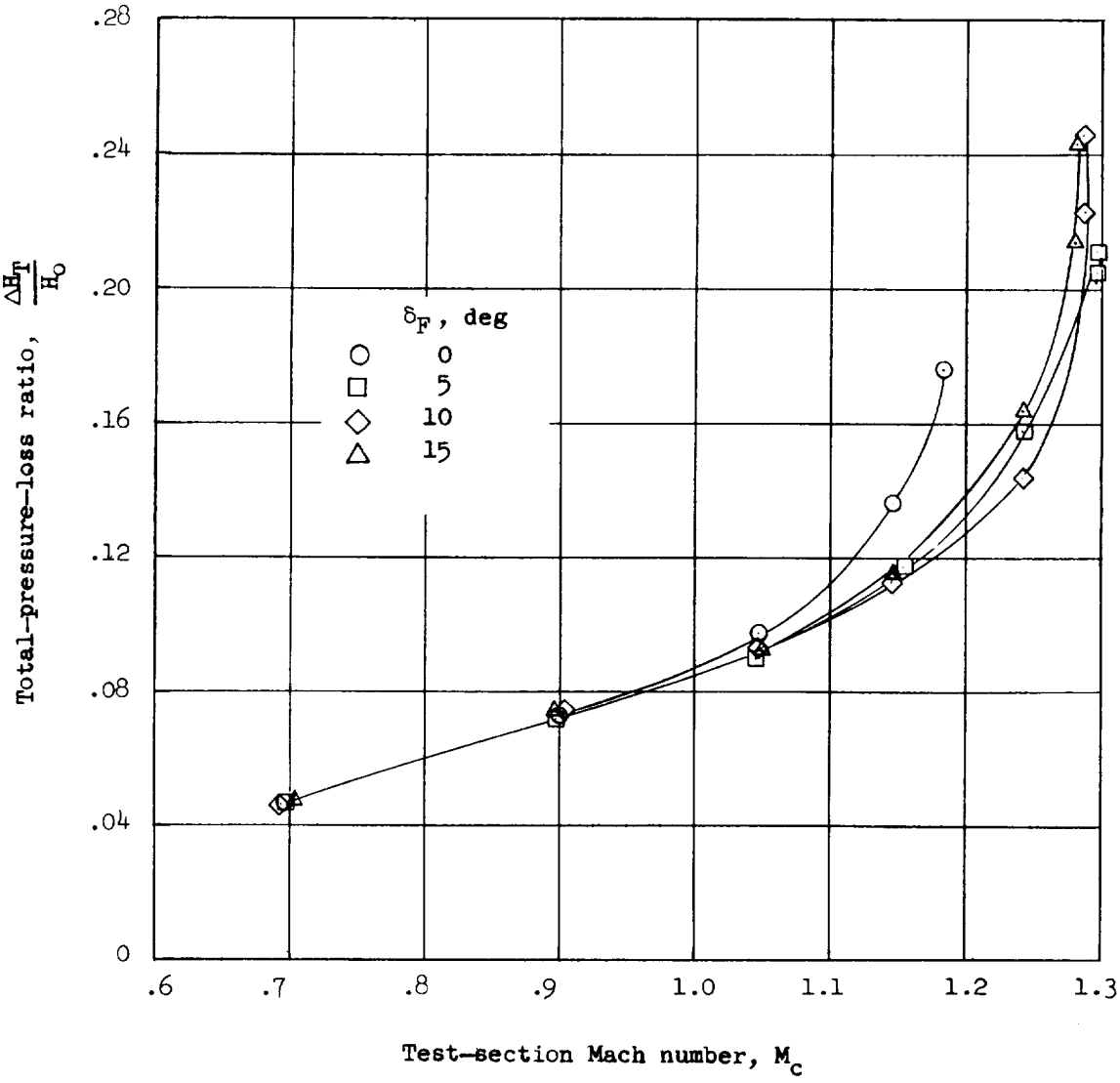

(a) $4^\circ, 20^\circ$ diffuser.

Figure 16.- Variation of total-pressure-loss ratio with test-section Mach number.

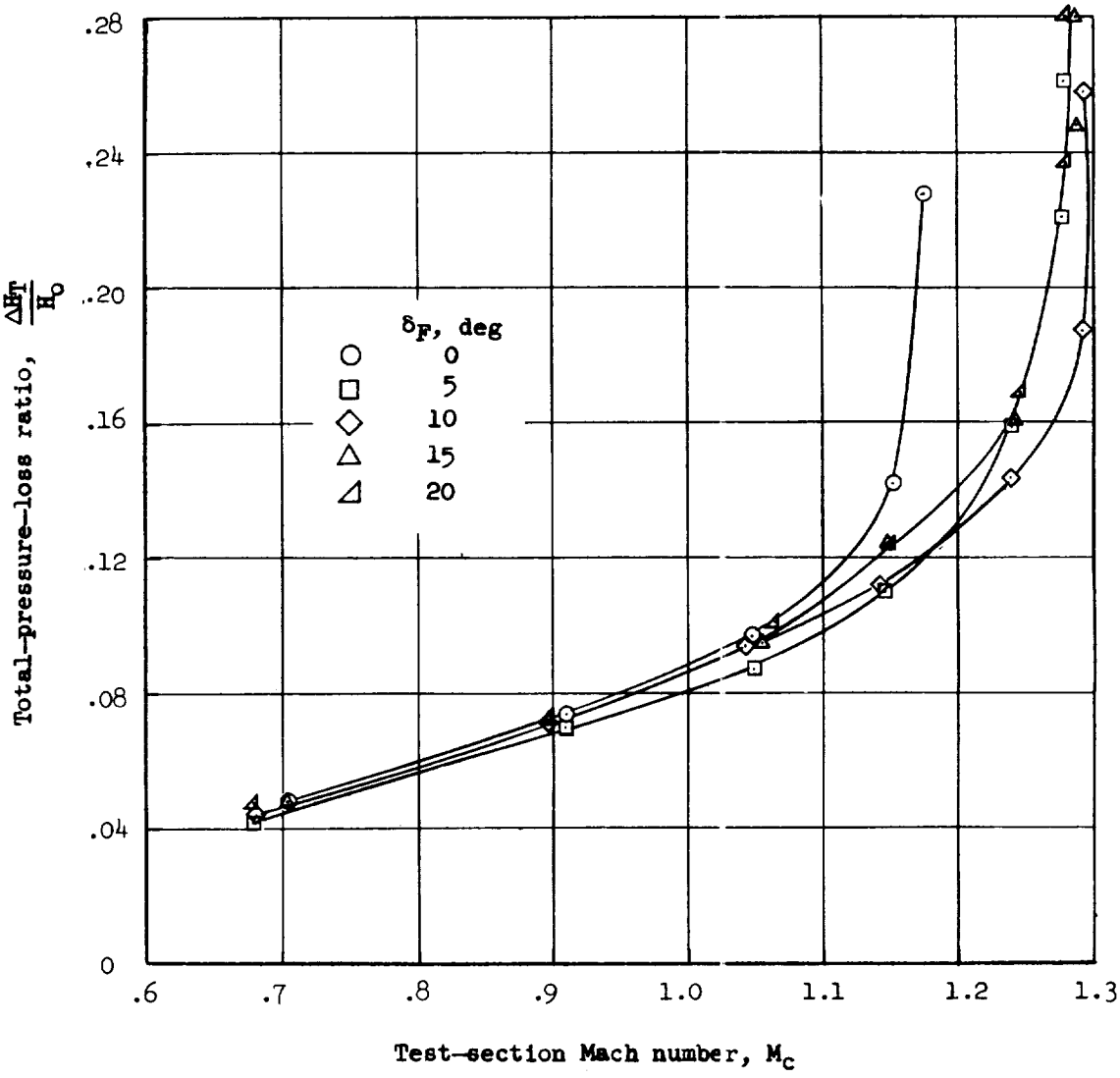

(b) $6^\circ,20^\circ$ diffuser.

Figure 16.- Continued.

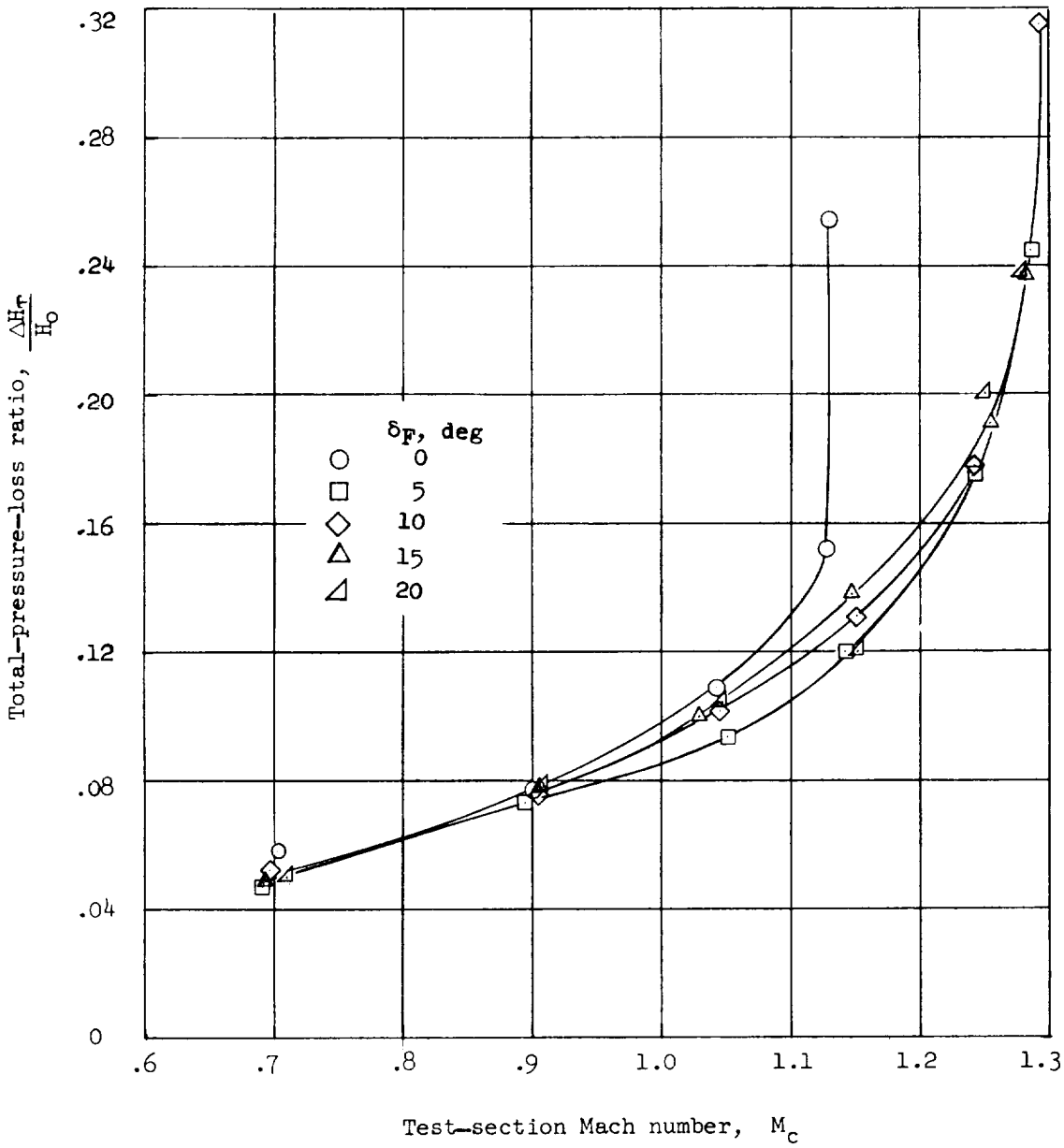

(c) $8^\circ, 20^\circ$ diffuser.

Figure 16.- Continued.

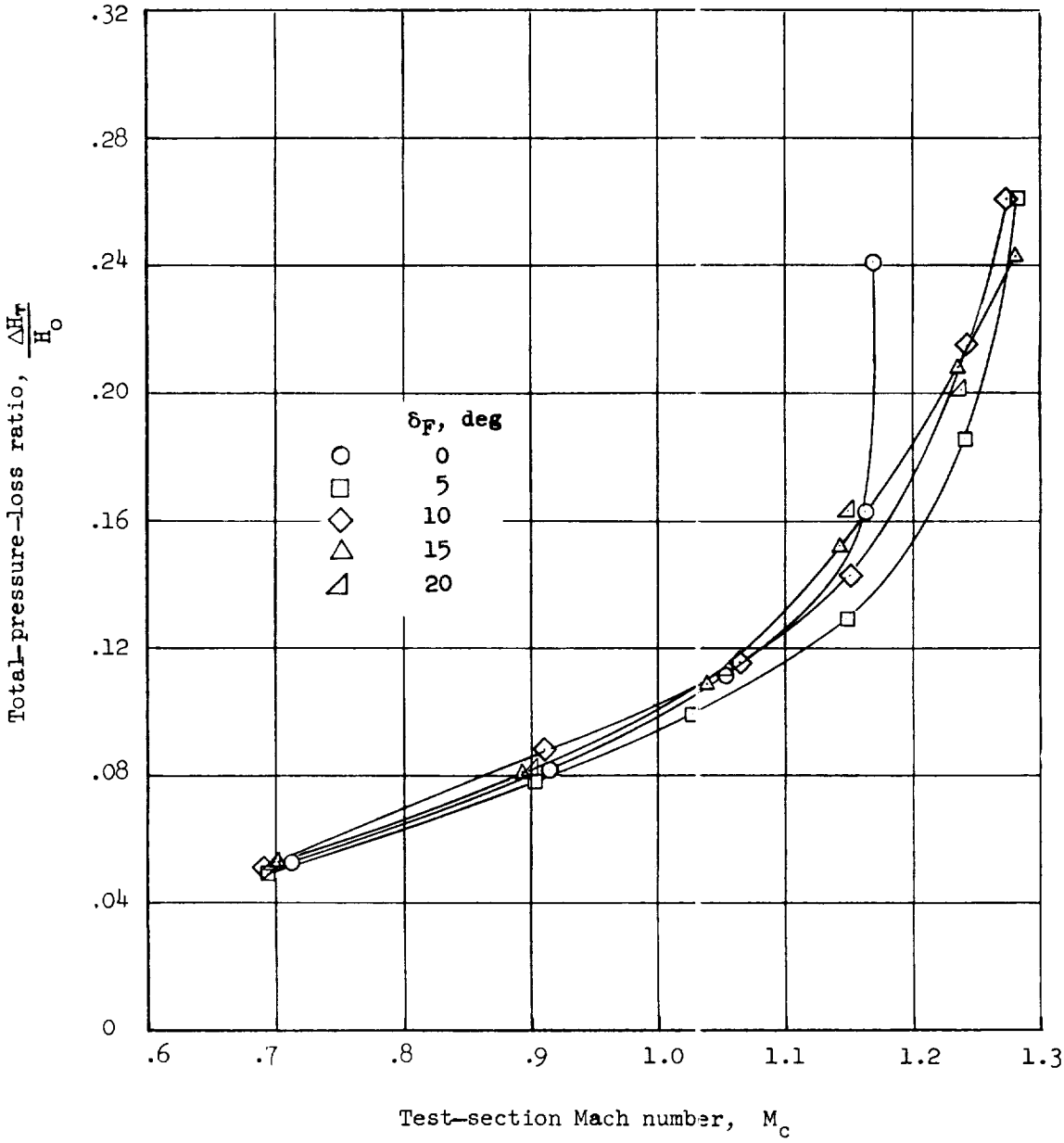

(d) 10° diffuser.

Figure 16.- Continued.

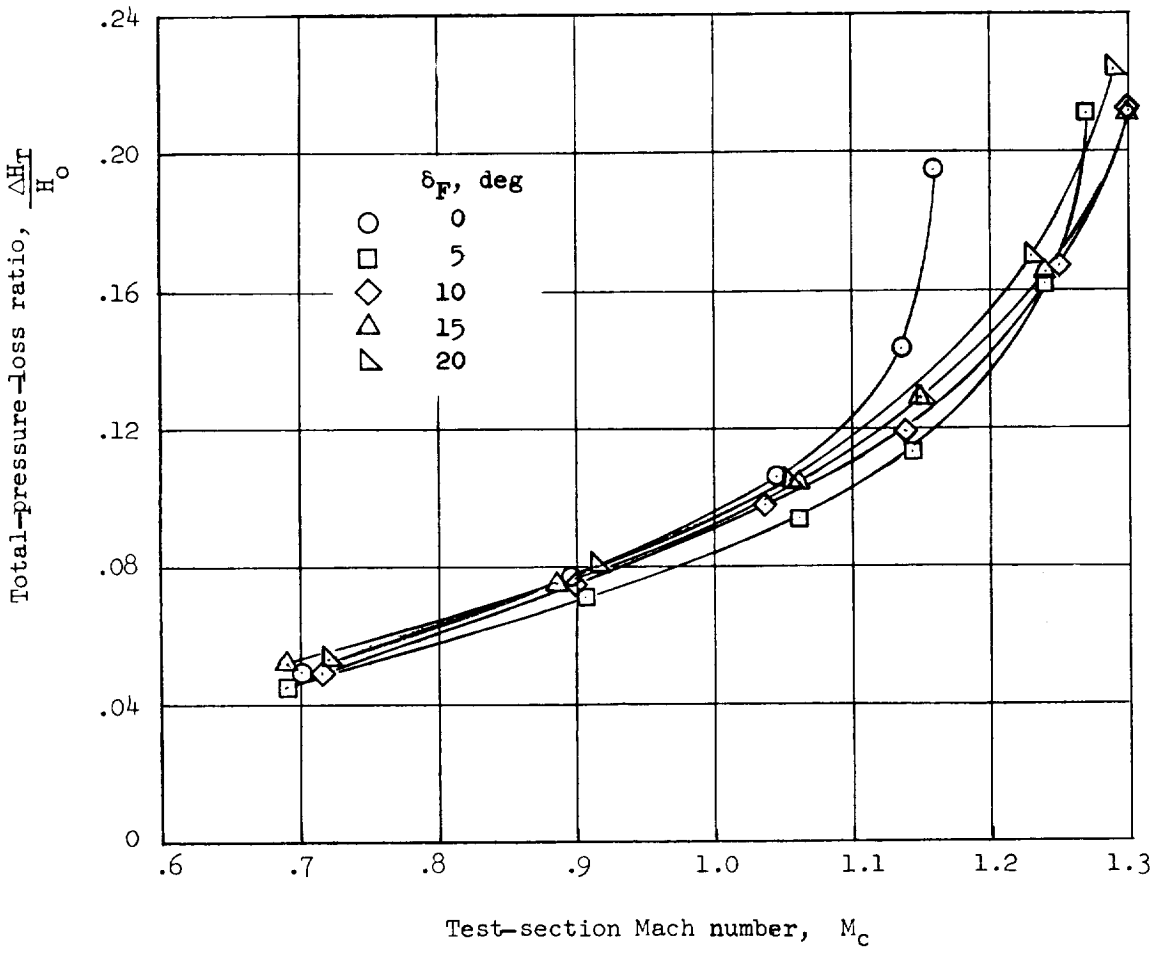

(e) 6.4° diffuser.

Figure 16.- Concluded.

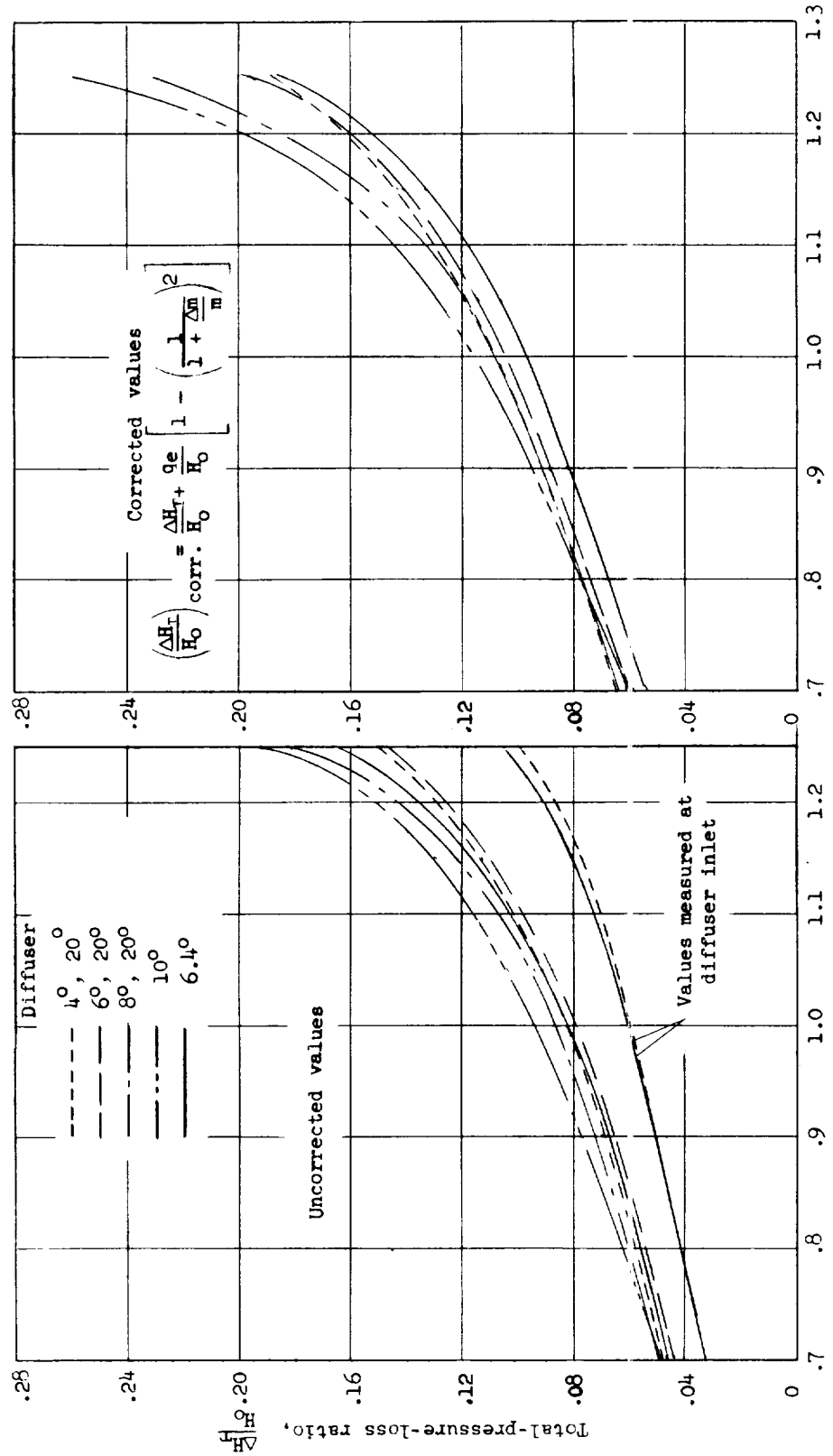

Figure 17.- Measured and corrected values for tunnel-total-pressure-loss ratio. Envelope curves.

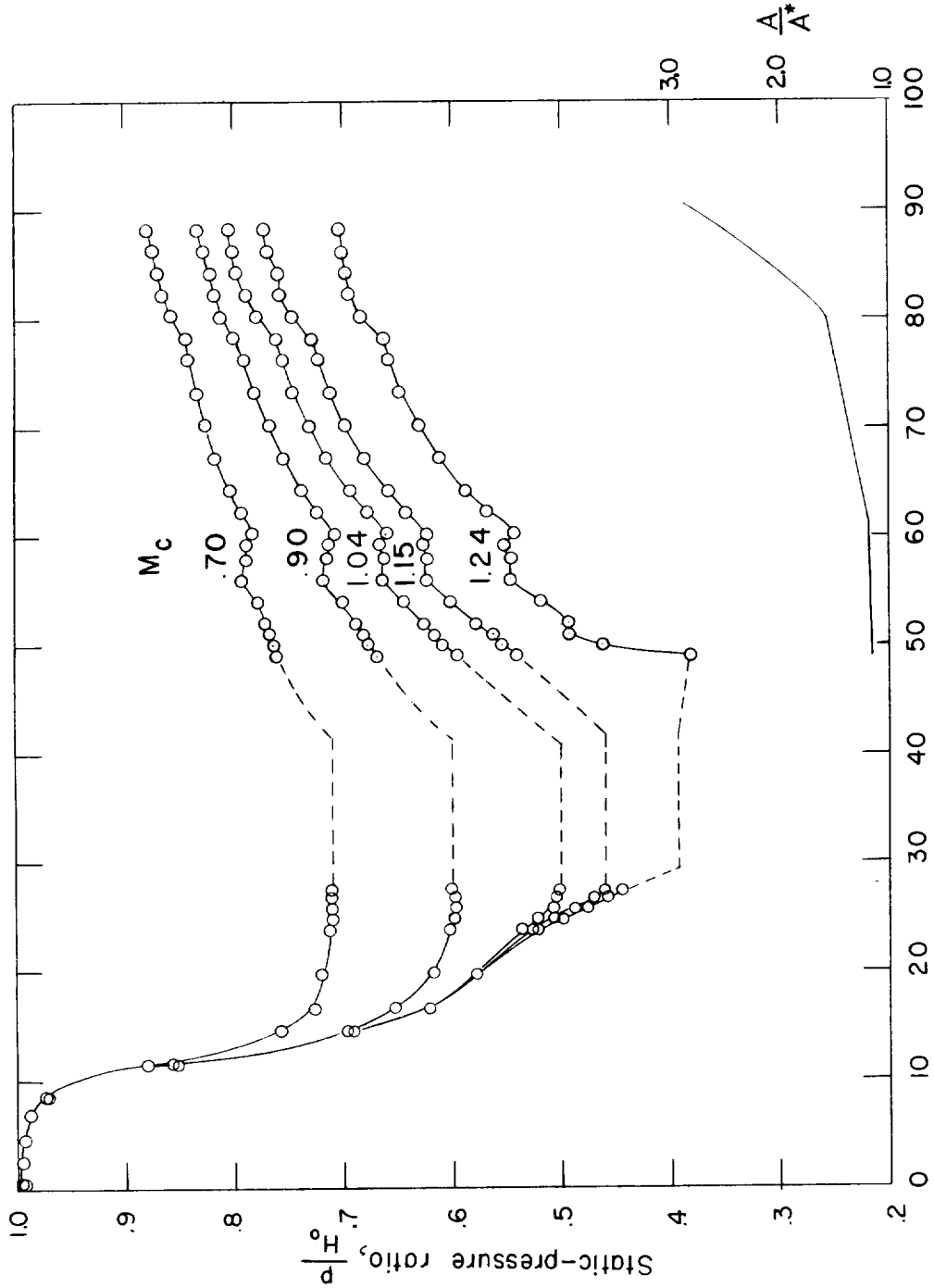

Figure 18.- Wall static-pressure distributions for the $4^\circ,20^\circ$ diffuser at $\delta_F = 5^\circ$.

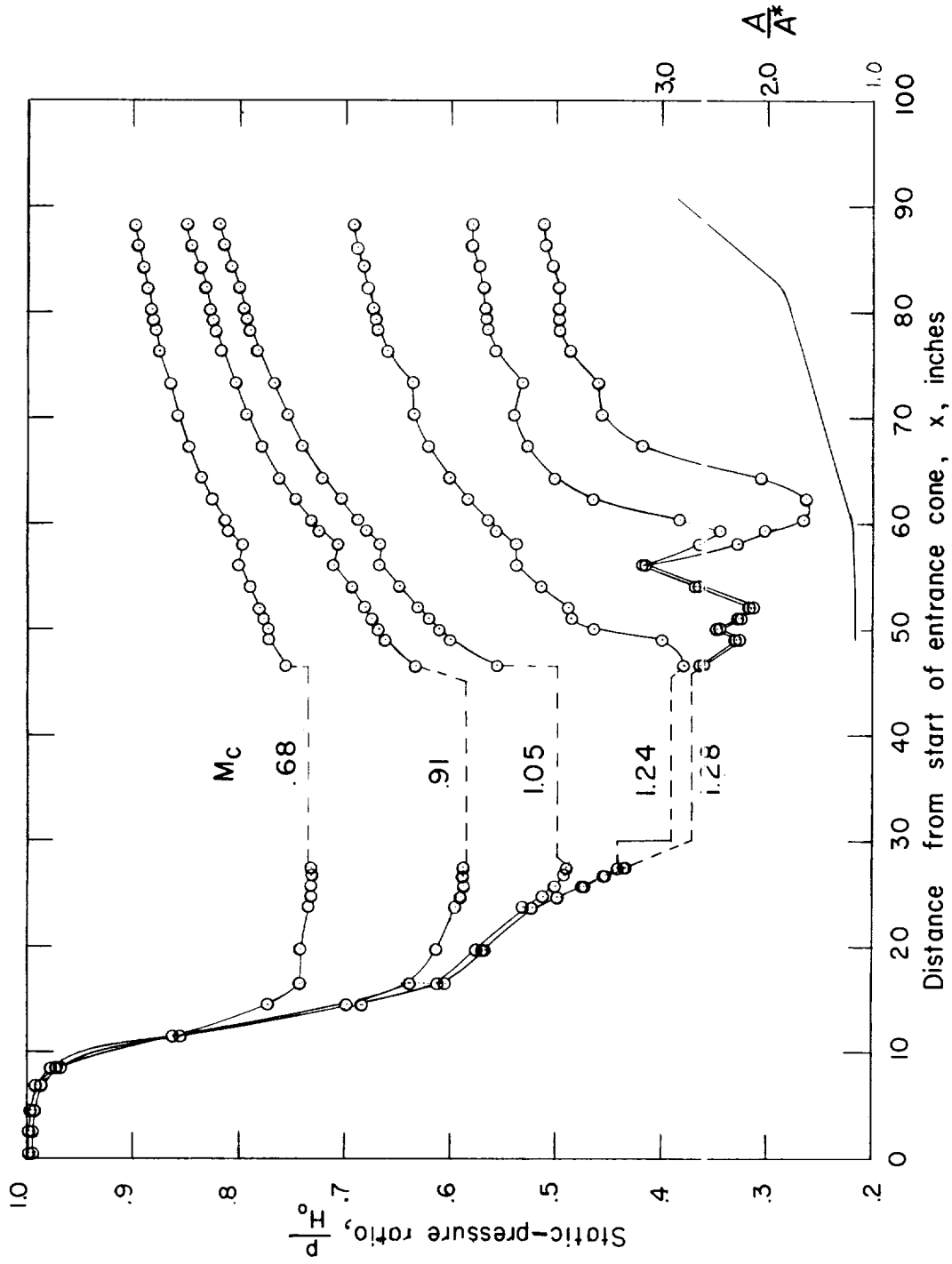

Figure 19.- Wall static-pressure distributions for the $6^o, 20^o$ diffuser at $\delta_F = 5^o$.

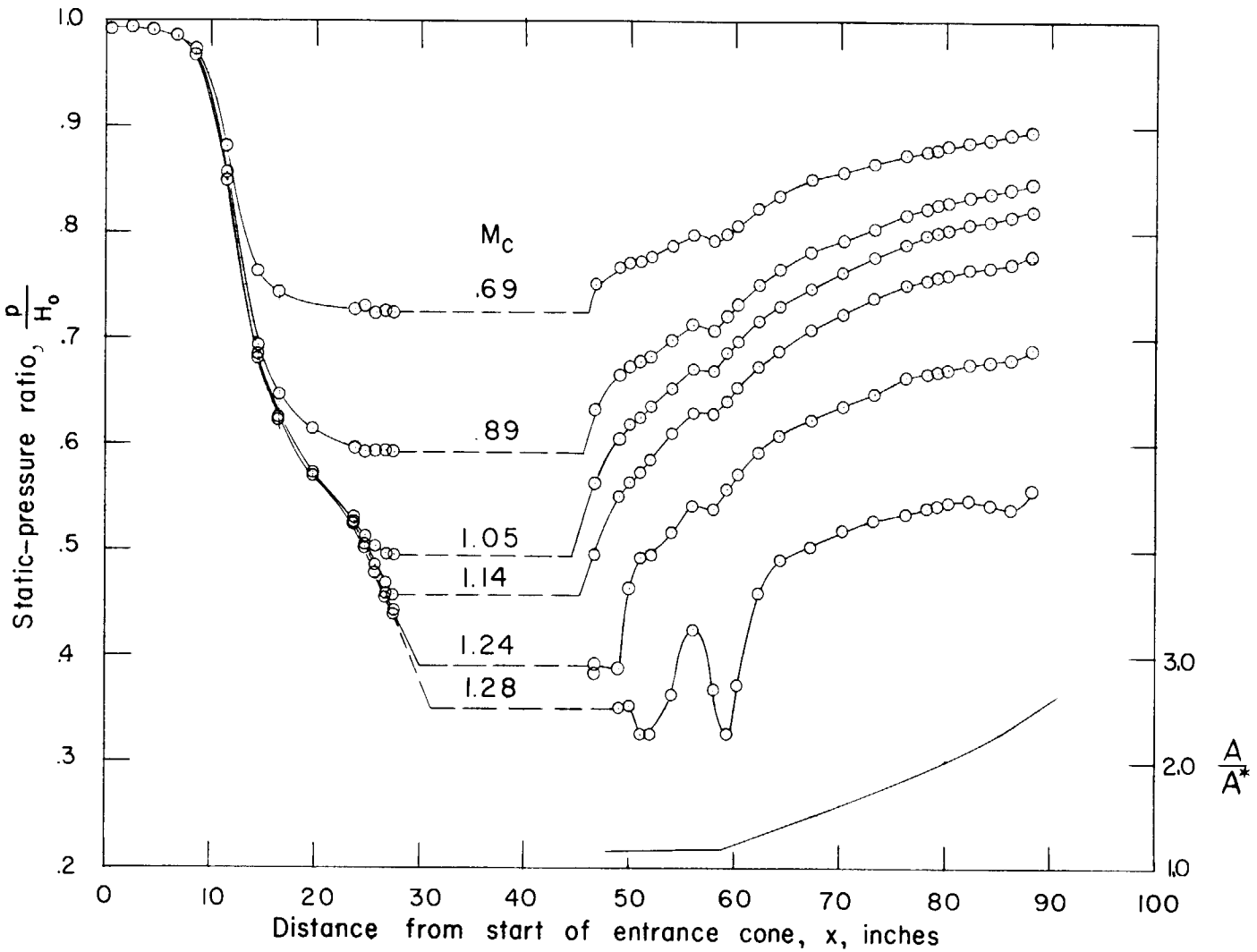

Figure 20.- Wall static-pressure distributions for the $8^\circ, 20^\circ$ diffuser at $\delta_F = 5^\circ$.

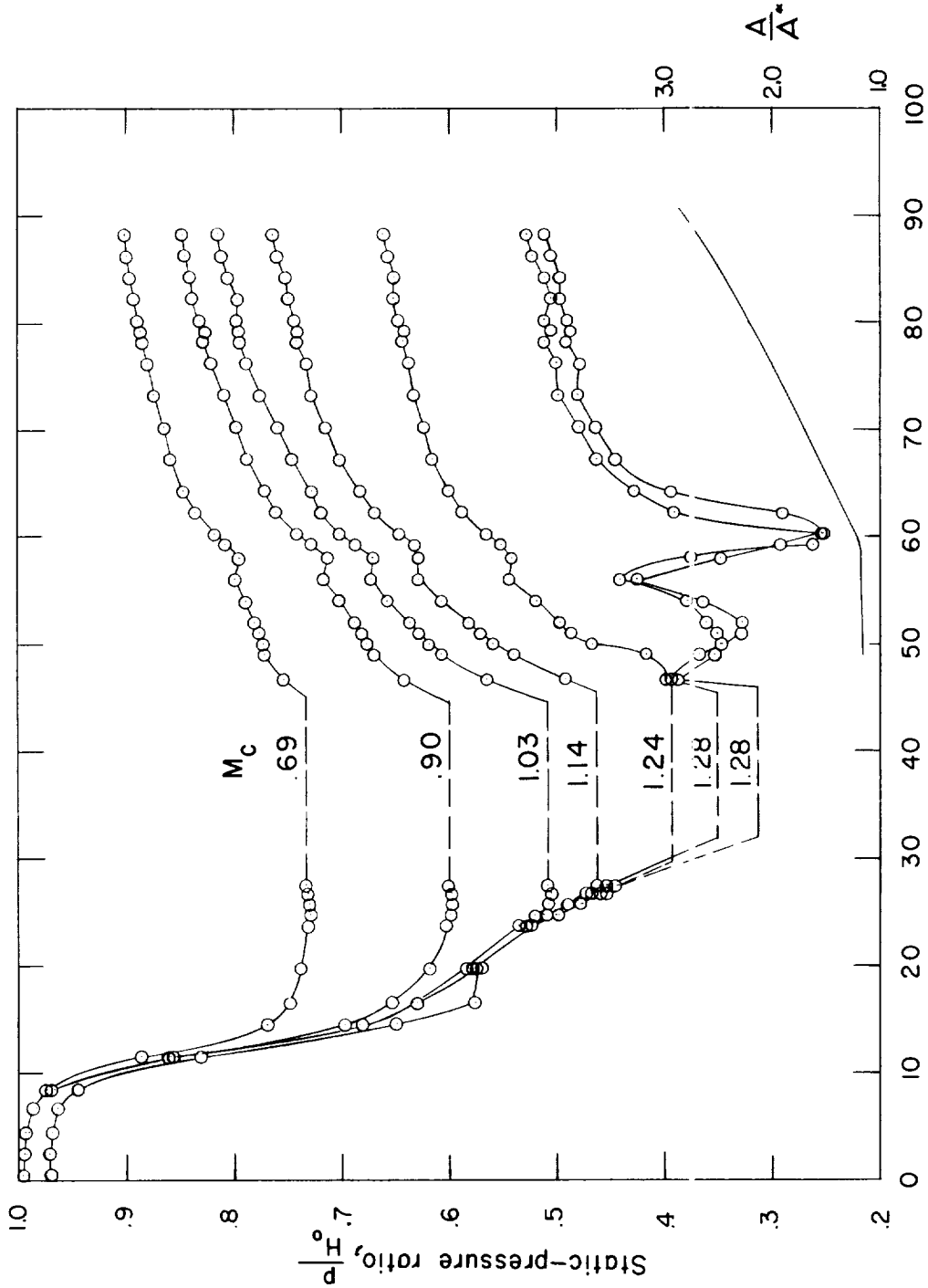

Figure 21.- Wall static-pressure distributions for the 10° diffuser at $\delta_F = 5°$.

L-1005

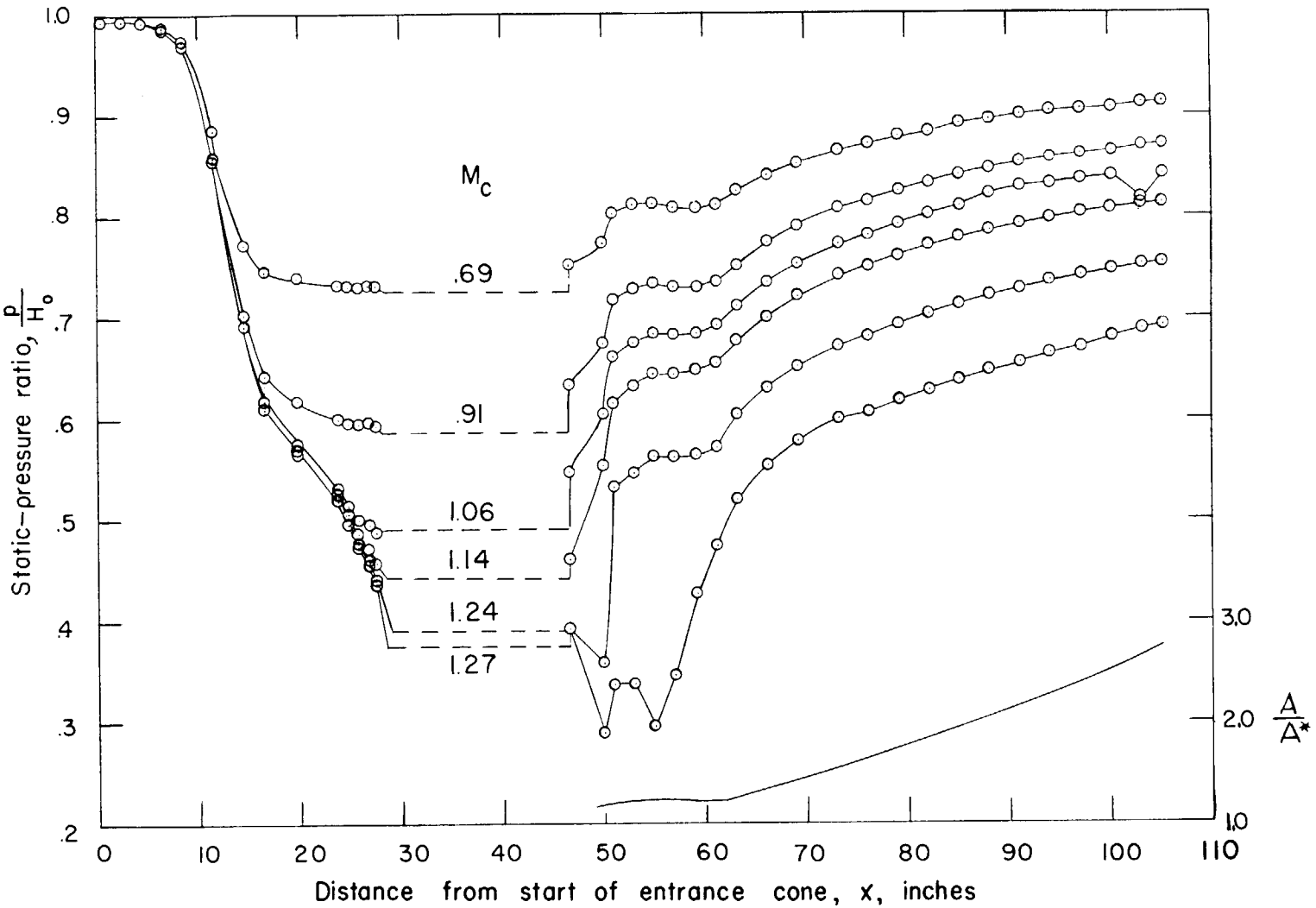

Figure 22.- Wall static-pressure distributions for the 6.4° diffuser at $\delta_F = 5°$.

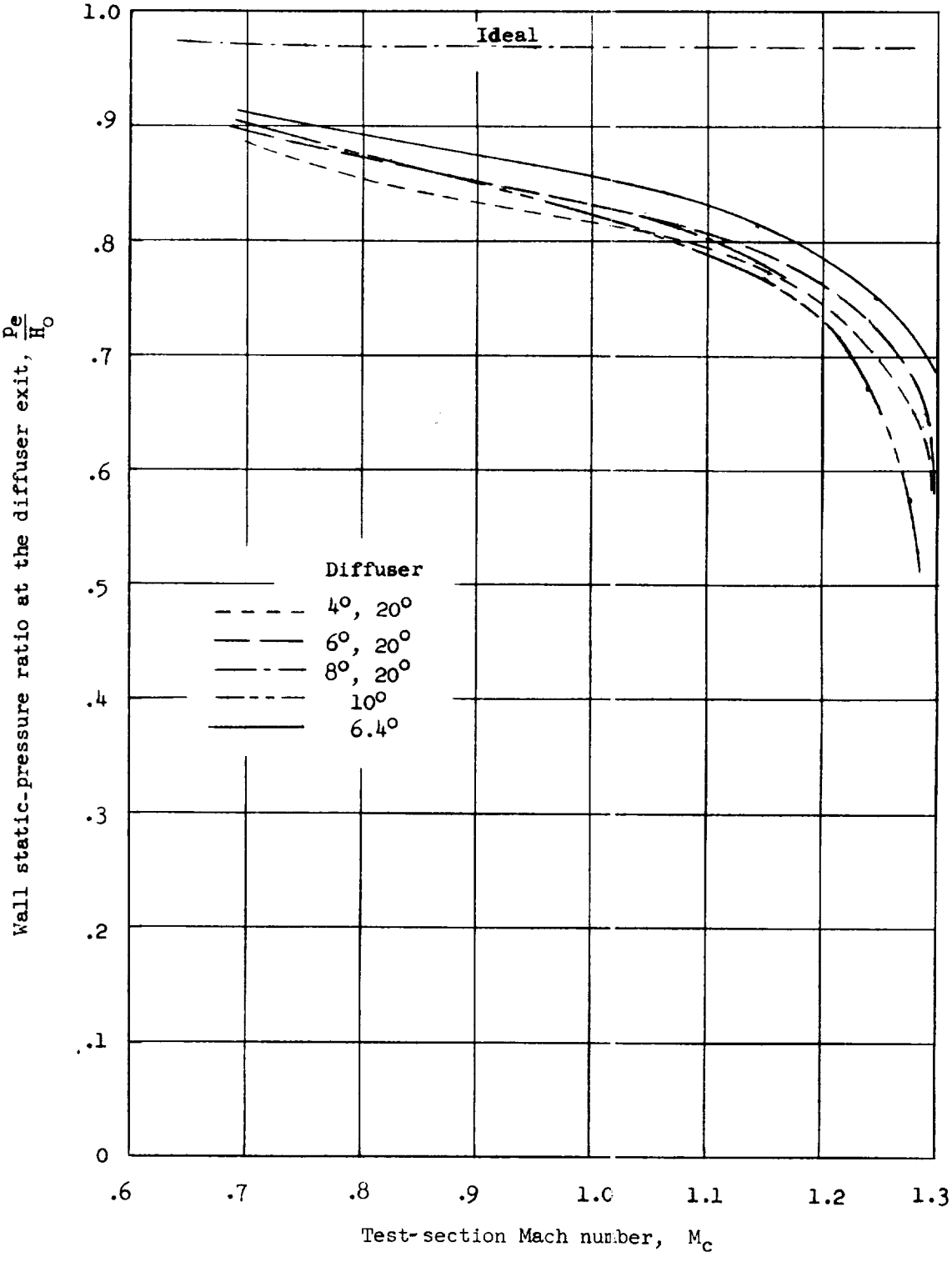

Figure 23.- Static-pressure recovery for different diffuser configurations at $\delta_F = 5°$.

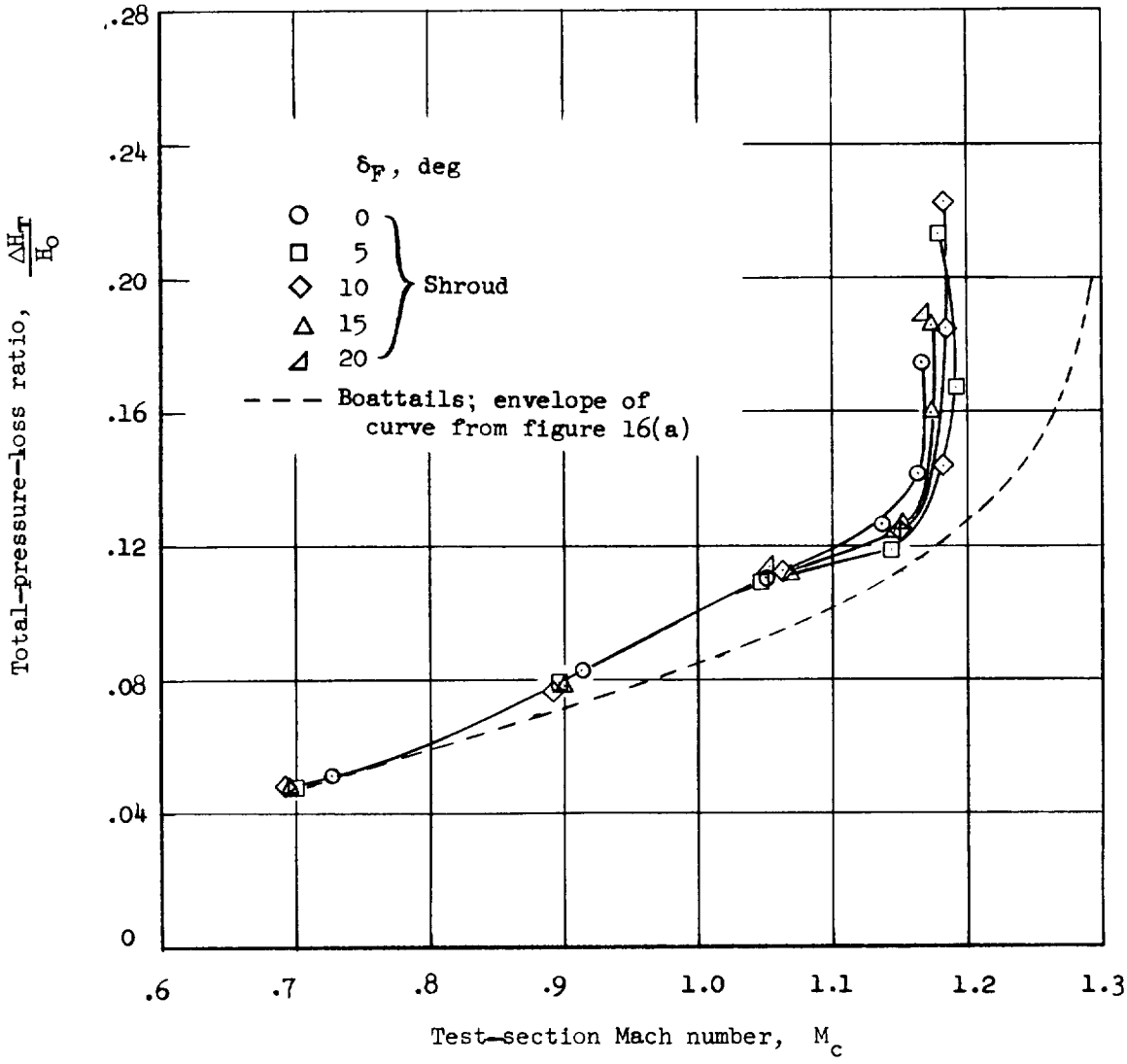

Figure 24.- Effect of the shrouded-diffuser re-entry section on total-pressure losses in the $4^\circ,20^\circ$ diffuser.

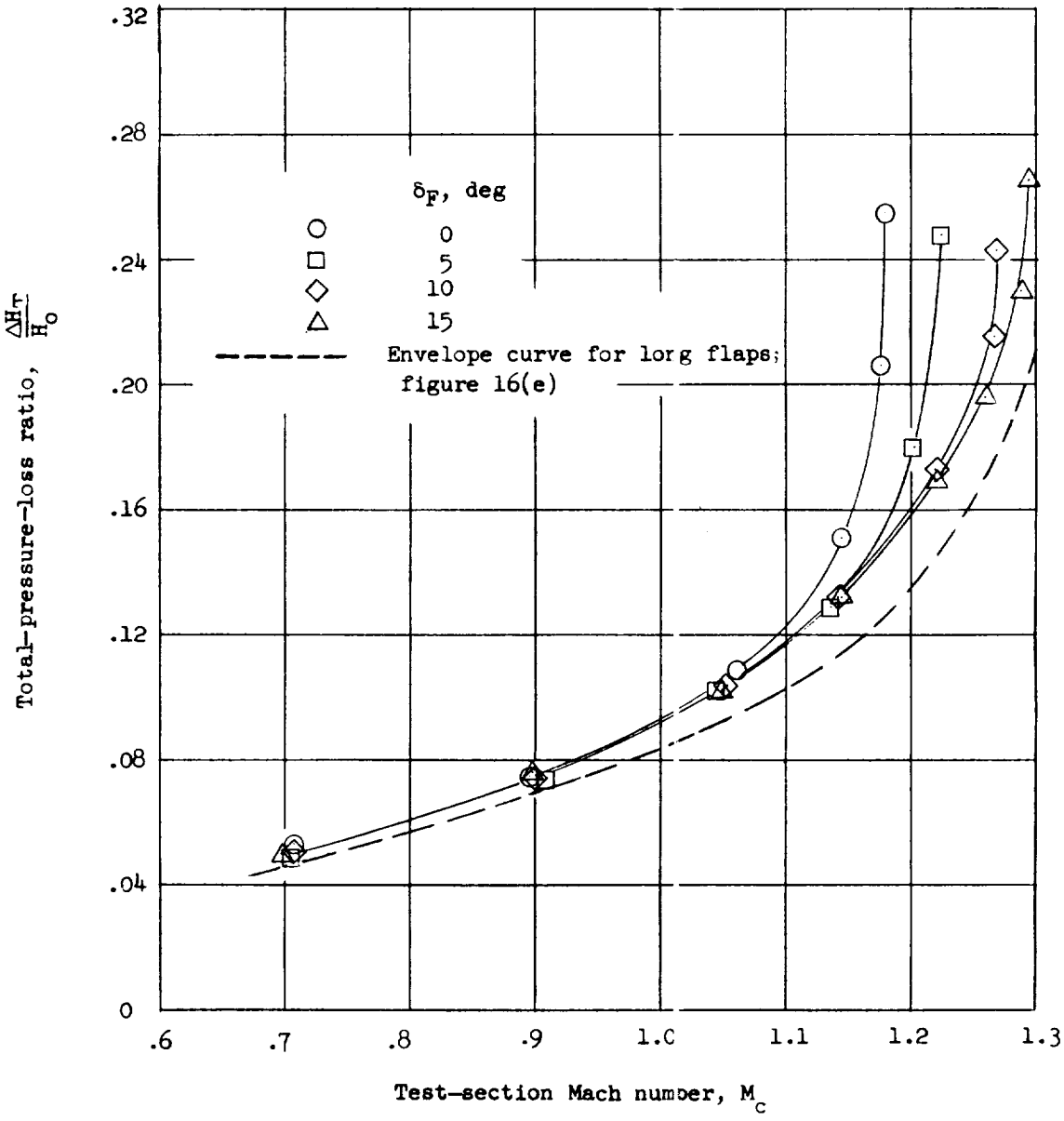

Figure 25.- Total-pressure-loss ratio for short-flap configuration. 6.4° diffuser.

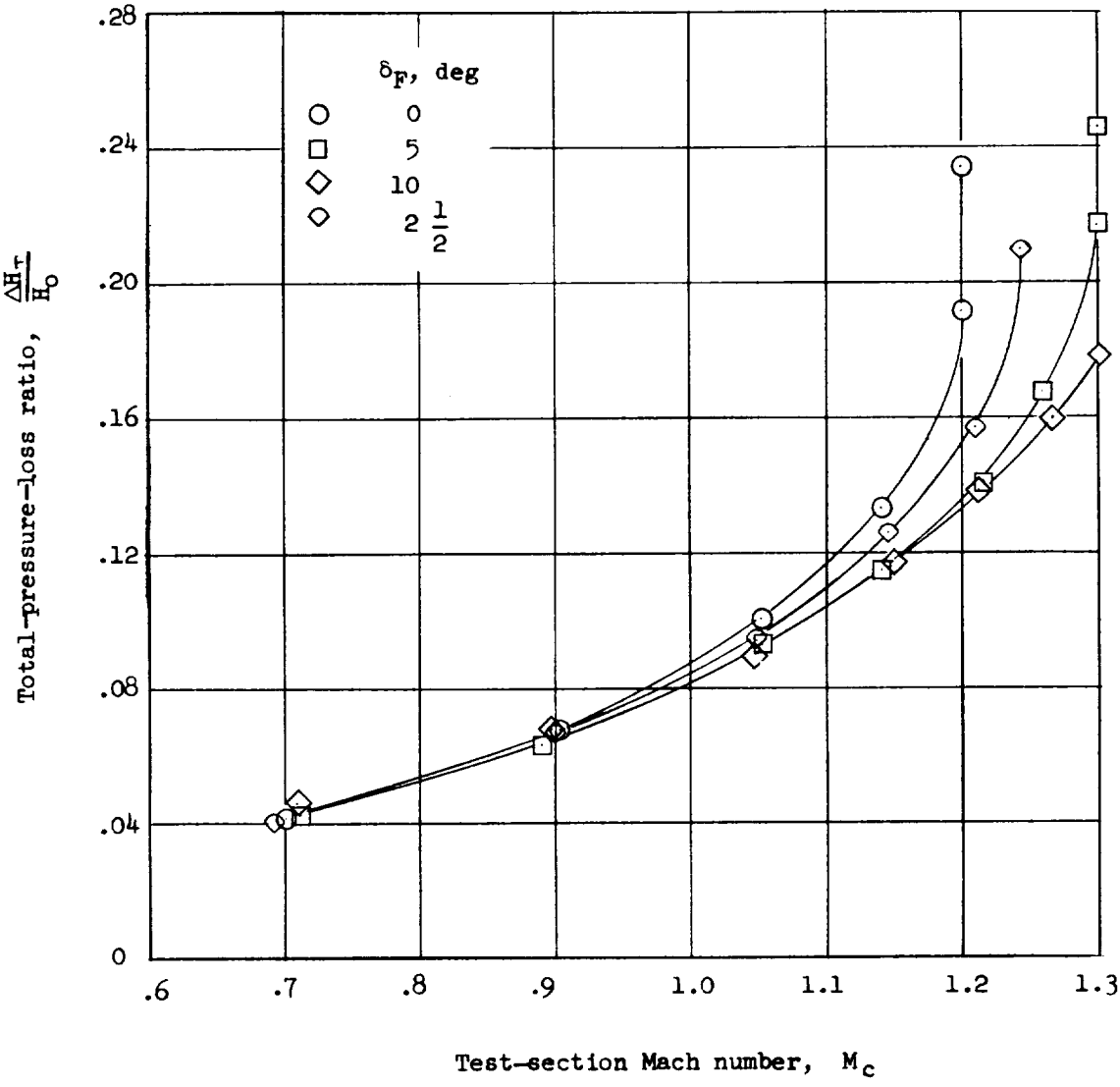

Figure 26.- Total-pressure-loss ratio for no-boattail configuration.

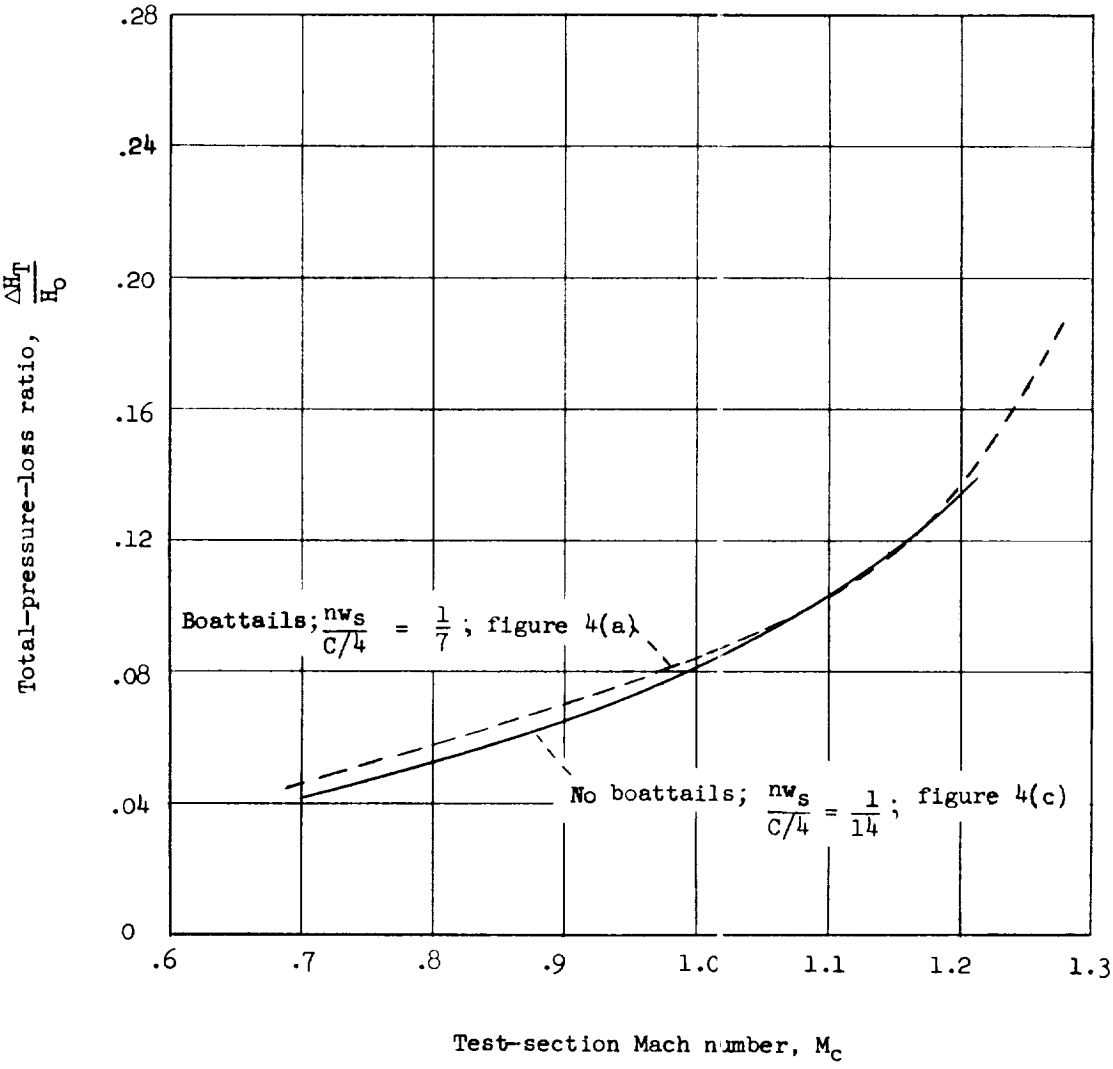

Figure 27.- Comparison of tunnel performance with and without boattails. Envelope curves.

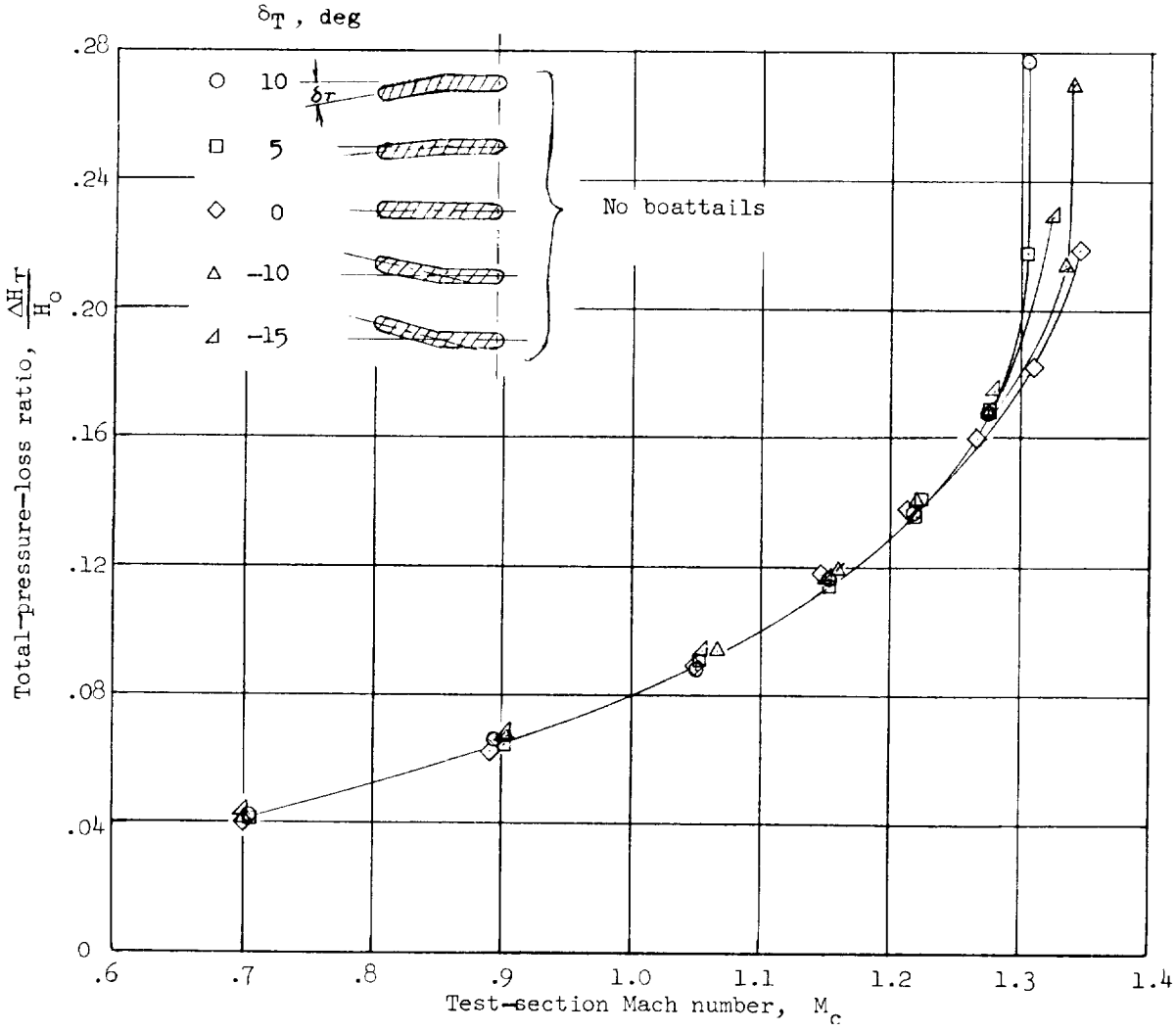

Figure 28.- Envelope curves showing the effect of flap geometry on total-pressure-loss ratios.

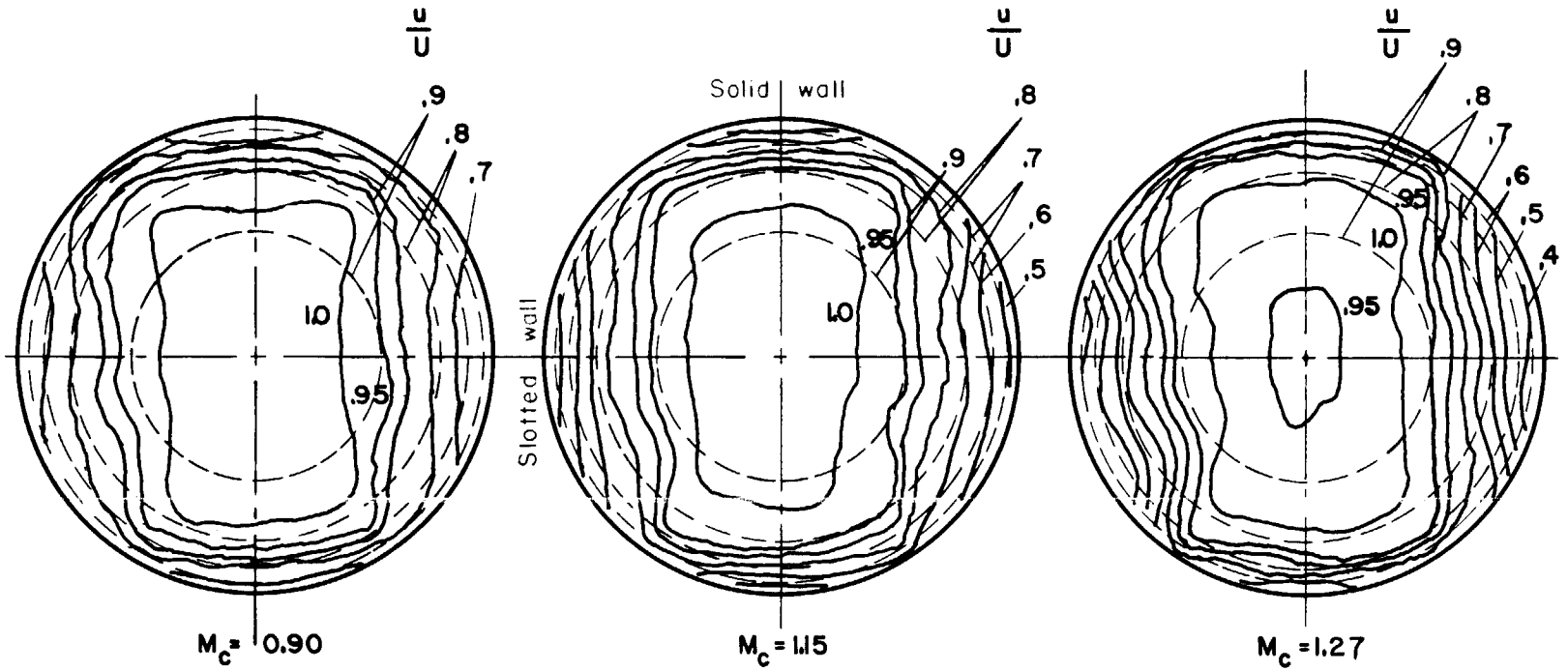

Figure 29.- Velocity contours at the diffuser inlet. $\delta_F = 5^o$. Dashed lines indicate fully developed turbulent flow.

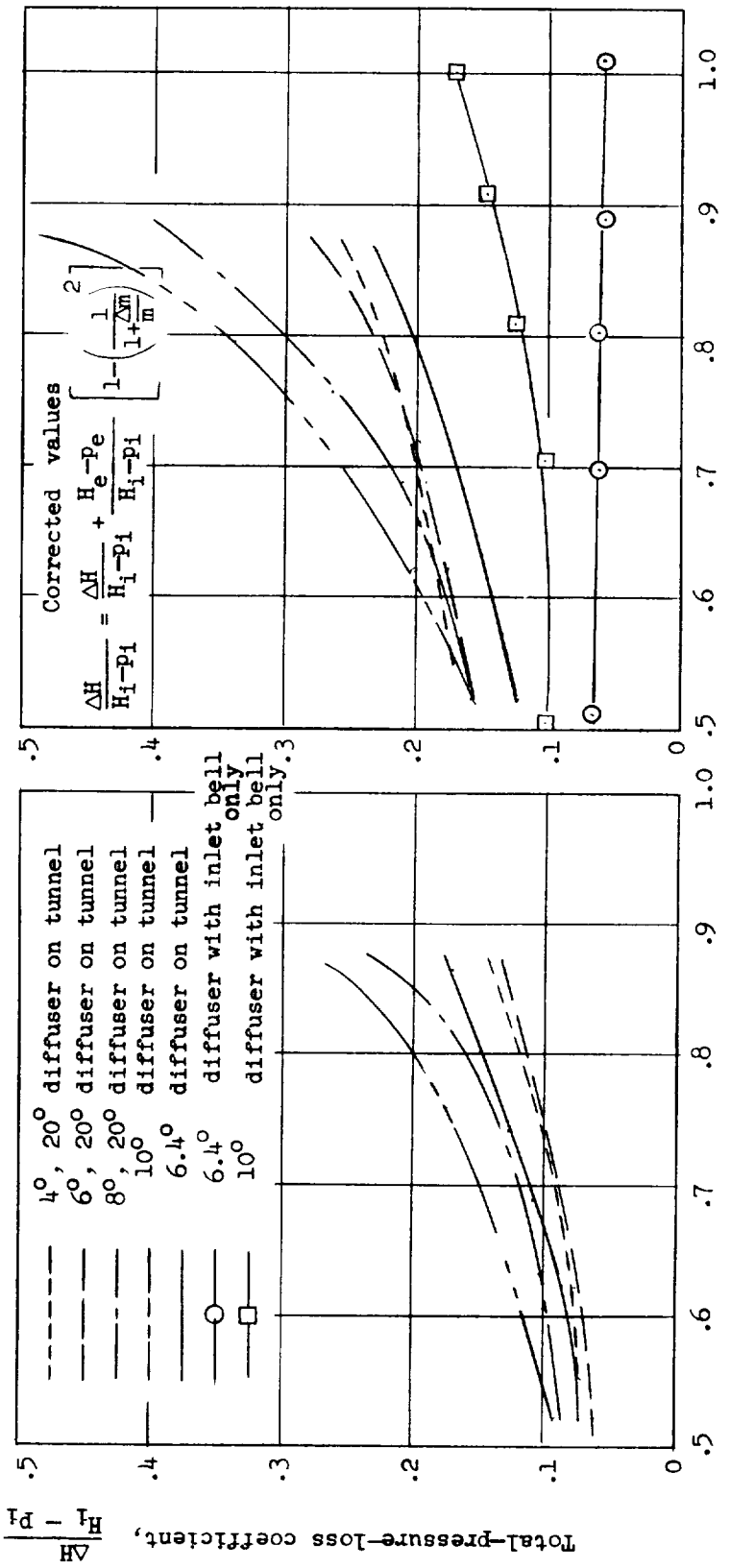

Figure 30.- Total-pressure-loss coefficients for the different diffusers. Envelope curves.

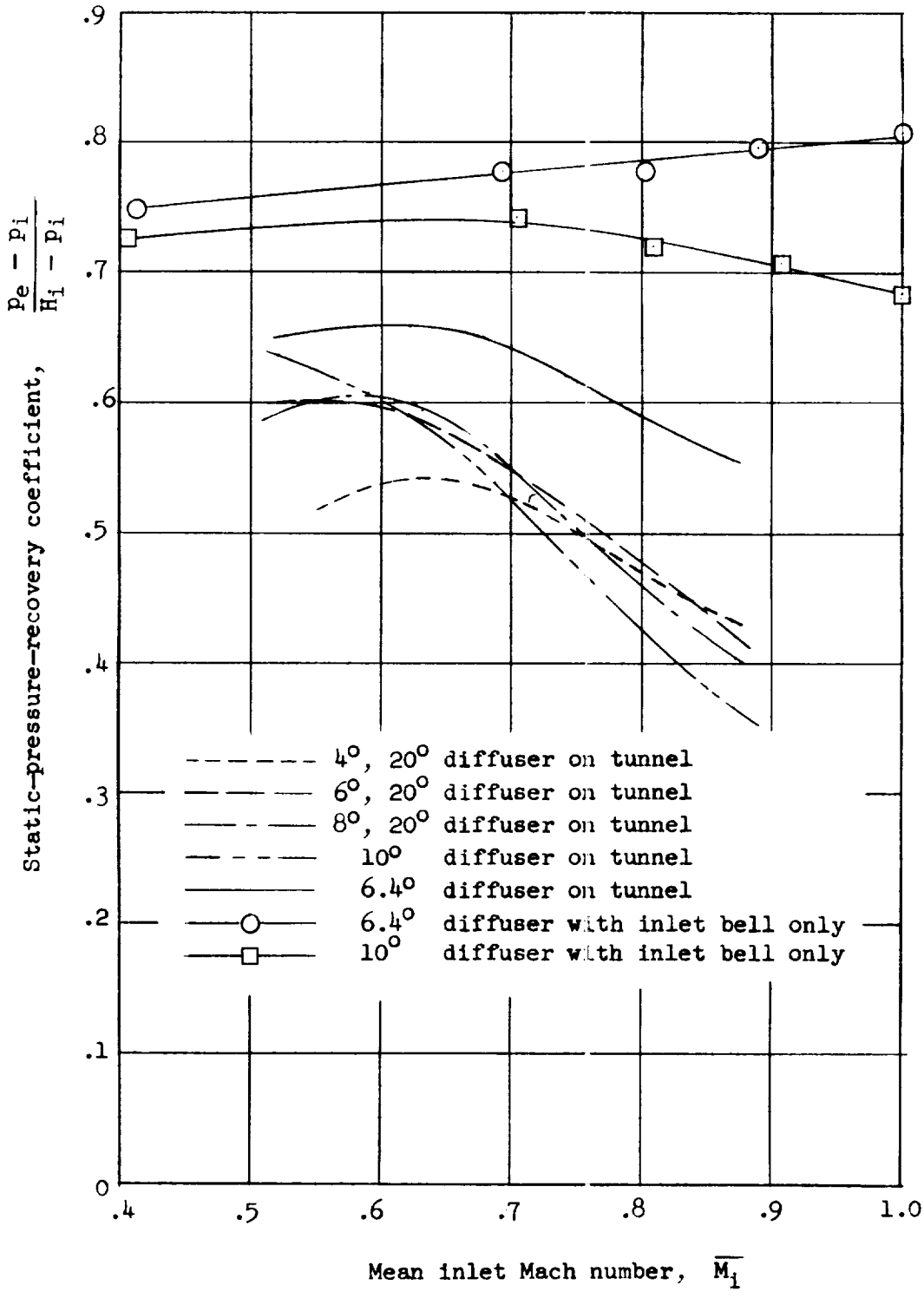

L-1005

Figure 31.- Static-pressure-recovery coefficients for the different diffusers. Envelope curves.

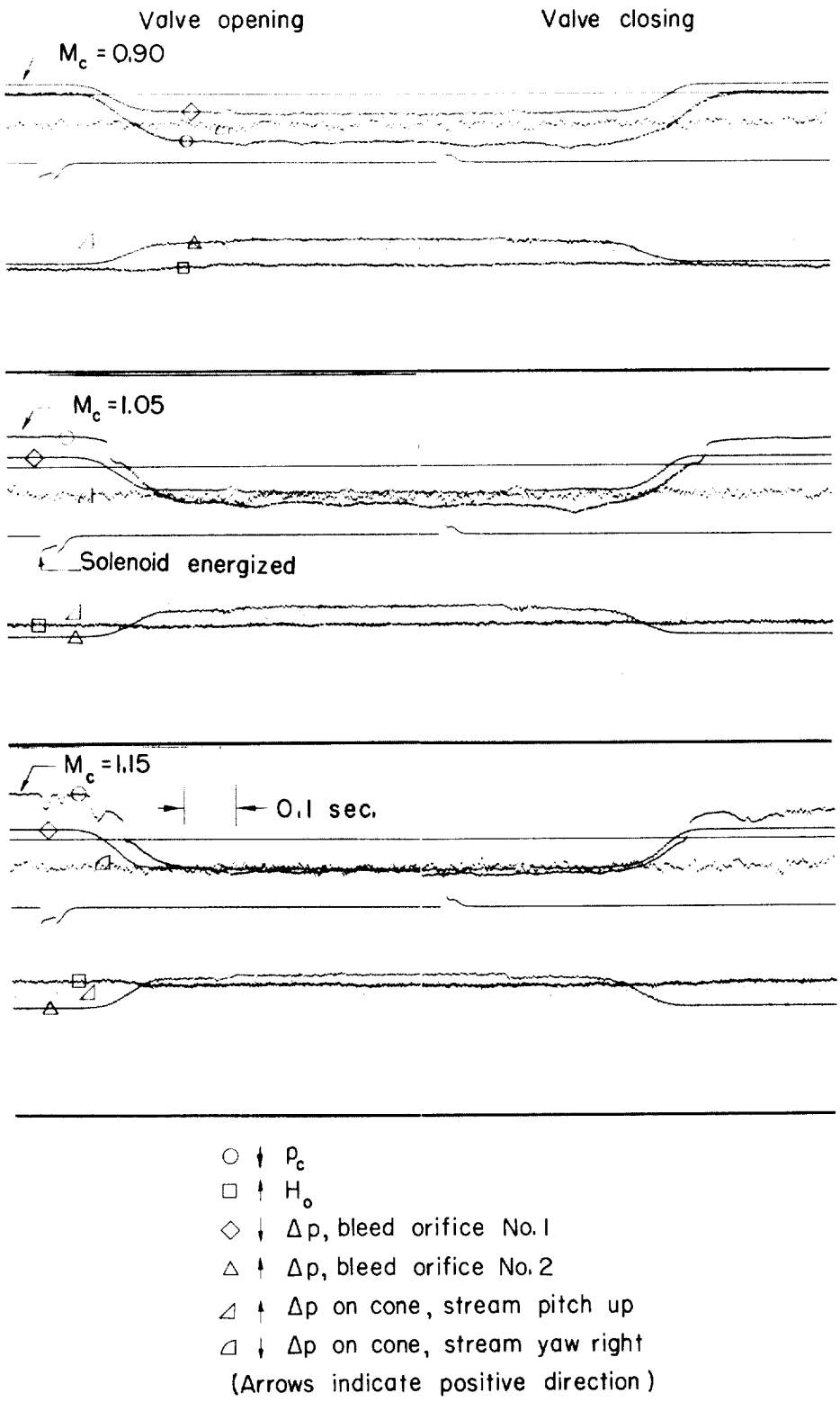

Figure 32.- Pressure-time records for rapid Mach number changes. $A_o/A^* = 0.103$.

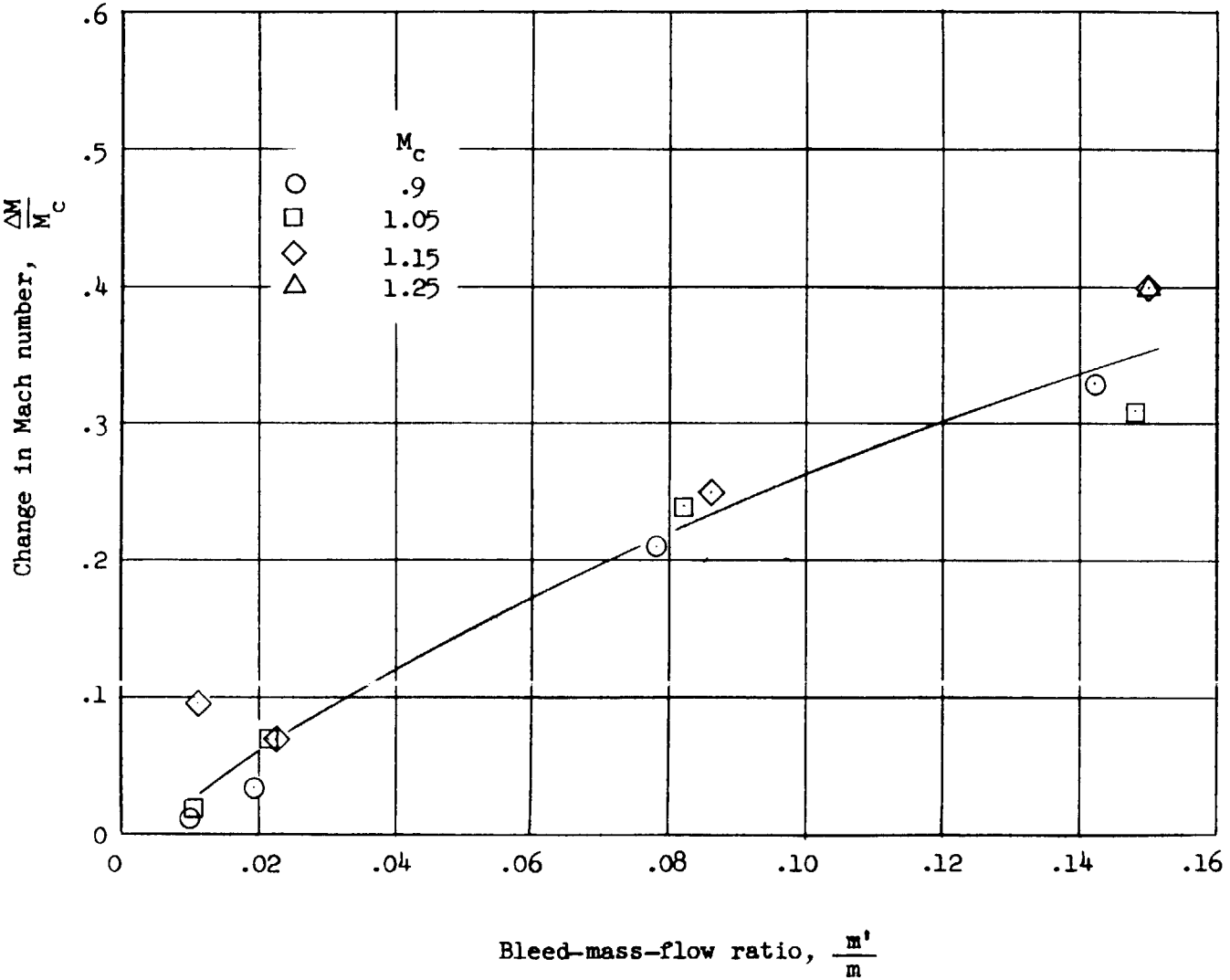

Figure 33.- Bleed mass flow required for Mach number change.

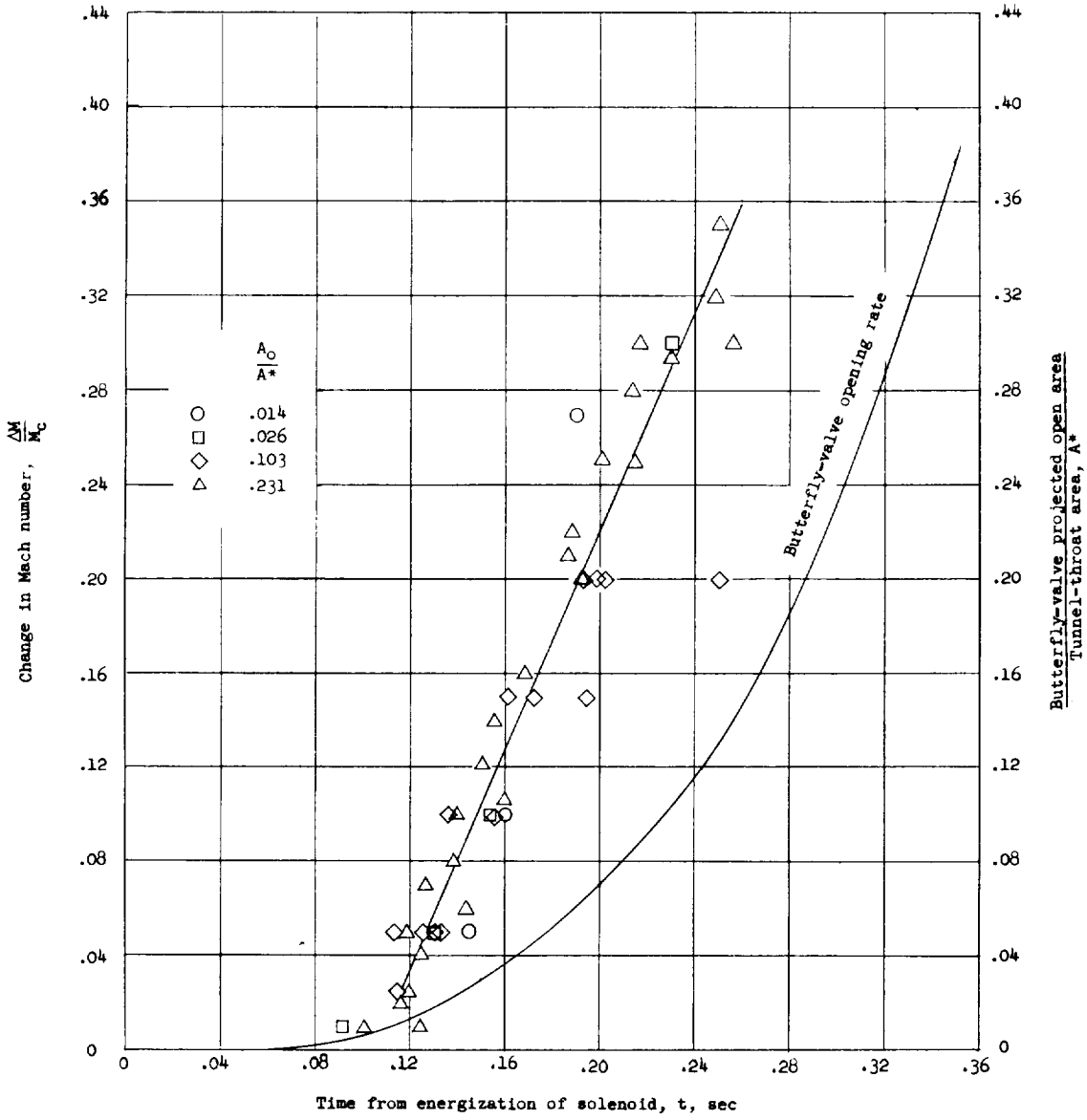

Figure 34.- Change in Mach number and butterfly-valve projected open area plotted against time.

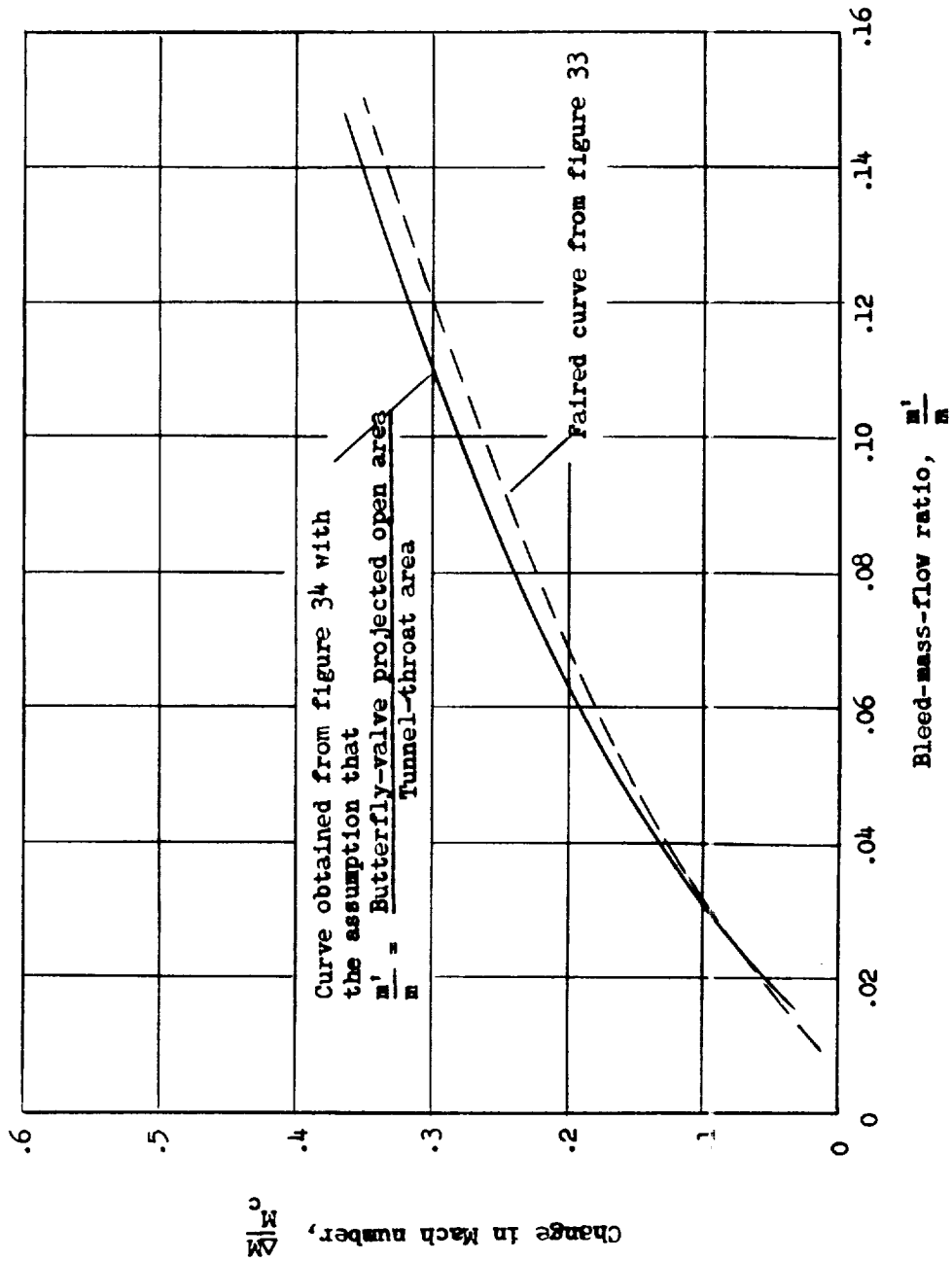

Figure 35.- Comparison of the variation of $\frac{\Delta M}{M_c}$ with $\frac{m'}{m}$ from orifices and butterfly valve.

L-1005